

Optimisation of locally advanced MSI-H/dMMR colorectal cancer treatment with neoadjuvant pembrolizumab using data-driven delay integro-differential equations

Georgio Hawi^{1, *}, Peter S. Kim^{1, †}, and Peter P. Lee^{2, †}

¹School of Mathematics and Statistics, University of Sydney, Sydney, Australia

²Department of Immuno-Oncology, Beckman Research Institute, City of Hope, Duarte, California, USA

*Corresponding author: georgio.hawi@sydney.edu.au

†These authors contributed comparably to this work

Abstract

Colorectal cancer (CRC) poses a major public health challenge due to its increasing prevalence, particularly among younger populations, with it being the third most commonly diagnosed cancer and the second leading cause of cancer-related deaths worldwide as of 2024. Microsatellite instability-high (MSI-H) CRC and deficient mismatch repair (dMMR) CRC comprise 15% of all CRC, and have shown remarkable response to immunotherapy, especially with PD-1 inhibitors. Despite this, there is still a significant need to optimise immunotherapeutic regimens to maximise clinical efficacy and patient quality of life, whilst minimising monetary costs. Mathematical models are a promising avenue for treatment optimisation, and we use delay integro-differential equations to model the interactions and dynamics of various cell types, immune checkpoints, damage-associated molecular patterns (DAMPs), and cytokines. We provide deterministic equations for the concentrations of cancer cells, DAMPs, CD4+ and CD8+ T cells, dendritic cells (DCs), cancer-associated fibroblasts (CAFs), neutrophils, macrophages, NK cells and various cytokines of pro-inflammatory (IL-2, IFN- γ , TNF, IL-12, IL-1 β) and immunosuppressive (TGF- β , IL-10, IL-4, IL-6) nature. We consider these cells and their phenotypes, noting that many of these cell types are being modelled deterministically for the first time in cancer, paving the way for a deeper understanding of the complex underlying immune dynamics. We consider two compartments: the tumour site and the tumour-draining lymph node (TDLN), taking into account phenomena such as DC migration, T cell proliferation, acquired resistance to pembrolizumab, and CD8+ T cell exhaustion and reinvigoration. The parameter values and initial conditions for the model are estimated from experimental data, incorporating various pharmacokinetic, bioanalytical, and radiographic studies, as well as deconvolution of bulk RNA-sequencing data from the TCGA COADREAD database. We finally optimise CRC treatment with neoadjuvant pembrolizumab — one of the most commonly used PD-1 inhibitors. We maximise treatment efficacy and efficiency in locally advanced MSI-H/dMMR CRC patients whilst accounting for toxicity, and improve upon currently FDA-approved therapeutic regimens for metastatic MSI-H/dMMR CRC. We demonstrate that a single medium-to-high dose of pembrolizumab is sufficient for effective tumour eradication, whilst being efficient, safe and practical.

1 Introduction

Colorectal cancer (CRC) is the third most common cancer worldwide accounting for approximately 10% of all cancer cases [1] with more than 1.85 million cases and 850,000 deaths annually [2]. The American Cancer Society estimates that in the United States, there will be 152,810 new cases of CRC diagnosed and 53,010 deaths due to CRC [3] with individual risk factors including a family history of CRC, inflammatory bowel disease, and type 2 diabetes [4]. Despite CRC being diagnosed mostly in adults 65 and older, there has been an increase in the incidence rate of CRC amongst younger populations [3, 5, 6] since the mid-1990s, with CRC being the leading cause of cancer-related deaths in adults under 55 [3]. In particular, since many people will not experience symptoms in the early stages of CRC, diagnoses often occur at a later stage when the disease is more advanced, where treatment is significantly less effective, and survival is much worse [7]. Of new CRC diagnoses, 20% of patients present with metastatic disease, while an additional 25% who initially have localised disease eventually develop metastases [2]. In the United States, the 5-year survival rates for stage IIIA, stage IIIB, and Stage IIIC colon cancer are 90%, 72%, and 53% respectively, whilst stage IV CRC has a 5-year survival of only 12% [8].

Whilst many systemic therapies are available for advanced CRC, chemotherapy has been the main treatment approach with fluoropyrimidine 5-fluorouracil being the only Food and Drug Administration (FDA) agent approved for metastatic CRC treatment for nearly 40 years [9]. Noting that folinic acid (leucovorin), a vitamin B derivative, increases the cytotoxicity of 5-fluorouracil [10], and with the approval of the topoisomerase I inhibitor irinotecan in 1996 and the platinum-based agent oxaliplatin, mainstay chemotherapy regimens such as FOLFOX (folinic acid, 5-fluorouracil, oxaliplatin) and FOLFIRI (folinic acid, 5-fluorouracil, irinotecan) have become integral to the treatment of advanced CRC [11]. However, the response rate of advanced CRC patients with 5-fluorouracil monotherapy remains at only 10 – 15%, with the addition of other anti-cancer drugs increasing response rates to only 40 – 50% [12].

Moreover, patients with the hypermutant microsatellite instability-high (MSI-H) phenotype who have reached metastasis are less responsive to conventional chemotherapy and have a poorer prognosis compared to patients with microsatellite stable (MSS) CRC [13]. MSI-H CRC is associated with the inactivation of mismatch repair (MMR) genes, including *MLH1*, *MSH2*, *MSH6*, and *PMS2*, leading to deficient MMR (dMMR) and impaired recognition and correction of spontaneous mutations by cells [14]. In particular, we note that in CRC, MSI-H and dMMR tumours are equivalent [15], and we denote these tumours as MSI-H/dMMR for the remainder of this work. Approximately 20% of stage II, 12% of stage III, and 4% of stage IV CRC tumours are diagnosed as MSI-H/dMMR [16, 17], with approximately 80% of sporadic MSI-H/dMMR CRC caused by *MLH1* promoter hypermethylation [18]. This leads to a highly increased mutational rate, with MSI-H/dMMR CRC tumours having 10 – 100 times more somatic tumours compared to microsatellite stable (MSS) CRC tumours [14], resulting in increased tumour mutation burden (TMB) and neoantigen load, and immunogenic tumour microenvironment (TME) with dense immune cell infiltration [19, 20]. This immunogenicity results in patients with MSI-H/dMMR CRC having good prognosis for immunotherapy treatment, in particular to immune checkpoint inhibitors (ICIs) [21].

Immune checkpoints, such as programmed cell death-1 (PD-1), cytotoxic T-lymphocyte-associated antigen 4 (CTLA-4), and lymphocyte-activation gene 3 (LAG-3) normally downregulate immune responses after antigen activation [22]. CTLA-4 is expressed on activated T and B cells and plays a major role in downmodulating the initial stages of T cell activation and proliferation [23]. PD-1, a cell

membrane receptor that is expressed on a variety of cell types including activated T cells, activated B cells and monocytes, has been extensively researched in the context of cancer such as MSI-H/dMMR CRC [24, 25]. When PD-1 interacts with its ligands (PD-L1 and PD-L2), effector T cell activity is inhibited, resulting in downregulation of pro-inflammatory cytokine secretion and upregulation of immunosuppressive regulatory T cells (Tregs) [26, 27]. Cancers can exploit this by expressing PD-L1 themselves, evading immunosurveillance, and impairing the proliferation and activity of cytotoxic T lymphocytes (CTLs) [28]. Blockade of PD-1/PD-L1 complex formation reinvigorates effector T cell activity, resulting in enhanced anti-tumour immunity and responses, leading to improved clinical outcomes in cancer patients [29, 30].

The KEYNOTE-177 phase III trial, NCT02563002, aimed to evaluate the efficacy of first-line pembrolizumab, an anti-PD-1 antibody, in metastatic MSI-H/dMMR CRC [18]. In the trial, 307 treatment-naive metastatic MSI-H/dMMR CRC patients were randomly assigned to receive pembrolizumab at a dose of 200 mg every 3 weeks or 5-fluorouracil-based chemotherapy every 2 weeks. A partial or complete response was observed in 43.8% of patients allocated to pembrolizumab therapy, compared with 33.1% of patients participating in 5-fluorouracil-based therapy. Furthermore, among patients who responded, 83% in the pembrolizumab group maintained response at 24 months, compared with 35% of patients receiving chemotherapy. These results motivated the FDA to approve pembrolizumab for the first-line treatment of unresectable or metastatic MSI-H/dMMR CRC on June 29, 2020 [31].

In the past couple of years, there has been a surge in research into the efficacy of neoadjuvant pembrolizumab in the treatment of high-risk stage II and stage III MSI-H/dMMR CRC. One such phase II study is the NEOPRISM-CRC, NCT05197322, 31 patients with a high TMR and high-risk stage II or stage III MSI-H/dMMR CRC were given 3 cycles of pembrolizumab, at a dose of 200mg every 3 weeks via IV infusion, and underwent surgery 4 – 6 weeks after the last dose was administered [32]. Seventeen patients exhibited pathologic complete responses (pCRs) (55%, 95% CI 36% – 73%), with the remaining patients having their tumours removed after surgery. After a median follow-up time of 6 months, recurrence was found in no patients, and the median cancer-free period was 9.7 months.

Another phase II trial, NCT04082572, aimed to evaluate the efficacy of neoadjuvant pembrolizumab on localised MSI-H/dMMR solid tumours [33]. As part of this, 27 MSI-H/dMMR CRC patients with locally advanced cancer were either given 200 mg pembrolizumab via IV infusion every 3 weeks for eight treatments followed by surgical resection, or 200 mg pembrolizumab via IV infusion every 3 weeks for 16 treatments. Of the 14 MSI-H/dMMR CRC patients who chose the resection approach, 11 of these had pCRs, and overall, 21 MSI-H/dMMR patients exhibited pcR. Additionally, after a median follow-up time of 9.5 months, only 2 patients who underwent surgical resection experienced recurrence or progression.

An important question to consider is the appropriate dosing and spacing of ICI therapies, to balance tumour reduction with factors such as monetary cost, toxicity, and side effects [34, 35]. A retrospective study by Dubé-Pelletier et al. of 80 patients with advanced non-small cell lung cancer (NSCLC) who received 4 mg/kg pembrolizumab every 6 weeks and 80 NSCLC patients who received 2 mg/kg pembrolizumab every 3 weeks, revealed that both therapies were comparable in terms of OS, toxicity and progression-free survival [36], despite the less frequent therapy being more cost-effective. Various pharmacokinetic models have been developed to optimise ICI therapy [37–40], with [41] showing that tripling the dosing interval of nivolumab, another anti-PD-1 antibody, from 240mg every 2 weeks to 240mg every 6 weeks leads to comparable efficacy despite financial costs decreasing threefold. Mathematical models provide a powerful framework for optimising treatment regimens, and in this work,

we construct a comprehensive data-driven model of the immunobiology of MSI-H/dMMR CRC using delay integro-differential equations and use this to evaluate and optimise neoadjuvant pembrolizumab therapy in locally advanced MSI-H/dMMR CRC.

To date, there are no existing mathematical models in the literature for ICI therapy in locally advanced CRC; however, there are numerous models of CRC. Kirshtein et al. developed an ordinary differential equation (ODE) model of CRC progression incorporating immunological components such as T helper cells, Tregs, dendritic cells (DCs), macrophages, as well as considered the effects of carcinogenic cytokines and immunosuppressive agents [42]. They used data from the TCGA COADREAD database [43] to perform estimates for the steady states and initial conditions of model variables, and considered data from all patients, regardless of TNM stage. Moreover, this model was extended in [44] to include FOLFIRI treatment. Bozkurt et al. presented a relatively simple ODE model of CRC treatment with anthracycline doxorubicin, and IL-2 immunotherapy, modelling cancer cells, natural killer (NK) cells, CD8+ T cells, and other lymphocytes [45]. dePillis et al. developed an ODE model of CRC with irinotecan and monoclonal antibody therapies, in particular cetuximab and panitumumab, modelling similar quantities [46].

ICI therapy has been modelled extensively in other cancers, and [47] provides a comprehensive review on the merits and weaknesses of various modelling approaches including continuum partial differential equations (PDEs), continuum ODEs, agent-based modelling (ABM) and hybrid modelling. We now summarise a few pre-existing differential-equation-based models of PD-1 blockade therapies. Lai et al. modelled the effects of anti-PD-1 and vaccines on cancer, taking into account DC maturation by high mobility group box 1 (HMGB1) and interleukin-2 (IL-2) and interleukin-12 (IL-12) in [48]. This model was adapted in [49] to optimise combination PD-1 and vascular endothelial growth factor (VEGF) inhibitor therapies in cancer. Siewe et al. modelled how transforming growth factor beta (TGF- β) can be used to overcome resistance to PD-1 blockade and also incorporated macrophages, Tregs, IL-2, IL-12, TGF- β , interleukin-10 (IL-10), and chemokine ligand 2 (CCL-2) [50]. This model was extended in [51] to model cancer therapy with PD-1 inhibitors with CSF-1 blockade, also including the cytokine tumour necrosis factor (TNF). Additionally, Liao et al. constructed a mathematical model that demonstrated the pro-cancer or anti-cancer nature of interleukin-27 (IL-27) in combination with anti-PD-1, incorporating the following cytokines: IL-27, TGF- β , IL-2, interferon-gamma (IFN- γ), and IL-10 [52].

There are, however, a multitude of limitations and drawbacks to these pre-existing models of CRC and ICI therapy. One of the biggest issues is that mature DC migration to the tumour-draining lymph node (TDLN) to activate naive T cells is not addressed, with T cell proliferation and migration to the tumour site (TS) also not being addressed. Kumbhari et al. attempted to address this in [53] and [54] in the context of optimising cancer vaccine therapy; however, activation is treated as occurring instantaneously which has been shown to be false experimentally [55]. Moreover, since T cell activation and proliferation take a non-negligible amount of time to occur, immune checkpoint inhibition of these processes must take this into account. No papers to date have properly considered this inhibition deterministically throughout the whole proliferation and activation programs, since examining inhibition at a single moment in time is insufficient to characterise this properly. Additionally, damage-associated molecular patterns (DAMPs), released by necrotic cancer cells, induce DC maturation. To date, DC maturation is considered only by HMGB1 in some models, with other important DAMPs such as calreticulin and extracellular ATP not being taken into account [56]. Furthermore, no deterministic model to date has adequately addressed CD8+ T cell exhaustion due to prolonged antigen exposure [57], nor their potential reinvigoration through immune checkpoint blockade.

Many immune cell types and cytokines that are prevalent and have important roles in the TME have not been incorporated in pre-existing deterministic models of cancer. These include neutrophils, which can either enhance anti-tumour immunity or reduce pro-tumour inflammation [58, 59], cancer-associated fibroblasts (CAFs) which are the most abundant component of the TME and produce immunosuppressive cytokines [60, 61], and cytokines such as interleukin-4 (IL-4), interleukin-6 (IL-6) and interleukin-1 beta (IL-1 β) [62]. One thing to note is that pre-existing deterministic models mostly estimate cytokine production parameters via biologically informed assumptions, which can lead to inaccuracies and is a somewhat ad hoc approach. In this work we construct a mathematical model using data-driven delay integro-differential equations that addresses these drawbacks, incorporating all of the aforementioned processes and species, and use this to optimise neoadjuvant pembrolizumab therapy in locally advanced MSI-H/dMMR CRC.

It is prudent for us to briefly outline the functions and processes of some immune cells in the TME since their interaction with cancer cells directly or through chemokine/cytokine signalling significantly influences the efficacy of therapeutic regimens [63]. T cell activation occurs in the lymph node and occurs through T cell receptor (TCR) recognition of cancer antigen presented by major histocompatibility complex (MHC) class I molecules, in the case of CD8+ T cells, and MHC class II molecules, in the case of CD4+ T cells, expressed on the surfaces of mature DCs [64]. CTLs recognise cancer cells through TCR detection of peptide major histocompatibility complexes (pMHCs) on cancer cell surfaces via MHC class I [65]. CD8+ cells, as well as NK cells, are amongst the most cytotoxic and important cells in cancer cell lysis [66], in addition to secreting pro-inflammatory cytokines such as IL-2, IFN- γ , and TNF [67]. These are also secreted by CD4+ T helper 1 (Th1) cells, and are an important part of cell-mediated immunity, allowing for neutrophil chemotaxis and macrophage activation [68]. On the other hand, CD4+ T helper 2 (Th2) cells produce various anti-inflammatory cytokines such as IL-4, IL-10, and interleukin 23 (IL-23), which induce increased antibody production, and eosinophil activation [69]. Furthermore, we must also consider CD4+ Tregs, which are vital in immune tissue homeostasis, since they are able to suppress the synthesis of pro-inflammatory cytokines, and control intestinal inflammatory processes [70]. This is done in a variety of ways, including the production of immunomodulatory and immunosuppressive cytokines such as TGF- β , IL-10, and interleukin 35 (IL-35) [71, 72]. We note that naive CD4+ T cells can differentiate towards multiple additional phenotypes such as Th9, Th22, Tfh and Th17 cells, each involved in the pathogenesis of cancer [73, 74].

Also of importance in CRC are macrophages which, like T cells, are able to produce pro-inflammatory and anti-inflammatory cytokines [75]. Naive macrophages, denoted M0 macrophages, can differentiate into two main phenotypes: classically activated M1 macrophages and alternatively activated M2 macrophages. These names were given since M1 macrophages promote Th1 cell responses, and M2 macrophages promote Th2 responses, with Th1-associated cytokines downregulating M2 activity, and vice-versa [76]. M1 macrophages contribute to the inflammatory response by activating endothelial cells, promoting the induction of nitric oxide synthase, and producing large amounts of pro-inflammatory cytokines such as TNF, IL-1 β , and IL-12 [77]. On the other hand, M2 macrophages are responsible for wound healing and the resolution of inflammation, through phagocytosing apoptotic cells, and releasing anti-inflammatory mediators such as IL-10, interleukin 13 α 1 (IL-13 α 1), and CC Motif Chemokine Ligand 17 (CCL17) [78].

Finally, we consider neutrophils in CRC which promote tumour growth, invasion, and metastasis [79], but like macrophages and T cells, secrete pro-inflammatory and immunosuppressive cytokines [80]. Similarly to macrophages, naive neutrophils, denoted N0 neutrophils, can differentiate into two

main phenotypes: anti-tumour N1 neutrophils and pro-tumour N2 neutrophils [81]. N1 neutrophils in CRC are characterised by their production of pro-inflammatory cytokines such as TNF, IL-12, and IL-1 β [82]. However, N2 neutrophils promote tumour growth and metastasis through the secretion of pro-angiogenic factors and immunosuppressive chemokines such as arginase, CCL2 and chemokine ligand 4 (CCL4) [81, 83].

It is important to note that the M1/M2 macrophage and N1/N2 and neutrophil dichotomies are somewhat of a simplification. Macrophages and neutrophils are highly plastic and have been demonstrated to integrate environmental signals to change their phenotype and physiology [84, 85]. To account for this, in the model, we incorporate macrophage and neutrophil polarisation and repolarisation between their anti-tumour and immunosuppressive phenotypes by various cytokines and proteins.

2 Mathematical Model

2.1 Model Assumptions

The variables and their units in the model are shown in Table 1. For simplicity, we ignore spatial effects in the model, ignoring the effects of diffusion, advection, and chemotaxis by all species. We assume the system has two compartments: one at the TS, located in the colon or rectum, and one at the tumour-draining lymph node (TDLN). We assume that cytokines in the TS are produced only by effector or activated cells and that DAMPs in the TS are only produced by necrotic cancer cells. We assume that all mature DCs in the TDLN are cancer-antigen bearing and that all T cells in the TS are primed with cancer antigens. Furthermore, we assume that all activated T cells in the TDLN are activated with cancer antigens and that T cell proliferation/division follows a deterministic program. We assume that CD4+ T cells, immediately upon activation, differentiate into the Th1 or Th2 phenotypes, ignoring CD4+ and CD8+ memory T cells. We also assume that all Tregs in the TS are natural Tregs (nTregs), ignoring induced Tregs (iTregs). We assume, for simplicity, that activated neutrophils polarise into the N1/N2 dichotomy, and that activated macrophages polarise into the M1/M2 dichotomy. We also assume that the duration of pembrolizumab infusion is negligible compared to the timescale of the model. Therefore, we treat their infusions as an intravenous bolus so that drug absorption occurs immediately after infusion. Finally, to ensure that all concentrations stay positive regardless of the initial conditions, for biological realism, we assume that cells do not interact before $t = 0$, setting their concentrations to nil for $t < 0$.

Table 1: Variables used in the model. Quantities in the top box are in units of cell/cm³, quantities in the second and bottom box are in units of g/cm³, and all other quantities are in units of molec/cm³. All quantities refer to tumour site density/concentration unless otherwise specified. TDLN denotes the tumour-draining lymph node, whilst TS denotes the tumour site.

Var	Description	Var	Description
C	Viable cancer cell density	N_c	Necrotic cell density
D_0	Immature DC density	D	Mature DC density at TS
D^{LN}	Mature DC density at TDLN	T_0^8	Naive CD8+ T cell density in TDLN
T_A^8	Effector CD8+ T cell density in TDLN	T_8	Effector CD8+ T cell density at TS
T_{ex}	Exhausted CD8+ T cell density at TS	T_0^4	Naive CD4+ T cell density in TDLN
T_A^1	Effector Th1 cell density in TDLN	T_A^2	Effector Th2 cell density in TDLN
T_1	Effector Th1 cell density at TS	T_2	Effector Th2 cell density at TS

T_0^r	Naive Treg density in TDLN	T_A^r	Effector Treg density in TDLN
T_r	Effector Treg density at TS	C_F	CAF density
N_0	Naive neutrophil density	N_1	N1 neutrophil density
N_2	N2 neutrophil density	M_0	Naive macrophage density
M_1	M1 macrophage density	M_2	M2 macrophage density
K_0	Naive NK cell density	K	Activated NK cell density
H	HMGB1 concentration	A	Extracellular ATP concentration
S	Calreticulin concentration	I_2	IL-2 concentration
I_γ	IFN- γ concentration	I_α	TNF concentration
I_β	TGF- β concentration	I_{12}	IL-12 concentration
I_{10}	IL-10 concentration	I_4	IL-4 concentration
I_6	IL-6 concentration	$I_{1\beta}$	IL-1 β concentration
P_D	PD-1 concentration at TS	P_D^{LN}	PD-1 concentration in TDLN
P_L	PD-L1 concentration at TS	P_L^{LN}	PD-L1 concentration in TDLN
Q	PD-1/PD-L1 concentration at TS	Q^{LN}	PD-1/PD-L1 concentration in TDLN
P_A	CTLA-4 concentration at TS	P_A^{LN}	CTLA-4 concentration in TDLN
A_1	Concentration of pembrolizumab at TS	A_1^{LN}	Concentration of pembrolizumab in TDLN

We assume that all species, X_i , degrade/die at a rate proportional to their concentration, with decay constant d_{X_i} . We assume that the rate of activation/polarisation of a species X_i by a species X_j follows the Michaelis-Menten kinetic law $\lambda_{X_i X_j} X_i \frac{X_j}{K_{X_i X_j} + X_j}$, for rate constant $\lambda_{X_i X_j}$, and half-saturation constant $K_{X_i X_j}$. Similarly, we model the rate of inhibition of a species X_i by a species X_j using a term with form $\lambda_{X_i X_j} \frac{X_i}{1 + X_j / K_{X_i X_j}}$ for rate constant $\lambda_{X_i X_j}$, and half-saturation constant $K_{X_i X_j}$. Production of X_i by X_j is modelled using mass-action kinetics unless otherwise specified so that the rate that X_i is formed is given by $\lambda_{X_i X_j} X_i X_j$ for some positive constant $\lambda_{X_i X_j}$. Finally, we assume that the rate of lysis of X_i by X_j follows mass-action kinetics in the case where X_j is a cell, and follows Michaelis-Menten kinetics in the case where X_j is a cytokine.

2.2 Model Summary

We now outline some of the main processes accounted for in the model, with all processes and equations being explained in [Section 2.3](#).

1. CD8+ T cells, CD4+ T cells, and NK cells induce apoptosis of cancer cells with this being inhibited by proteins including TGF- β , IL-6, PD-1 and PD-L1. However, TNF and IFN- γ induce necroptosis of cancer cells, causing them to become necrotic before they are removed.
2. Necrotic cancer cells release DAMPs such as HMGB1, calreticulin, and extracellular ATP which stimulate immature DCs to mature.
3. Some mature DCs migrate to the T cell zone of the TDLN and activate naive CD4+ and CD8+ T cells, with this being inhibited by PD-1 and CTLA-4.
4. Activated CD4+ and CD8+ T cells undergo clonal expansion and proliferate rapidly in the TDLN, with this proliferation being inhibited by the PD-1/PD-L1 complex and CTLA-4.

5. CD4+ and CD8+ T cells that have completed proliferation migrate to the TS and perform effector functions including the secretion of pro-inflammatory (IL-2, IFN- γ , TNF, IL-12, IL-1 β) and immunosuppressive (TGF- β , IL-10, IL-4, IL-6) cytokines. Extended exposure to the cancer antigen can lead CD8+ T cells to become exhausted, however, this exhaustion can be reversed by pembrolizumab.
6. In addition, mature DCs, NK cells, neutrophils, macrophages and CAFs secrete cytokines that can activate NK cells, and polarise and repolarise macrophages and neutrophils into pro-inflammatory and immunosuppressive phenotypes.

2.3 Model Equations

Cancer cells are killed by effector CD8+ T cells [86], activated NK cells [87] and Th1 cells [88, 89] through direct contact, whilst TNF and IFN- γ indirectly eliminate cancer cells via activating cell death pathways [90–92]. In particular, TNF and IFN- γ induce the necroptosis, programmed necrotic cell death, of cancer cells [91, 93]. We note that TGF- β and PD-L1 have been shown to inhibit cancer cell lysis by CD8+ T cells [94, 95], and IL-6 and PD-1 have been shown to inhibit NK cell cytotoxicity [96, 97]. We assume that cancer cells grow logistically, as is done in many CRC models [42, 44, 46], due to space and resource competition in the TME. Combining these, we have

$$\begin{aligned} \frac{dC}{dt} = & \underbrace{\lambda_C C \left(1 - \frac{C}{C_0}\right)}_{\text{growth}} - \underbrace{\lambda_{CT_8} T_8 \frac{1}{1 + I_\beta/K_{CI_\beta}} \frac{1}{1 + P_L/K_{CP_L}} C}_{\substack{\text{elimination by } T_8 \\ \text{inhibited by } I_\beta \text{ and } P_L}} - \underbrace{\lambda_{CT_1} T_1 C}_{\text{elimination by } T_1} \\ & - \underbrace{\lambda_{CK} K \frac{1}{1 + I_6/K_{CI_6}} \frac{1}{1 + P_D/K_{CP_D}} C}_{\substack{\text{elimination by } K \\ \text{inhibited by } I_6 \text{ and } P_D}} - \underbrace{\lambda_{CI_\alpha} \frac{I_\alpha}{K_{CI_\alpha} + I_\alpha} C}_{\text{elimination by } I_\alpha} - \underbrace{\lambda_{CI_\gamma} \frac{I_\gamma}{K_{CI_\gamma} + I_\gamma} C}_{\text{elimination by } I_\gamma}, \end{aligned} \quad (2.1)$$

$$\frac{dN_c}{dt} = \underbrace{\lambda_{CI_\alpha} \frac{I_\alpha}{K_{CI_\alpha} + I_\alpha} C}_{\text{Elimination by } I_\alpha} + \underbrace{\lambda_{CI_\gamma} \frac{I_\gamma}{K_{CI_\gamma} + I_\gamma} C}_{\text{Elimination by } I_\gamma} - \underbrace{d_{N_c} N_c}_{\text{Removal}}. \quad (2.2)$$

The molecule HMGB1 is released by necrotic cancer cells [98] and CAFs [99] so that

$$\frac{dH}{dt} = \underbrace{\lambda_{HN_c} N_c}_{\text{production by } N_c} + \underbrace{\lambda_{HC_F} C_F}_{\text{production by } C_F} - \underbrace{d_H H}_{\text{degradation}}. \quad (2.3)$$

Necrotic cancer cells release ATP [100] and calreticulin [101] so that

$$\frac{dA}{dt} = \underbrace{\lambda_{AN_c} N_c}_{\text{production by } N_c} - \underbrace{d_A A}_{\text{degradation}}, \quad (2.4)$$

$$\frac{dS}{dt} = \underbrace{\lambda_{SN_c} N_c}_{\text{production by } N_c} - \underbrace{d_S S}_{\text{degradation}}. \quad (2.5)$$

Immature DCs are stimulated to mature via DAMPs such as HMGB1, ATP, and calreticulin [56]; however, we employ Michaelis-Menten kinetics to accommodate for the limited rate of receptor recycling

time [48]. In addition, NK cells have been shown to efficiently kill immature DCs but not mature DCs [102, 103]. Assuming that immature DCs are supplied at a rate \mathcal{A}_{D_0} , we have that

$$\frac{dD_0}{dt} = \underbrace{\mathcal{A}_{D_0}}_{\text{source}} - \underbrace{\lambda_{DH}D_0 \frac{H}{K_{DH} + H}}_{D_0 \rightarrow D \text{ by } H} - \underbrace{\lambda_{DA}D_0 \frac{A}{K_{DA} + A}}_{D_0 \rightarrow D \text{ by } A} - \underbrace{\lambda_{DS}D_0 \frac{S}{K_{DS} + S}}_{D_0 \rightarrow D \text{ by } S} - \underbrace{\lambda_{D_0K}D_0K}_{\text{elimination by } K} - \underbrace{d_{D_0}D_0}_{\text{death}}, \quad (2.6)$$

$$\frac{dD}{dt} = \underbrace{\lambda_{DH}D_0 \frac{H}{K_{DH} + H}}_{D_0 \rightarrow D \text{ by } H} + \underbrace{\lambda_{DA}D_0 \frac{A}{K_{DA} + A}}_{D_0 \rightarrow D \text{ by } A} + \underbrace{\lambda_{DS}D_0 \frac{S}{K_{DS} + S}}_{D_0 \rightarrow D \text{ by } S} - \underbrace{\lambda_{DD^{\text{LN}}}D}_{D \text{ migration to TDLN}} - \underbrace{d_D D}_{\text{death}}. \quad (2.7)$$

We also need to consider that some mature DCs migrate into the T cell zone of the TDLN and stimulate naive CD8+ T cells, causing them to be activated, hence no longer naive [104, 105]. We assume a fixed DC migration time of τ_m and also assume that only $e^{-d_D\tau_m}$ of the mature DCs that leave the TS survive migration. Taking into account the volume change between the TS site and the TDLN, we have that

$$\frac{dD^{\text{LN}}}{dt} = \frac{V_{\text{TS}}}{V_{\text{LN}}} \underbrace{\lambda_{DD^{\text{LN}}}e^{-d_D\tau_m} D(t - \tau_m)\theta(t - \tau_m)}_{D \text{ migration to TDLN}} - \underbrace{d_D D^{\text{LN}}}_{\text{death}}, \quad (2.8)$$

where $\theta(x)$ is the Heaviside function which equals 1 if $x \geq 0$, and 0 otherwise. The Heaviside function ensures positive invariance of the system by preventing cells from interacting before $t = 0$.

We now consider the concentration of naive T cells in the TDLN. We assume that naive CD8+ T cells come into the TDLN at a constant rate and that they have not undergone cell division, nor will they until their activation. For simplicity, we do not consider cytokines in the TDLN, absorbing their influence into $\lambda_{T_0^s T_A^s}$. We do, however, explicitly take into account the influence of PD-1 and CTLA-4 in the TDLN, which have been shown to inhibit T cell activation through limiting naive T cells from binding to mature DCs [106, 107]. Thus, taking this all into account leads to

$$\frac{dT_0^s}{dt} = \underbrace{\mathcal{A}_{T_0^s}}_{\text{source}} - \underbrace{R^s(t)}_{\text{CD8+ T cell activation}} - \underbrace{d_{T_0^s}T_0^s}_{\text{death}}, \quad (2.9)$$

where $R^s(t)$ is defined as

$$R^s(t) := \frac{\lambda_{T_0^s T_A^s} e^{-d_{T_0^s} \tau_8^{\text{act}}} D^{\text{LN}}(t - \tau_8^{\text{act}}) T_0^s(t - \tau_8^{\text{act}}) \theta(t - \tau_8^{\text{act}})}{\underbrace{\left(1 + \int_{t-\tau_8^{\text{act}}}^t P_D^{\text{LN}}(s) ds / K_{T_0^s P_D^{\text{LN}}}\right) \left(1 + \int_{t-\tau_8^{\text{act}}}^t P_A^{\text{LN}}(s) ds / K_{T_0^s P_A^{\text{LN}}}\right)}_{\text{CD8+ T cell activation inhibited by } P_D^{\text{LN}} \text{ and } P_A^{\text{LN}}}}. \quad (2.10)$$

In particular, since PD-1 and CTLA-4 inhibit T cell activation during the whole activation process, it is not sufficient to consider point estimates of PD-1 and CTLA-4 concentration. Instead, we resort to considering the integrals of the concentration of these immune checkpoint proteins throughout the entire τ_8^{act} time that the CD8+ T cell takes to complete activation. This is because these integrals are proportional (with a proportionality constant of $1/\tau_8^{\text{act}}$) to the average concentration of these proteins throughout activation, allowing us to properly incorporate its inhibition by PD-1 and CTLA-4.

We now are interested in finding the concentration of effector CD8+ T cells over time. It is known

that activated CD8+ T cells undergo clonal expansion in the TDLN and differentiate before they stop proliferating and migrate to the TS [108, 109].

We assume that activated CD8+ T cells proliferate up to n_{\max}^8 times upon which they stop dividing. For simplicity, we assume that the death rate of CD8+ T cells that have not completed their division program is equal to $d_{T_0^8}$, the death rate of naive CD8+ T cells, regardless of the number of cell divisions previously undergone. We also assume that only activated CD8+ T cells that have undergone n_{\max}^8 divisions become effector CD8+ T cells which will leave the TDLN and migrate to the TS. Furthermore, we assume a constant cell cycle time Δ_8 , except for the first cell division which has cycle time Δ_8^0 . Thus, the duration of the activated CD8+ T cell division program to n_{\max}^8 divisions is given by

$$\tau_{T_A^8} = \Delta_8^0 + (n_{\max}^8 - 1)\Delta_8. \quad (2.11)$$

In particular, we must take into account that some T cells will die before the division program is complete, and so we must introduce a shrinkage factor of $e^{-d_{T_0^8}\tau_{T_A^8}}$. Furthermore, we must also take into account that the PD-1/PD-L1 complex and CTLA-4 inhibit CD8+ T cell proliferation throughout the program [23, 110]. We finally assume that the death rate of CD8+ T cells that have completed their division program is equal to the death rate of CD8+ T cells in the TS. Taking this all into account leads to

$$\frac{dT_A^8}{dt} = \frac{2^{n_{\max}^8} e^{-d_{T_0^8}\tau_{T_A^8}} R^8(t - \tau_{T_A^8})}{\underbrace{\left(1 + \int_{t-\tau_{T_A^8}}^t Q^{\text{LN}}(s) ds / K_{T_A^8 Q^{\text{LN}}}\right) \left(1 + \int_{t-\tau_{T_A^8}}^t P^{\text{LN}}(s) ds / K_{T_A^8 P^{\text{LN}}}\right)}_{\text{CD8+ T cell proliferation inhibited by } Q^{\text{LN}} \text{ and } P^{\text{LN}}}} - \underbrace{\lambda_{T_A^8 T_8} T_A^8}_{T_A^8 \text{ migration to TS}} - \underbrace{d_{T_8} T_A^8}_{\text{death}}. \quad (2.12)$$

One thing we must consider is that these CD8+ T cells must first migrate to the TS before they are able to attack and kill cancer cells. We denote $T_8(t)$ as the concentration of effector CD8+ T cells in the TS, and we assume that it takes τ_a amount of time for effector CD8+ T cells in the TDLN to migrate to the TS. We must also account for CTL expansion due to positive growth factors such as IL-2 [111], with this being inhibited by PD-1/PD-L1 complexes [112]. Furthermore, the death of CD8+ T cells is resisted by IL-10 [113, 114].

However, chronic antigen exposure can cause effector CD8+ T cells to enter a state of exhaustion, where they lose their ability to kill cancer cells, and the rate of cytokine secretion significantly decreases [57, 115, 116]. We denote this exhausted CD8+ T cell population as $T_{\text{ex}}(t)$. It has also been shown that pembrolizumab can “reinvigorate” these cells back into the effector state [29, 117]. We model the re-invigoration and exhaustion using Michaelis-Menten terms in A_1 and $\int_{t-\tau_l}^t C(s) ds$ respectively, where τ_l is the median time that CD8+ T cells take to become exhausted after entering the TS. In particular, this has been shown to be more appropriate than simple mass-action kinetics as it accounts for extended antigen exposure [118]. As before, we introduce a Heaviside function $\theta(t - \tau_l)$, as we assume that CD8+ T cells need to spend at least τ_l in the TS for them to be able to be exhausted.

As such, remembering to take the volume change between the TDLN and the TS into account, this

implies that

$$\begin{aligned} \frac{dT_8}{dt} = & \frac{V_{\text{LN}}}{V_{\text{TS}}} \underbrace{\lambda_{T_A^8 T_8} e^{-d_{T_8} \tau_a} T_A^8 (t - \tau_a) \theta(t - \tau_a)}_{T_A^8 \text{ migration to TS}} + \underbrace{\lambda_{T_8 I_2} \frac{T_8^{\text{TS}} I_2}{K_{T_8 I_2} + I_2}}_{\text{growth by } I_2} \underbrace{\frac{1}{1 + Q/K_{T_8 Q}}}_{\text{Inhibition by } Q} \\ & - \underbrace{\lambda_{T_8 C} \frac{T_8 \int_{t-\tau_l}^t C(s) ds}{K_{T_8 C} + \int_{t-\tau_l}^t C(s) ds}}_{T_8 \rightarrow T_{\text{ex}} \text{ from } C \text{ exposure}} \theta(t - \tau_l) + \underbrace{\lambda_{T_{\text{ex}} A_1} \frac{T_{\text{ex}} A_1}{K_{T_{\text{ex}} A_1} + A_1}}_{T_{\text{ex}} \rightarrow T_8 \text{ by } A_1} - \underbrace{\frac{d_{T_8} T_8}{1 + I_{10}/K_{T_8 I_{10}}}}_{\text{death inhibited by } I_{10}}, \end{aligned} \quad (2.13)$$

$$\frac{dT_{\text{ex}}}{dt} = \underbrace{\lambda_{T_8 C} \frac{T_8 \int_{t-\tau_l}^t C(s) ds}{K_{T_8 C} + \int_{t-\tau_l}^t C(s) ds}}_{T_8 \rightarrow T_{\text{ex}} \text{ from } C \text{ exposure}} \theta(t - \tau_l) - \underbrace{\lambda_{T_{\text{ex}} A_1} \frac{T_{\text{ex}} A_1}{K_{T_{\text{ex}} A_1} + A_1}}_{T_{\text{ex}} \rightarrow T_8 \text{ by } A_1} - \underbrace{\frac{d_{T_{\text{ex}}} T_{\text{ex}}}{1 + I_{10}/K_{T_{\text{ex}} I_{10}}}}_{\text{death inhibited by } I_{10}}. \quad (2.14)$$

We perform a similar process for CD4+ T helper cells and first consider naive CD4+ T cells in the TDLN. For simplicity, we consider only Th1 and Th2 subtypes that naive CD4+ T cells differentiate into upon activation, absorbing the influence of cytokines via the kinetic rate constants $\lambda_{T_0^4 T_A^1}$ and $\lambda_{T_0^4 T_A^2}$ respectively. Taking into account that PD-1 and CTLA-4 inhibit CD4+ T cell activation and some mature DCs migrate into the TDLN and activate naive CD4+ T cells, causing them to no longer be naive, and assuming that naive CD4+ T cells come into the TDLN at a rate $\mathcal{A}_{T_0^4}$, we can write a similar equation to (2.9):

$$\frac{dT_0^4}{dt} = \underbrace{\mathcal{A}_{T_0^4}}_{\text{source}} - \underbrace{(R^1(t) + R^2(t))}_{\text{CD4+ T cell activation}} - \underbrace{d_{T_0^4} T_0^4}_{\text{death}}, \quad (2.15)$$

where $R^i(t)$, for $i = 1, 2$, is defined as,

$$R^i(t) = \frac{\lambda_{T_0^4 T_A^i} e^{-d_{T_0^4} \tau_{\text{act}}^4} D^{\text{LN}}(t - \tau_{\text{act}}^4) T_0^4 (t - \tau_{\text{act}}^4) \theta(t - \tau_{\text{act}}^4)}{\underbrace{\left(1 + \int_{t-\tau_{\text{act}}^4}^t P_D^{\text{LN}}(s) ds / K_{T_0^4 P_D^{\text{LN}}}\right) \left(1 + \int_{t-\tau_{\text{act}}^4}^t P_A^{\text{LN}}(s) ds / K_{T_0^4 P_A^{\text{LN}}}\right)}_{T_A^i \text{ activation inhibited by } P_D^{\text{LN}} \text{ and } P_A^{\text{LN}}}}. \quad (2.16)$$

As before, we are interested in finding the concentration of effector Th1 and Th2 cells over time, and for simplicity, we only consider the differentiation of CD4+ T cells into Th1 cells and Th2 cells. We assume that Th1 cells and Th2 cells proliferate up to n_{max}^1 and n_{max}^2 times, respectively, upon which they stop dividing. As before, we assume that the death rate of Th1 and Th2 cells that have not completed their division program is equal to $d_{T_0^4}$, the death rate of naive CD4+ T cells, regardless of the number of cell divisions previously undergone or their phenotype. We assume a constant cell cycle time Δ_i , except for the first cell division which has cycle time Δ_i^0 . Thus, the duration of the activated CD4+ T cell division program to n_{max}^i divisions is given by

$$\tau_{T_A^i} = \Delta_i^0 + (n_{\text{max}}^i - 1) \Delta_i. \quad (2.17)$$

In particular, we must take into account that some T cells will die before the division program is complete, so we must introduce a shrinkage factor of $e^{-d_{T_0^4} \tau_{T_A^i}}$. Furthermore, we must also take into account that the PD-1/PD-L1 complex and CTLA-4 inhibit CD4+ T cell proliferation throughout the program [23, 110]. We finally assume that the death rate of CD4+ T cells that have completed their division program is equal to the corresponding degradation rate in the TS. Taking this all into

account, for $i = 1, 2$, leads to

$$\frac{dT_A^i}{dt} = \frac{2^{n_{\max}^i} e^{-d_{T_0^i} \tau_{T_A^i}} R^i(t - \tau_{T_A^i})}{\underbrace{\left(1 + \int_{t-\tau_{T_A^i}}^t Q^{\text{LN}}(s) ds / K_{T_A^i}^{\text{QLN}}\right) \left(1 + \int_{t-\tau_{T_A^i}}^t P_A^{\text{LN}}(s) ds / K_{T_A^i}^{\text{P}^{\text{LN}}}\right)}_{\text{CD4+ T cell proliferation inhibited by } Q^{\text{LN}} \text{ and } P_A^{\text{LN}}}} - \underbrace{\lambda_{T_A^i T_i} T_A^i}_{T_A^i \text{ migration to TS}} - \underbrace{d_{T_i} T_A^i}_{\text{death}}. \quad (2.18)$$

We also assume that it takes τ_a amount of time for these cells to migrate to the TS. We take into account the fact that IL-2 induces the growth of activated Th1 cells [119]; however, this is inhibited by PD-1/PD-L1. Hence,

$$\frac{dT_1}{dt} = \frac{V_{\text{LN}}}{V_{\text{TS}}} \underbrace{\lambda_{T_A^1 T_1} e^{-d_{T_1} \tau_a} T_A^1(t - \tau_a) \theta(t - \tau_a)}_{T_A^1 \text{ migration to TS}} + \underbrace{\lambda_{T_1 I_2} \frac{T_1 I_2}{K_{T_1 I_2} + I_2}}_{\text{growth by } I_2} \underbrace{\frac{1}{1 + Q/K_{T_1 Q}}}_{\text{Inhibition by } Q} - \underbrace{d_{T_1} T_1}_{\text{death}}, \quad (2.19)$$

$$\frac{dT_2}{dt} = \frac{V_{\text{LN}}}{V_{\text{TS}}} \underbrace{\lambda_{T_A^2 T_2} e^{-d_{T_2} \tau_a} T_A^2(t - \tau_a) \theta(t - \tau_a)}_{T_A^2 \text{ migration to TS}} - \underbrace{d_{T_2} T_2}_{\text{death}}. \quad (2.20)$$

Finally, we consider the concentration of Tregs in the TDLN, following the same procedure as for CD8+ T cells and CD4+ T helper cells. We absorb the influence of cytokines on Treg activation via the kinetic rate constant $\lambda_{T_0^r T_A^r}$. We also take into account that PD-1 and CTLA-4 inhibit Treg activation and some mature DCs migrate into the TDLN and activate naive Tregs, causing them to no longer be naive. Assuming that naive Tregs come into the TDLN at a rate $\mathcal{A}_{T_0^r}$, we can write a similar equation to (2.9) and (2.15):

$$\frac{dT_0^r}{dt} = \underbrace{\mathcal{A}_{T_0^r}}_{\text{source}} - \underbrace{R^r(t)}_{\text{Treg activation}} - \underbrace{d_{T_0^r} T_0^r}_{\text{death}}, \quad (2.21)$$

where

$$R^r(t) = \frac{\lambda_{T_0^r T_A^r} e^{-d_{T_0^r} \tau_{\text{act}}^r} D^{\text{LN}}(t - \tau_{\text{act}}^r) T_0^r(t - \tau_{\text{act}}^r) \theta(t - \tau_{\text{act}}^r)}{\underbrace{\left(1 + \int_{t-\tau_{\text{act}}^r}^t P_D^{\text{LN}}(s) ds / K_{T_0^r}^{\text{P}^{\text{LN}}}\right) \left(1 + \int_{t-\tau_{\text{act}}^r}^t P_A^{\text{LN}}(s) ds / K_{T_0^r}^{\text{P}^{\text{LN}}}\right)}_{T_A^r \text{ activation inhibited by } P_D^{\text{LN}} \text{ and } P_A^{\text{LN}}}}. \quad (2.22)$$

We assume that activated Tregs proliferate up to n_{\max}^r , times upon which they stop dividing, and become effector Tregs. As before, we assume that the death rate of Tregs that have not completed their division program is equal to $d_{T_0^r}$, the death rate of naive Tregs. We assume a constant cell cycle time Δ_r , except for the first cell division which has cycle time Δ_r^0 . Thus, the duration of the activated Treg division program to n_{\max}^r divisions is given by

$$\tau_{T_A^r} = \Delta_r^0 + (n_{\max}^r - 1) \Delta_r. \quad (2.23)$$

In particular, we must take into account that some T cells will die before the division program is complete, so we must introduce a shrinkage factor of $e^{-d_{T_0^r} \tau_{T_A^r}}$. Furthermore, we must also take into account that the PD-1/PD-L1 complex and CTLA-4 inhibit Treg proliferation throughout the program [110, 120]. We finally assume that the death rate of effector Tregs in the TDLN is equal to the

corresponding degradation rate in the TS. Taking this all into account leads to

$$\frac{dT_A^r}{dt} = \underbrace{\frac{2^{n_{\max}^r} e^{-d_{T_0^r} \tau_{T_A^r}} R^r(t - \tau_{T_A^r})}{\left(1 + \int_{t-\tau_{T_A^r}}^t Q^{\text{LN}}(s) ds / K_{T_A^r Q^{\text{LN}}}\right) \left(1 + \int_{t-\tau_{T_A^r}}^t P^{\text{LN}}(s) ds / K_{T_A^r P^{\text{LN}}}\right)}}_{\text{Treg proliferation inhibited by } Q^{\text{LN}} \text{ and } P^{\text{LN}}_A} - \underbrace{\frac{\lambda_{T_A^r T_r} T_A^r}{T_A^r}}_{\text{migration to TS}} - \underbrace{d_{T_r} T_A^r}_{\text{death}}. \quad (2.24)$$

Assuming that it also takes τ_a amount of time for Tregs to migrate to the TS, we have that

$$\frac{dT_r}{dt} = \frac{V_{\text{LN}}}{V_{\text{TS}}} \underbrace{\lambda_{T_A^r T_r} e^{-d_{T_r} \tau_a} T_A^r(t - \tau_a) \theta(t - \tau_a)}_{T_A^r \text{ migration to TS}} - \underbrace{d_{T_r} T_r}_{\text{death}}. \quad (2.25)$$

We assume that CAFs grow logistically for the same reason as cancer cells. We take into account the growth rate of CAFs, their induced growth due to fibrotic signalling via TGF- β [121] and their induced growth by inflammatory signalling via IL-1 β [122, 123]. In particular, we note that their effects are saturation-limited and need to be incorporated via Michaelis-Menten kinetics. Hence,

$$\frac{dC_F}{dt} = \left(\underbrace{\lambda_{C_F}}_{\text{growth}} + \underbrace{\lambda_{C_F I_\beta} \frac{I_\beta}{K_{C_F I_\beta} + I_\beta}}_{I_\beta\text{-induced growth}} + \underbrace{\lambda_{C_F I_{1\beta}} \frac{I_{1\beta}}{K_{C_F I_{1\beta}} + I_{1\beta}}}_{I_{1\beta}\text{-induced growth}} \right) \underbrace{C_F \left(1 - \frac{C_F}{C_{F0}}\right)}_{\text{growth}} - \underbrace{d_{C_F} C_F}_{\text{death}}. \quad (2.26)$$

Naive neutrophils are polarised to N1 neutrophils under the influence of IL-1 β [124] and IFN- γ [125], whilst N0 neutrophils are polarised to the N2 phenotype by IL-6 [126], and TGF- β [81]. Assuming a production rate \mathcal{A}_{N_0} of naive neutrophils, we have that

$$\begin{aligned} \frac{dN_0}{dt} = & \underbrace{\mathcal{A}_{N_0}}_{\text{source}} - \underbrace{\lambda_{N_1 I_{1\beta}} N_0 \frac{I_{1\beta}}{K_{N_1 I_{1\beta}} + I_{1\beta}}}_{N_0 \rightarrow N_1 \text{ by } I_{1\beta}} - \underbrace{\lambda_{N_1 I_\gamma} N_0 \frac{I_\gamma}{K_{N_1 I_\gamma} + I_\gamma}}_{N_0 \rightarrow N_1 \text{ by } I_\gamma} - \underbrace{\lambda_{N_2 I_6} N_0 \frac{I_6}{K_{N_2 I_6} + I_6}}_{N_0 \rightarrow N_2 \text{ by } I_6} \\ & - \underbrace{\lambda_{N_2 I_\beta} N_0 \frac{I_\beta}{K_{N_2 I_\beta} + I_\beta}}_{N_0 \rightarrow N_2 \text{ by } I_\beta} - \underbrace{d_{N_0} N_0}_{\text{death}}, \end{aligned} \quad (2.27)$$

$$\frac{dN_1}{dt} = \underbrace{\lambda_{N_1 I_{1\beta}} N_0 \frac{I_{1\beta}}{K_{N_1 I_{1\beta}} + I_{1\beta}}}_{N_0 \rightarrow N_1 \text{ by } I_{1\beta}} + \underbrace{\lambda_{N_1 I_\gamma} N_0 \frac{I_\gamma}{K_{N_1 I_\gamma} + I_\gamma}}_{N_0 \rightarrow N_1 \text{ by } I_\gamma} - \underbrace{d_{N_1} N_1}_{\text{death}}, \quad (2.28)$$

$$\frac{dN_2}{dt} = \underbrace{\lambda_{N_2 I_6} N_0 \frac{I_6}{K_{N_2 I_6} + I_6}}_{N_0 \rightarrow N_2 \text{ by } I_6} + \underbrace{\lambda_{N_2 I_\beta} N_0 \frac{I_\beta}{K_{N_2 I_\beta} + I_\beta}}_{N_0 \rightarrow N_2 \text{ by } I_\beta} - \underbrace{d_{N_2} N_2}_{\text{death}}. \quad (2.29)$$

TNF and IFN- γ polarise naive macrophages into M1 macrophages [127–130], whilst IL-4, IL-10 and PD-L1 polarise naive macrophages into the M2 phenotype [131–135]. In addition, TGF- β and IL-6 induce M1 macrophages to convert into M2 macrophages [136–138]. Furthermore, M2 macrophages change phenotype to M1 under the influence of IL-12 [139] and TNF [127] whilst IFN- γ induces M2 to M1 phenotype change [140]. Assuming a production rate \mathcal{A}_{M_0} of naive macrophages, we thus have

that

$$\begin{aligned} \frac{dM_0}{dt} = & \underbrace{\mathcal{A}_{M_0}}_{\text{source}} - \underbrace{\lambda_{M_1 I_\alpha} M_0 \frac{I_\alpha}{K_{M_1 I_\alpha} + I_\alpha}}_{M_0 \rightarrow M_1 \text{ by } I_\alpha} - \underbrace{\lambda_{M_1 I_\gamma} M_0 \frac{I_\gamma}{K_{M_1 I_\gamma} + I_\gamma}}_{M_0 \rightarrow M_1 \text{ by } I_\gamma} - \underbrace{\lambda_{M_2 I_4} M_0 \frac{I_4}{K_{M_2 I_4} + I_4}}_{M_0 \rightarrow M_2 \text{ by } I_4} \\ & - \underbrace{\lambda_{M_2 I_{10}} M_0 \frac{I_{10}}{K_{M_2 I_{10}} + I_{10}}}_{M_0 \rightarrow M_2 \text{ by } I_{10}} - \underbrace{\lambda_{M_2 P_L} M_0 \frac{P_L}{K_{M_2 P_L} + P_L}}_{M_0 \rightarrow M_2 \text{ by } P_L} - \underbrace{d_{M_0} M_0}_{\text{degradation}}, \end{aligned} \quad (2.30)$$

$$\begin{aligned} \frac{dM_1}{dt} = & \underbrace{\lambda_{M_1 I_\alpha} M_0 \frac{I_\alpha}{K_{M_1 I_\alpha} + I_\alpha}}_{M_0 \rightarrow M_1 \text{ by } I_\alpha} + \underbrace{\lambda_{M_1 I_\gamma} M_0 \frac{I_\gamma}{K_{M_1 I_\gamma} + I_\gamma}}_{M_0 \rightarrow M_1 \text{ by } I_\gamma} + \underbrace{\lambda_{M I_{12}} M_2 \frac{I_{12}}{K_{M I_{12}} + I_{12}}}_{M_2 \rightarrow M_1 \text{ by } I_{12}} + \underbrace{\lambda_{M I_\gamma} M_2 \frac{I_\gamma}{K_{M I_\gamma} + I_\gamma}}_{M_2 \rightarrow M_1 \text{ by } I_\gamma} \\ & + \underbrace{\lambda_{M I_\alpha} M_2 \frac{I_\alpha}{K_{M I_\alpha} + I_\alpha}}_{M_2 \rightarrow M_1 \text{ by } I_\alpha} - \underbrace{\lambda_{M I_\beta} M_1 \frac{I_\beta}{K_{M I_\beta} + I_\beta}}_{M_1 \rightarrow M_2 \text{ by } I_\beta} - \underbrace{\lambda_{M I_6} M_1 \frac{I_6}{K_{M I_6} + I_6}}_{M_1 \rightarrow M_2 \text{ by } I_6} - \underbrace{d_{M_1} M_1}_{\text{degradation}}, \end{aligned} \quad (2.31)$$

$$\begin{aligned} \frac{dM_2}{dt} = & \underbrace{\lambda_{M_2 I_4} M_0 \frac{I_4}{K_{M_2 I_4} + I_4}}_{M_0 \rightarrow M_2 \text{ by } I_4} + \underbrace{\lambda_{M_2 I_{10}} M_0 \frac{I_{10}}{K_{M_2 I_{10}} + I_{10}}}_{M_0 \rightarrow M_2 \text{ by } I_{10}} + \underbrace{\lambda_{M_2 P_L} M_0 \frac{P_L}{K_{M_2 P_L} + P_L}}_{M_0 \rightarrow M_2 \text{ by } P_L} - \underbrace{\lambda_{M I_{12}} M_2 \frac{I_{12}}{K_{M I_{12}} + I_{12}}}_{M_2 \rightarrow M_1 \text{ by } I_{12}} \\ & - \underbrace{\lambda_{M I_\gamma} M_2 \frac{I_\gamma}{K_{M I_\gamma} + I_\gamma}}_{M_2 \rightarrow M_1 \text{ by } I_\gamma} - \underbrace{\lambda_{M I_\alpha} M_2 \frac{I_\alpha}{K_{M I_\alpha} + I_\alpha}}_{M_2 \rightarrow M_1 \text{ by } I_\alpha} + \underbrace{\lambda_{M I_\beta} M_1 \frac{I_\beta}{K_{M I_\beta} + I_\beta}}_{M_1 \rightarrow M_2 \text{ by } I_\beta} + \underbrace{\lambda_{M I_6} M_1 \frac{I_6}{K_{M I_6} + I_6}}_{M_1 \rightarrow M_2 \text{ by } I_6} \\ & - \underbrace{d_{M_2} M_2}_{\text{degradation}}. \end{aligned} \quad (2.32)$$

Naive NK cells are activated by IL-2 and IL-12 [141, 142]. In addition, immature and mature DCs activate NK cells [143]. Thus, assuming a supply rate \mathcal{A}_{K_0} of naive NK cells, we have that

$$\begin{aligned} \frac{dK_0}{dt} = & \underbrace{\mathcal{A}_{K_0}}_{\text{source}} - \underbrace{\lambda_{K I_2} K_0 \frac{I_2}{K_{K I_2} + I_2}}_{K_0 \rightarrow K \text{ by } I_2} - \underbrace{\lambda_{K I_{12}} K_0 \frac{I_{12}}{K_{K I_{12}} + I_{12}}}_{K_0 \rightarrow K \text{ by } I_{12}} - \underbrace{\lambda_{K D_0} K_0 \frac{D_0}{K_{K D_0} + D_0}}_{K_0 \rightarrow K \text{ by } D_0} - \underbrace{\lambda_{K D} K_0 \frac{D}{K_{K D} + D}}_{K_0 \rightarrow K \text{ by } D} \\ & - \underbrace{d_{K_0} K_0}_{\text{degradation}}, \end{aligned} \quad (2.33)$$

$$\begin{aligned} \frac{dK}{dt} = & \underbrace{\lambda_{K I_2} K_0 \frac{I_2}{K_{K I_2} + I_2}}_{K_0 \rightarrow K \text{ by } I_2} + \underbrace{\lambda_{K I_{12}} K_0 \frac{I_{12}}{K_{K I_{12}} + I_{12}}}_{K_0 \rightarrow K \text{ by } I_{12}} + \underbrace{\lambda_{K D_0} K_0 \frac{D_0}{K_{K D_0} + D_0}}_{K_0 \rightarrow K \text{ by } D_0} + \underbrace{\lambda_{K D} K_0 \frac{D}{K_{K D} + D}}_{K_0 \rightarrow K \text{ by } D} - \underbrace{d_K K}_{\text{degradation}}. \end{aligned} \quad (2.34)$$

IL-2 is produced by CD8+ T cells [144, 145] and Th1 cells [146], so that

$$\frac{dI_2}{dt} = \underbrace{\lambda_{I_2 T_8} T_8}_{\text{production by } T_8} + \underbrace{\lambda_{I_2 T_1} T_1}_{\text{production by } T_1} - \underbrace{d_{I_2} I_2}_{\text{degradation}}. \quad (2.35)$$

IFN- γ is produced by CD8+ T cells [147] and Th1 cells [93, 148], with both expressions being inhibited by Tregs [149]. Activated NK cells also produce IFN- γ [150]; however, this is inhibited by CTLA-4 [151]. Thus,

$$\frac{dI_\gamma}{dt} = \left(\underbrace{\lambda_{I_\gamma T_8} T_8}_{\text{production by } T_8} + \underbrace{\lambda_{I_\gamma T_1} T_1}_{\text{production by } T_1} \right) \underbrace{\frac{1}{1 + T_r/K_{I_\gamma T_r}}}_{\text{inhibition by } T_r} + \underbrace{\lambda_{I_\gamma K} \frac{K}{1 + P_A/K_{I_\gamma P_A}}}_{\substack{\text{production by } K \\ \text{inhibition by } P_A}} - \underbrace{d_{I_\gamma} I_\gamma}_{\text{degradation}} . \quad (2.36)$$

TNF is produced by CD8+ T cells [67, 152], Th1 cells [153, 154], M1 macrophages [155], N1 neutrophils [82], and activated NK cells [156, 157]. Hence,

$$\frac{dI_\alpha}{dt} = \underbrace{\lambda_{I_\alpha T_8} T_8}_{\text{production by } T_8} + \underbrace{\lambda_{I_\alpha T_1} T_1}_{\text{production by } T_1} + \underbrace{\lambda_{I_\alpha M_1} M_1}_{\text{production by } M_1} + \underbrace{\lambda_{I_\alpha N_1} N_1}_{\text{production by } N_1} + \underbrace{\lambda_{I_\alpha K} K}_{\text{production by } K} - \underbrace{d_{I_\alpha} I_\alpha}_{\text{degradation}} . \quad (2.37)$$

TGF- β is produced by cancer cells [158], Tregs [159] and CAFs [123]. Thus,

$$\frac{dI_\beta}{dt} = \underbrace{\lambda_{I_\beta C} C}_{\text{production by } C} + \underbrace{\lambda_{I_\beta T_r} T_r}_{\text{production by } T_r} + \underbrace{\lambda_{I_\beta C_F} C_F}_{\text{production by } C_F} - \underbrace{d_{I_\beta} I_\beta}_{\text{degradation}} . \quad (2.38)$$

IL-12 is produced by N1 neutrophils [82, 160] and M1 macrophages with IL-10 suppressing this expression of IL-12 [161–163]. Additionally, mature DCs also produce IL-12; however, extracellular ATP has been shown to inhibit this production [164]. Taking all of these factors into account, we have

$$\frac{dI_{12}}{dt} = \underbrace{\lambda_{I_{12} D} \frac{D}{1 + A/K_{I_{12} A}}}_{\substack{\text{production by } D \\ \text{inhibited by } A}} + \underbrace{\lambda_{I_{12} N_1} N_1}_{\text{production by } N_1} + \underbrace{\lambda_{I_{12} M_1} \frac{M_1}{1 + I_{10}/K_{I_{12} I_{10}}}}_{\substack{\text{production by } M_1 \\ \text{inhibited by } I_{10}}} - \underbrace{d_{I_{12}} I_{12}}_{\text{degradation}} . \quad (2.39)$$

IL-10 is produced by cancer cells [165, 166], Th2 cells [167, 168], and M2 macrophages [169, 170]. Additionally, Tregs secrete IL-10 [171] with IL-2 enhancing this production [172]. In particular, IL-2 binds to its cognate receptors and is rapidly internalised [173] which we account for using Michaelis-Menten kinetics. Hence,

$$\frac{dI_{10}}{dt} = \underbrace{\lambda_{I_{10} C} C}_{\text{production by } C} + \underbrace{\lambda_{I_{10} T_2} T_2}_{\text{production by } T_2} + \underbrace{\lambda_{I_{10} M_2} M_2}_{\text{production by } M_2} + \underbrace{\lambda_{I_{10} T_r} T_r \left(1 + \lambda_{I_{10} I_2} \frac{I_2}{K_{I_{10} I_2} + I_2} \right)}_{\substack{\text{production by } T_r \\ \text{enhanced by } I_2}} - \underbrace{d_{I_{10}} I_{10}}_{\text{degradation}} . \quad (2.40)$$

IL-4 is produced by Th2 cells [174] so

$$\frac{dI_4}{dt} = \underbrace{\lambda_{I_4 T_2} T_2}_{\text{production by } T_2} - \underbrace{d_{I_4} I_4}_{\text{Degradation}} . \quad (2.41)$$

IL-6 is produced by mature DCs [175] and CAFs [176]. As such,

$$\frac{dI_6}{dt} = \underbrace{\lambda_{I_6 D} D}_{\text{production by } D} + \underbrace{\lambda_{I_6 C_F} C_F}_{\text{production by } C_F} - \underbrace{d_{I_6} I_6}_{\text{degradation}}. \quad (2.42)$$

IL-1 β is produced by mature DCs [179, 180], N1 neutrophils [177], and M1 macrophages [178]. Thus,

$$\frac{dI_{1\beta}}{dt} = \underbrace{\lambda_{I_{1\beta} D} D}_{\text{production by } D} + \underbrace{\lambda_{I_{1\beta} N_1} N_1}_{\text{production by } N_1} + \underbrace{\lambda_{I_{1\beta} M_1} M_1}_{\text{production by } M_1} - \underbrace{d_{I_{1\beta}} I_{1\beta}}_{\text{degradation}}. \quad (2.43)$$

It is known that PD-1 is expressed on the surface of effector and exhausted CD8+ T cells [181–183], effector Th1 cells [184], effector Tregs [185], and M2 macrophages [186, 187]. In the case where no pembrolizumab is administered, we assume that PD-1 expression is proportional to the density of the cell expressing it. For example the total number of PD-1 molecules expressed by Th1 cells in the TS is $\rho_{P_D^1} T_1$ for some constant $\rho_{P_D^1}$. If no pembrolizumab is present, then P_D simply follows

$$P_D = \rho_{P_D^8} T_8 + \rho_{P_D^{\text{ex}}} T_{\text{ex}} + \rho_{P_D^1} T_1 + \rho_{P_D^r} T_r + \rho_{P_D^{M2}} M_2. \quad (2.44)$$

However, when pembrolizumab is injected, PD-1 on these PD-1-expressing cells can bind to the pembrolizumab drug, causing their depletion [27] and in turn changing the number of PD-1 molecules expressed on each cell. We assume, however, that the ratio of the number of PD-1 molecules expressed on each cell stays invariant. We must finally take into account acquired resistance to pembrolizumab [188–190]. We incorporate resistance by considering an accumulation penalty for PD-1-pembrolizumab in the form of an inhibition term in $\int_0^t A_1(s) ds$. Properly accounting for depletion and resistance, and denoting $d_{P_D A_1}$ as the rate at which PD-1 binds to pembrolizumab, leads to

$$\frac{dP_D}{dt} = P_D \frac{\left(\rho_{P_D^8} \frac{dT_8}{dt} + \rho_{P_D^{\text{ex}}} \frac{dT_{\text{ex}}}{dt} + \rho_{P_D^1} \frac{dT_1}{dt} + \rho_{P_D^r} \frac{dT_r}{dt} + \rho_{P_D^{M2}} \frac{dM_2}{dt} \right)}{\underbrace{\rho_{P_D^8} T_8 + \rho_{P_D^{\text{ex}}} T_{\text{ex}} + \rho_{P_D^1} T_1 + \rho_{P_D^r} T_r + \rho_{P_D^{M2}} M_2}_{\text{surface expression}}} - \frac{d_{P_D A_1} P_D A_1}{\underbrace{1 + \int_0^t A_1(s) ds / K_{P_D A_1}}_{\text{depletion inhibited by } A_1}}. \quad (2.45)$$

A derivation of (2.45) can be found in Appendix A. For simplicity, we assume that only activated T cells that have undergone their maximum possible divisions express PD-1 on their surface, and that the number of PD-1 molecules on T cells in the TDLN is the same as for those in the TS. Accounting for depletion and resistance as in (2.45), we have that

$$\frac{dP_D^{\text{LN}}}{dt} = P_D^{\text{LN}} \frac{\left(\rho_{P_D^8} \frac{dT_A^8}{dt} + \rho_{P_D^1} \frac{dT_A^1}{dt} + \rho_{P_D^r} \frac{dT_A^r}{dt} \right)}{\underbrace{\rho_{P_D^8} T_A^8 + \rho_{P_D^1} T_A^1 + \rho_{P_D^r} T_A^r}_{\text{surface expression}}} - \frac{d_{P_D^{\text{LN}} A_1^{\text{LN}}} P_D^{\text{LN}} A_1^{\text{LN}}}{\underbrace{1 + \int_0^t A_1^{\text{LN}}(s) ds / K_{P_D^{\text{LN}} A_1^{\text{LN}}}}_{\text{depletion inhibited by } A_1^{\text{LN}}}}. \quad (2.46)$$

We also know that PD-L1 is expressed on the surface of cancer cells [191], DCs [192], effector CD8+ T cells [193, 194], effector Th1 cells [195], effector Tregs [185], CAFs [196–198], M2 macrophages [199], and N1 and N2 neutrophils [200, 201]. The equation for P_L has a similar form to (2.45), except there is no anti-PD-L1 present, so that

$$P_L = \underbrace{\rho_{P_L^C} C + \rho_{P_L^D} D + \rho_{P_L^8} T_8 + \rho_{P_L^1} T_1 + \rho_{P_L^r} T_r + \rho_{P_L^{C_F}} C_F + \rho_{P_L^{M2}} M_2 + \rho_{P_L^{N1}} N_1 + \rho_{P_L^{N2}} N_2}_{\text{surface expression}}. \quad (2.47)$$

For simplicity, we do not consider PD-L1 on DCs in the TDLN, so that

$$P_L^{\text{LN}} = \underbrace{\rho_{P_L^s} T_A^s + \rho_{P_L^1} T_A^1 + \rho_{P_L^r} T_A^r}_{\text{surface expression}}. \quad (2.48)$$

PD-L1 binds to PD-1 on the surfaces of effector and exhausted CD8+ cells, effector Th1 cells, effector Tregs and M2 macrophages forming the PD-1/PD-L1 complex [202]. This formation is a reversible chemical process, with association occurring at a rate of $\alpha_{P_D P_L}$ and dissociation occurring at a rate of d_Q , so that the reaction can be expressed as $P_D + P_L \xrightleftharpoons[d_Q]{\alpha_{P_D P_L}} Q$. Hence,

$$\frac{dQ}{dt} = \underbrace{\alpha_{P_D P_L} P_D P_L}_{\text{formation}} - \underbrace{d_Q Q}_{\text{dissociation}}. \quad (2.49)$$

Since the half-life of Q is very small, being less than 1 second ($\approx 1.16 \times 10^{-5}$ days) [203], we employ a quasi-steady state approximation for Q , so that $\frac{dQ}{dt} = 0 \implies \alpha_{P_D P_L} P_D P_L - d_Q Q$, or equivalently

$$Q = \frac{\alpha_{P_D P_L}}{d_Q} P_D P_L, \quad (2.50)$$

and similarly,

$$Q^{\text{LN}} = \frac{\alpha_{P_D P_L}}{d_Q} P_D^{\text{LN}} P_L^{\text{LN}}. \quad (2.51)$$

We assume that pembrolizumab is injected intravenously at times t_1, t_2, \dots, t_n with doses $\gamma_1, \gamma_2, \dots, \gamma_n$ respectively. Accounting for depletion due to blocking PD-1, the systemic nature of pembrolizumab distribution, and assuming that the duration of infusion is negligible in comparison to the time period of interest, we have that

$$\frac{dA_1}{dt} = \underbrace{\sum_{j=1}^n \gamma_j \delta(t - t_j)}_{\text{infusion}} - \underbrace{\frac{d_{P_D A_1} P_D A_1}{1 + \int_0^t A_1(s) ds / K_{P_D A_1}}}_{\text{depletion due to blocking PD-1 inhibited by } A_1} - \underbrace{d_{A_1} A_1}_{\text{degradation}}, \quad (2.52)$$

and

$$\frac{dA_1^{\text{LN}}}{dt} = \underbrace{\sum_{j=1}^n \gamma_j \delta(t - t_j)}_{\text{infusion}} - \underbrace{\frac{d_{P_D^{\text{LN}} A_1^{\text{LN}}} P_D^{\text{LN}} A_1^{\text{LN}}}{1 + \int_0^t A_1^{\text{LN}}(s) ds / K_{P_D^{\text{LN}} A_1^{\text{LN}}}}}_{\text{depletion due to blocking PD-1 inhibited by } A_1^{\text{LN}}} - \underbrace{d_{A_1} A_1^{\text{LN}}}_{\text{degradation}}. \quad (2.53)$$

We now consider CTLA-4. We know that CTLA-4 is expressed on the surface of effector and exhausted CD8+ T cells [204, 205], effector Th1 cells and Th2 cells [206], and effector Tregs [207, 208]. However, it was found in [206] that the surface expression of CTLA-4 by Th1 cells is almost undetectable, whereas Th2 cell CTLA-4 surface expression was easily detected. Thus, we do not consider CTLA-4 expression by Th1 cells. The equations for CTLA-4 are identical in structure to those for PD-L1, so that

$$P_A = \underbrace{\rho_{P_A^s} T_8 + \rho_{P_A^{\text{ex}}} T_{\text{ex}} + \rho_{P_A^2} T_2 + \rho_{P_A^r} T_r}_{\text{surface expression}}. \quad (2.54)$$

For simplicity, we also assume that only activated T cells that have undergone their maximum possible divisions express CTLA-4 on their surface, and that the number of CTLA-4 molecules on T cells in the TDLN is the same as for those in the TS, so that

$$\frac{dP_A^{\text{LN}}}{dt} = \underbrace{\rho_{P_A^8} T_A^8 + \rho_{P_A^2} T_A^2 + \rho_{P_A^r} T_A^r}_{\text{surface expression}}. \quad (2.55)$$

2.4 Model Parameters

The model parameter values are estimated in [Appendix C](#) and are listed in [Table 2](#).

Table 2: Parameter values for the model. TDLN denotes the tumour-draining lymph node, whilst TS denotes the tumour site. est. denotes estimated parameters.

Parameter	Description	Value	Unit	References
\mathcal{A}_{D_0}	Source of D_0	1.20×10^6	$(\text{cell}/\text{cm}^3) \text{ day}^{-1}$	est.
$\mathcal{A}_{T_0^8}$	Source of T_0^8	3.72×10^5	$(\text{cell}/\text{cm}^3) \text{ day}^{-1}$	est.
$\mathcal{A}_{T_0^4}$	Source of T_0^4	2.75×10^5	$(\text{cell}/\text{cm}^3) \text{ day}^{-1}$	est.
$\mathcal{A}_{T_0^r}$	Source of T_0^r	2.36×10^5	$(\text{cell}/\text{cm}^3) \text{ day}^{-1}$	est.
\mathcal{A}_{N_0}	Source of N_0	4.38×10^6	$(\text{cell}/\text{cm}^3) \text{ day}^{-1}$	est.
\mathcal{A}_{M_0}	Source of M_0	8.75×10^5	$(\text{cell}/\text{cm}^3) \text{ day}^{-1}$	est.
\mathcal{A}_{K_0}	Source of K_0	3.82×10^5	$(\text{cell}/\text{cm}^3) \text{ day}^{-1}$	est.
λ_C	Growth rate of C	6.27×10^{-1}	day^{-1}	est.
λ_{CT_8}	Elimination rate of C by T_8	5.22×10^{-7}	$(\text{cell}/\text{cm}^3)^{-1} \text{ day}^{-1}$	est.
λ_{CT_1}	Elimination rate of C by T_1	1.63×10^{-8}	$(\text{cell}/\text{cm}^3)^{-1} \text{ day}^{-1}$	est.
λ_{CK}	Elimination rate of C by K	5.22×10^{-7}	$(\text{cell}/\text{cm}^3)^{-1} \text{ day}^{-1}$	est.
λ_{CI_α}	Elimination rate of C by I_α	4.69×10^{-2}	day^{-1}	est.
λ_{CI_γ}	Elimination rate of C by I_γ	9.38×10^{-3}	day^{-1}	est.
λ_{HN_c}	Production rate of H by N_c	1.57×10^{-14}	$(\text{g}/\text{cell}) \text{ day}^{-1}$	est.
λ_{HC_F}	Production rate of H by C_F	1.74×10^{-15}	$(\text{g}/\text{cell}) \text{ day}^{-1}$	est.
λ_{AN_c}	Production rate of A by N_c	1.93×10^{-8}	$(\text{g}/\text{cell}) \text{ day}^{-1}$	est.
λ_{SN_c}	Production rate of S by N_c	1.70×10^{-14}	$(\text{g}/\text{cell}) \text{ day}^{-1}$	est.
λ_{DH}	Maturation rate of D_0 by H	2.04×10^{-1}	day^{-1}	est.
λ_{DA}	Maturation rate of D_0 by A	4.07×10^{-2}	day^{-1}	est.
λ_{DS}	Maturation rate of D_0 by S	2.04×10^{-2}	day^{-1}	est.
λ_{D_0K}	Killing rate of D_0 by K	1.32×10^{-7}	$(\text{cell}/\text{cm}^3)^{-1} \text{ day}^{-1}$	est.
$\lambda_{DD^{\text{LN}}}$	Migration rate of D to TDLN	1.71×10^{-2}	day^{-1}	est.
$\lambda_{T_0^8 T_A^8}$	Kinetic rate constant for T_0^8 activation	8.64×10^{-11}	$(\text{cell}/\text{cm}^3)^{-1}$	est.
$\lambda_{T_A^8 T_8}$	Kinetic rate constant for T_A^8 migration to TS	3.42×10^{-1}	day^{-1}	est.
$\lambda_{T_8 I_2}$	Growth rate of T_8 by I_2	1.62×10^{-3}	day^{-1}	est.
$\lambda_{T_8 C}$	Exhaustion rate of T_8 due to C exposure	7.16×10^{-3}	day^{-1}	est.
$\lambda_{T_{\text{ex}} A_1}$	Reinvigoration rate of T_{ex} by A_1	2.25×10^{-3}	day^{-1}	est.

$\lambda_{T_0^4 T_A^1}$	Kinetic rate constant for T_0^4 activation into T_A^1	2.06×10^{-10}	$(\text{cell}/\text{cm}^3)^{-1}$	est.
$\lambda_{T_0^4 T_A^2}$	Kinetic rate constant for T_0^4 activation into T_A^2	3.48×10^{-10}	$(\text{cell}/\text{cm}^3)^{-1}$	est.
$\lambda_{T_A^1 T_1}$	Kinetic rate constant for T_A^1 migration to TS	4.22×10^{-2}	day^{-1}	est.
$\lambda_{T_A^2 T_2}$	Kinetic rate constant for T_A^2 migration to TS	1.86×10^{-2}	day^{-1}	est.
$\lambda_{T_1 I_2}$	Growth rate of T_1 by I_2	1.60×10^{-3}	day^{-1}	est.
$\lambda_{T_0^r T_A^r}$	Kinetic rate constant for T_0^r activation into T_A^r	1.07×10^{-7}	$(\text{cell}/\text{cm}^3)^{-1}$	est.
$\lambda_{T_A^r T_r}$	Kinetic rate constant for T_A^r migration to TS	7.13×10^{-1}	day^{-1}	est.
λ_{C_F}	Growth rate of C_F	6.93×10^{-1}	day^{-1}	[209]
$\lambda_{C_F I_\beta}$	Growth rate of C_F by I_β	7.89×10^{-1}	day^{-1}	est.
$\lambda_{C_F I_{1\beta}}$	Growth rate of C_F by $I_{1\beta}$	1.97×10^{-1}	day^{-1}	est.
$\lambda_{N_1 I_{1\beta}}$	Polarisation rate of N_0 into N_1 by $I_{1\beta}$	1.72	day^{-1}	est.
$\lambda_{N_1 I_\gamma}$	Polarisation rate of N_0 into N_1 by I_γ	2.04	day^{-1}	est.
$\lambda_{N_2 I_6}$	Polarisation rate of N_0 into N_2 by I_6	4.06	day^{-1}	est.
$\lambda_{N_2 I_\beta}$	Polarisation rate of N_0 into N_2 by I_β	3.46	day^{-1}	est.
$\lambda_{M_1 I_\alpha}$	Polarisation rate of M_0 into M_1 by I_α	2.71×10^{-1}	day^{-1}	est.
$\lambda_{M_1 I_\gamma}$	Polarisation rate of M_0 into M_1 by I_γ	3.15×10^{-1}	day^{-1}	est.
$\lambda_{M_2 I_4}$	Polarisation rate of M_0 into M_2 by I_4	1.86×10^{-1}	day^{-1}	est.
$\lambda_{M_2 I_{10}}$	Polarisation rate of M_0 into M_2 by I_{10}	1.71×10^{-1}	day^{-1}	est.
$\lambda_{M_2 P_L}$	Polarisation rate of M_0 into M_2 by P_L	2.36	day^{-1}	est.
$\lambda_{M I_{12}}$	Polarisation rate of M_2 into M_1 by I_{12}	2.65×10^{-2}	day^{-1}	est.
$\lambda_{M I_\gamma}$	Polarisation rate of M_2 into M_1 by I_γ	1.59×10^{-1}	day^{-1}	est.
$\lambda_{M I_\alpha}$	Polarisation rate of M_2 into M_1 by I_α	1.32×10^{-1}	day^{-1}	est.
$\lambda_{M I_\beta}$	Polarisation rate of M_1 into M_2 by I_β	5.71×10^{-2}	day^{-1}	est.
$\lambda_{M I_6}$	Polarisation rate of M_1 into M_2 by I_6	1.14×10^{-2}	day^{-1}	est.
$\lambda_{K I_2}$	Maturation rate of K_0 by I_2	6.94×10^{-2}	day^{-1}	est.
$\lambda_{K I_{12}}$	Maturation rate of K_0 by I_{12}	6.69×10^{-2}	day^{-1}	est.
$\lambda_{K D_0}$	Maturation rate of K_0 by D_0	4.54×10^{-2}	day^{-1}	est.

λ_{KD}	Maturation rate of K_0 by D	2.27×10^{-1}	day ⁻¹	est.
$\lambda_{I_2T_8}$	Production rate of I_2 by T_8	5.79×10^{-13}	(g/cell) ⁻¹ day ⁻¹	est.
$\lambda_{I_2T_1}$	Production rate of I_2 by T_1	1.70×10^{-12}	(g/cell) ⁻¹ day ⁻¹	est.
$\lambda_{I_\gamma T_8}$	Production rate of I_γ by T_8	1.49×10^{-14}	(g/cell) ⁻¹ day ⁻¹	est.
$\lambda_{I_\gamma T_1}$	Production rate of I_γ by T_1	5.22×10^{-15}	(g/cell) ⁻¹ day ⁻¹	est.
$\lambda_{I_\gamma K}$	Production rate of I_γ by K	2.76×10^{-13}	(g/cell) ⁻¹ day ⁻¹	est.
$\lambda_{I_\alpha T_8}$	Production rate of I_α by T_8	2.71×10^{-13}	(g/cell) ⁻¹ day ⁻¹	est.
$\lambda_{I_\alpha T_1}$	Production rate of I_α by T_1	4.48×10^{-13}	(g/cell) ⁻¹ day ⁻¹	est.
$\lambda_{I_\alpha M_1}$	Production rate of I_α by M_1	1.64×10^{-13}	(g/cell) ⁻¹ day ⁻¹	est.
$\lambda_{I_\alpha N_1}$	Production rate of I_α by N_1	2.25×10^{-12}	(g/cell) ⁻¹ day ⁻¹	est.
$\lambda_{I_\alpha K}$	Production rate of I_α by K	4.72×10^{-13}	(g/cell) ⁻¹ day ⁻¹	est.
$\lambda_{I_\beta C}$	Production rate of I_β by C	6.74×10^{-9}	(g/cell) ⁻¹ day ⁻¹	est.
$\lambda_{I_\beta T_r}$	Production rate of I_β by T_r	3.90×10^{-8}	(g/cell) ⁻¹ day ⁻¹	est.
$\lambda_{I_\beta C_F}$	Production rate of I_β by C_F	1.35×10^{-8}	(g/cell) ⁻¹ day ⁻¹	est.
$\lambda_{I_{12}D}$	Production rate of I_{12} by D	2.05×10^{-15}	(g/cell) ⁻¹ day ⁻¹	est.
$\lambda_{I_{12}N_1}$	Production rate of I_{12} by N_1	1.20×10^{-16}	(g/cell) ⁻¹ day ⁻¹	est.
$\lambda_{I_{12}M_1}$	Production rate of I_{12} by M_1	2.34×10^{-15}	(g/cell) ⁻¹ day ⁻¹	est.
$\lambda_{I_{10}C}$	Production rate of I_{10} by C	1.54×10^{-14}	(g/cell) ⁻¹ day ⁻¹	est.
$\lambda_{I_{10}T_2}$	Production rate of I_{10} by T_2	5.12×10^{-16}	(g/cell) ⁻¹ day ⁻¹	est.
$\lambda_{I_{10}M_2}$	Production rate of I_{10} by M_2	3.09×10^{-14}	(g/cell) ⁻¹ day ⁻¹	est.
$\lambda_{I_{10}T_r}$	Production rate of I_{10} by T_r	5.83×10^{-13}	(g/cell) ⁻¹ day ⁻¹	est.
$\lambda_{I_{10}I_2}$	Production ratio of I_{10} by I_2	3	dimensionless	est.
$\lambda_{I_4T_2}$	Production rate of I_4 by T_2	3.35×10^{-11}	(g/cell) ⁻¹ day ⁻¹	est.
λ_{I_6D}	Production rate of I_6 by D	4.24×10^{-11}	(g/cell) ⁻¹ day ⁻¹	est.
$\lambda_{I_6C_F}$	Production rate of I_6 by C_F	3.67×10^{-10}	(g/cell) ⁻¹ day ⁻¹	est.
$\lambda_{I_{1\beta}D}$	Production rate of $I_{1\beta}$ by D	3.68×10^{-13}	(g/cell) ⁻¹ day ⁻¹	est.
$\lambda_{I_{1\beta}N_1}$	Production rate of $I_{1\beta}$ by N_1	5.15×10^{-13}	(g/cell) ⁻¹ day ⁻¹	est.
$\lambda_{I_{1\beta}M_1}$	Production rate of $I_{1\beta}$ by M_1	3.41×10^{-14}	(g/cell) ⁻¹ day ⁻¹	est.
K_{CI_α}	Half-saturation constant of I_α for C	9.00×10^{-8}	g/cm ³	[210] est.
K_{CI_γ}	Half-saturation constant of I_γ for C	1.69×10^{-8}	g/cm ³	[211] est.
K_{DH}	Half-saturation constant of H for D	1.33×10^{-8}	g/cm ³	[212] est.
K_{DA}	Half-saturation constant of A for D	3.55×10^{-4}	g/cm ³	[213–215] est.
K_{DS}	Half-saturation constant of S for D	4.50×10^{-8}	g/cm ³	[216] est.
$K_{T_8I_2}$	Half-saturation constant of I_2 for T_8	2.00×10^{-9}	g/cm ³	[217] est.
K_{T_8C}	Half-saturation constant T_8 exhaustion due to C exposure	6.97×10^8	(cell/cm ³) day	est.
$K_{T_{ex}A_1}$	Half-saturation constant of T_{ex} reinvigoration by A_1	5.08×10^{-5}	g/cm ³	est.
$K_{T_1I_2}$	Half-saturation constant of I_2 for T_1	2.00×10^{-9}	g/cm ³	[217] est.
$K_{C_F I_\beta}$	Half-saturation constant of I_β for C_F	1.51×10^{-3}	g/cm ³	[218] est.

$K_{C_F I_{1\beta}}$	Half-saturation constant of $I_{1\beta}$ for C_F	1.92×10^{-7}	g/cm ³	[211] est.
$K_{N_1 I_{1\beta}}$	Half-saturation constant of $I_{1\beta}$ for N_1	1.92×10^{-7}	g/cm ³	[211] est.
$K_{N_1 I_\gamma}$	Half-saturation constant of I_γ for N_1	1.69×10^{-8}	g/cm ³	[211] est.
$K_{N_2 I_6}$	Half-saturation constant of I_6 for N_2	3.11×10^{-3}	g/cm ³	[218] est.
$K_{N_2 I_\beta}$	Half-saturation constant of I_β for N_2	1.51×10^{-3}	g/cm ³	[218] est.
$K_{M_1 I_\alpha}$	Half-saturation constant of I_α for M_1	9.00×10^{-8}	g/cm ³	[210] est.
$K_{M_1 I_\gamma}$	Half-saturation constant of I_γ for M_1	1.69×10^{-8}	g/cm ³	[211] est.
$K_{M_2 I_4}$	Half-saturation constant of I_4 for M_2	9.20×10^{-8}	g/cm ³	[210] est.
$K_{M_2 I_{10}}$	Half-saturation constant of I_{10} for M_2	1.84×10^{-7}	g/cm ³	[210] est.
$K_{M_2 P_L}$	Half-saturation constant of P_L for M_2	1.65×10^{11}	molec/cm ³	est.
$K_{M I_{12}}$	Half-saturation constant of I_{12} for M_1/M_2	6.00×10^{-10}	g/cm ³	[219] est.
$K_{M I_\gamma}$	Half-saturation constant of I_γ for M_1/M_2	1.69×10^{-8}	g/cm ³	[211] est.
$K_{M I_\alpha}$	Half-saturation constant of I_α for M_1/M_2	9.00×10^{-8}	g/cm ³	[210] est.
$K_{M I_\beta}$	Half-saturation constant of I_β for M_1/M_2	1.51×10^{-3}	g/cm ³	[218] est.
$K_{M I_6}$	Half-saturation constant of I_6 for M_1/M_2	3.11×10^{-3}	g/cm ³	[218] est.
$K_{K I_2}$	Half-saturation constant of I_2 for K	2.00×10^{-9}	g/cm ³	[217] est.
$K_{K I_{12}}$	Half-saturation constant of I_{12} for K	6.00×10^{-10}	g/cm ³	[219] est.
$K_{K D_0}$	Half-saturation constant of D_0 for K	1.70×10^6	cell/cm ³	est.
$K_{K D}$	Half-saturation constant of D for K	6.67×10^5	cell/cm ³	est.
$K_{I_{10} I_2}$	Half-saturation constant of I_2 for I_{10}	2.00×10^{-9}	g/cm ³	[217] est.
C_0	Carrying capacity of C	8.02×10^8	cell/cm ³	est.
$K_{C I_\beta}$	Inhibition constant of T_8 elimination of C by I_β	1.51×10^{-3}	g/cm ³	[218] est.
$K_{C P_L}$	Inhibition constant of T_8 elimination of C by P_L	1.65×10^{11}	molec/cm ³	est.
$K_{C I_6}$	Inhibition constant of K elimination of C by I_6	3.11×10^{-3}	g/cm ³	[218] est.

K_{CP_D}	Inhibition constant of K elimination of C by P_D	5.66×10^9	molec/cm ³	est.
V_{TS}	Volume of the TS	2.71×10^1	cm ³	[220]
V_{LN}	Volume of the TDLN	9.20×10^{-2}	cm ³	[221] est.
$K_{T_0^8 P_D^{LN}}$	Inhibition constant of T_0^8 activation by P_D^{LN}	4.98×10^{10}	(molec/cm ³) day	est.
$K_{T_0^8 P_A^{LN}}$	Inhibition constant of T_0^8 activation by P_A^{LN}	4.90×10^{10}	(molec/cm ³) day	est.
$K_{T_A^8 Q^{LN}}$	Inhibition constant of T_A^8 proliferation by Q^{LN}	6.14×10^5	(molec/cm ³) day	est.
$K_{T_A^8 P_A^{LN}}$	Inhibition constant of T_A^8 proliferation by P_A^{LN}	1.19×10^9	(molec/cm ³) day	est.
$K_{T_8 Q}$	Inhibition constant of T_8 growth by I_2 by Q	1.99×10^5	molec/cm ³	est.
$K_{T_8 I_{10}}$	Inhibition constant of T_8 death by I_{10}	1.84×10^{-7}	g/cm ³	est.
$K_{T_{ex} I_{10}}$	Inhibition constant of T_{ex} death by I_{10}	1.84×10^{-7}	g/cm ³	est.
$K_{T_0^4 P_D^{LN}}$	Inhibition constant of T_0^4 activation by P_D^{LN}	3.74×10^{10}	(molec/cm ³) day	est.
$K_{T_0^4 P_A^{LN}}$	Inhibition constant of T_0^4 activation by P_A^{LN}	3.68×10^{10}	(molec/cm ³) day	est.
$K_{T_A^1 Q^{LN}}$	Inhibition constant of T_A^1 proliferation by Q^{LN}	5.20×10^5	(molec/cm ³) day	est.
$K_{T_A^1 P_A^{LN}}$	Inhibition constant of T_A^1 proliferation by Q^{LN}	1.01×10^{11}	(molec/cm ³) day	est.
$K_{T_A^2 Q^{LN}}$	Inhibition constant of T_A^2 proliferation by Q^{LN}	5.20×10^5	(molec/cm ³) day	est.
$K_{T_A^2 P_A^{LN}}$	Inhibition constant of T_A^2 proliferation by P_A^{LN}	1.01×10^{11}	(molec/cm ³) day	est.
$K_{T_1 Q}$	Inhibition constant of T_1 growth by I_2 by Q	1.99×10^5	molec/cm ³	est.
$K_{T_0^r P_D^{LN}}$	Inhibition constant of T_0^r activation by P_D^{LN}	3.74×10^{10}	(molec/cm ³) day	est.
$K_{T_0^r P_A^{LN}}$	Inhibition constant of T_0^r activation by P_A^{LN}	3.68×10^{10}	(molec/cm ³) day	est.
$K_{T_A^r Q^{LN}}$	Inhibition constant of T_A^r proliferation by Q^{LN}	3.62×10^5	(molec/cm ³) day	est.
$K_{T_A^r P_A^{LN}}$	Inhibition constant of T_A^r proliferation by P_A^{LN}	7.03×10^{10}	(molec/cm ³) day	est.
C_{F0}	Carrying Capacity of C_F	1.12×10^7	cell/cm ³	est.
$K_{I_\gamma T_r}$	Inhibition constant of T cell production of I_γ by T_r	1.81×10^5	cell/cm ³	est.
$K_{I_\gamma P_A}$	Inhibition constant of K production of I_γ by P_A	8.32×10^8	molec/cm ³	est.
$K_{I_{12} A}$	Inhibition constant of D production of I_{12} by A	3.55×10^{-4}	g/cm ³	[213–215] est.

$K_{I_{12}I_{10}}$	Inhibition constant of M_1 production of I_{12} by I_{10}	1.84×10^{-7}	g/cm^3	[210] est.
$K_{P_D A_1}$	Inhibition constant of A_1 depletion of P_D by A_1	6.33×10^{-2}	$(\text{g/cm}^3) \text{ day}$	est.
$K_{P_D^{\text{LN}} A_1^{\text{LN}}}$	Inhibition constant of A_1^{LN} depletion of P_D^{LN} by A_1^{LN}	6.33×10^{-2}	$(\text{g/cm}^3) \text{ day}$	est.
d_{N_c}	Removal rate of N_c	5.34×10^{-1}	day^{-1}	est.
d_H	Degradation rate of H	5.55	day^{-1}	[222] est.
d_A	Degradation rate of A	2.00×10^2	day^{-1}	[223] est.
d_S	Degradation rate of S	1.39	day^{-1}	[224, 225] est.
d_{D_0}	Death rate of D_0	3.60×10^{-2}	day^{-1}	[226] est.
d_D	Death rate of D	0.32	day^{-1}	[227] est.
$d_{T_0^8}$	Death rate of T_0^8	3.22×10^{-2}	day^{-1}	[228] est.
d_{T_8}	Death rate of T_8	9×10^{-3}	day^{-1}	[229]
$d_{T_{\text{ex}}}$	Death rate of T_{ex}	9×10^{-3}	day^{-1}	[229]
$d_{T_0^4}$	Death rate of T_0^4	4.03×10^{-2}	day^{-1}	[228] est.
d_{T_1}	Death rate of T_1	8×10^{-3}	day^{-1}	[229]
d_{T_2}	Death rate of T_2	8×10^{-3}	day^{-1}	[229]
$d_{T_0^r}$	Death rate of T_0^r	2.2×10^{-3}	day^{-1}	[54]
d_{T_r}	Death rate of T_r	6.30×10^{-2}	day^{-1}	[230] est.
d_{C_F}	Death rate of C_F	1.98×10^{-1}	day^{-1}	[231] est.
d_{N_0}	Death rate of N_0	0.98	day^{-1}	[232, 233] est.
d_{N_1}	Death rate of N_1	0.98	day^{-1}	[232, 233] est.
d_{N_2}	Death rate of N_2	0.98	day^{-1}	[232, 233] est.
d_{M_0}	Death rate of M_0	0.72	day^{-1}	[234]
d_{M_1}	Death rate of M_1	0.99	day^{-1}	[234]
d_{M_2}	Death rate of M_2	1.35×10^{-1}	day^{-1}	[234]
d_{K_0}	Death rate of K_0	7×10^{-2}	day^{-1}	[103, 235, 236] est.
d_K	Death rate of K	7×10^{-2}	day^{-1}	[103, 235, 236] est.
d_{I_2}	Degradation rate of I_2	1.44×10^2	day^{-1}	[237, 238] est.
d_{I_γ}	Degradation rate of I_γ	3.33×10^1	day^{-1}	[239] est.
d_{I_α}	Degradation rate of I_α	5.48×10^1	day^{-1}	[240, 241] est.
d_{I_β}	Degradation rate of I_β	3.99×10^2	day^{-1}	[242] est.
$d_{I_{12}}$	Degradation rate of I_{12}	2.13	day^{-1}	[243] est.
$d_{I_{10}}$	Degradation rate of I_{10}	6.16	day^{-1}	[244] est.
d_{I_4}	Degradation rate of I_4	5.25×10^1	day^{-1}	[245] est.
d_{I_6}	Degradation rate of I_6	1.11	day^{-1}	[246] est.
$d_{I_{1\beta}}$	Degradation rate of $I_{1\beta}$	4.75	day^{-1}	[247] est.
$d_{P_D A_1}$	Depletion rate of P_D by A_1	5.24×10^{-13}	$(\text{molec/cm}^3)^{-1} \text{ day}^{-1}$	est.
$d_{P_D^{\text{LN}} A_1^{\text{LN}}}$	Depletion rate of P_D^{LN} by A_1^{LN}	1.19×10^{-13}	$(\text{molec/cm}^3)^{-1} \text{ day}^{-1}$	est.
d_{A_1}	Degradation rate of A_1/A_1^{LN}	2.67×10^{-2}	day^{-1}	[39, 248, 249] est.
$\alpha_{P_D P_L}$	Formation rate of Q/Q^{LN}	2.64×10^{-11}	$(\text{molec/cm}^3)^{-1} \text{ day}^{-1}$	[250]
d_Q	Dissociation rate of Q/Q^{LN}	1.24×10^5	day^{-1}	[250]
$\rho_{P_D^8}$	Number of P_D molecules expressed on T_8	2.76×10^3	molec/cell	[251]
$\rho_{P_D^{\text{ex}}}$	Number of P_D molecules expressed on T_{ex}	1.38×10^4	molec/cell	[251] est.

$\rho_{P_D^1}$	Number of P_D molecules expressed on T_1	2.05×10^3	molec/cell	[251]
$\rho_{P_D^r}$	Number of P_D molecules expressed on T_r	2.05×10^3	molec/cell	[251]
$\rho_{P_D^{M2}}$	Number of P_D molecules expressed on M_2	1.47×10^3	molec/cell	
$\rho_{P_L^C}$	Number of P_L molecules expressed on C	1.67×10^3	molec/cell	[252] est.
$\rho_{P_L^D}$	Number of P_L molecules expressed on D	1.77×10^4	molec/cell	[250, 253]
$\rho_{P_L^8}$	Number of P_L molecules expressed on T_8	1.49×10^3	molec/cell	[250, 252]
$\rho_{P_L^1}$	Number of P_L molecules expressed on T_1	2.08×10^3	molec/cell	[250, 252]
$\rho_{P_L^r}$	Number of P_L molecules expressed on T_r	2.08×10^3	molec/cell	[250, 252]
$\rho_{P_L^{CF}}$	Number of P_L molecules expressed on C_F	2.81×10^3	molec/cell	[252] est.
$\rho_{P_L^{M2}}$	Number of P_L molecules expressed on M_2	1.79×10^3	molec/cell	[50, 254] est.
$\rho_{P_L^{N1}}$	Number of P_L molecules expressed on N_1	1.79×10^3	molec/cell	[252] est.
$\rho_{P_L^{N2}}$	Number of P_L molecules expressed on N_2	1.79×10^3	molec/cell	[252] est.
$\rho_{P_A^8}$	Number of P_A molecules expressed on T_8	6.90×10^2	molec/cell	est.
$\rho_{P_A^{\text{ex}}}$	Number of P_A molecules expressed on T_{ex}	8.28×10^2	molec/cell	est.
$\rho_{P_A^2}$	Number of P_A molecules expressed on T_2	5.61×10^2	molec/cell	est.
$\rho_{P_A^r}$	Number of P_A molecules expressed on T_r	2.79×10^3	molec/cell	est.
τ_m	DC migration time from TDLN to TS	0.75	day	[255] est.
τ_8^{act}	CD8+ T cell activation time	2	day	[256]
Δ_8^0	Time taken for first CTL division	1.63	day	[55]
n_{max}^8	Maximal number of CTL divisions in TDLN	10	dimensionless	[257, 258] est.
Δ_8	Time taken for successive CTL divisions	0.36	day	[257]
$\tau_{T_A^8}$	Time taken for CTL division program	4.87	day	est.
τ_a	T cell migration time from TDLN to TS	0.27	day	est.
τ_l	Time for CTL to become exhausted in TS	10	day	[57, 259] est.

τ_4^{act}	CD4+ T cell activation time	1.5	day	[260] est.
Δ_1^0	Time taken for first Th1 cell division	0.77	day	[261] est.
n_{max}^1	Maximal number of Th1 cell divisions in TDLN	9	dimensionless	[262] est.
Δ_1	Time taken for successive Th1 cell divisions	0.42	day	[261] est.
$\tau_{T_A^1}$	Time taken for Th1 cell division program	4.13	day	est.
Δ_2^0	Time taken for first Th2 cell division	0.77	day	[261] est.
n_{max}^2	Maximal number of Th2 cell divisions in TDLN	9	dimensionless	[262] est.
Δ_2	Time taken for successive Th2 cell divisions	0.42	day	[261] est.
$\tau_{T_A^2}$	Time taken for Th2 cell division program	4.13	day	est.
τ_r^{act}	Treg activation time	1.5	day	[260] est.
Δ_r^0	Time taken for first Treg division	0.77	day	[261] est.
n_{max}^r	Maximal number of Treg divisions in TDLN	6	dimensionless	[263] est.
Δ_r	Time taken for successive Treg divisions	0.42	day	[261] est.
$\tau_{T_A^r}$	Time taken for Treg division program	2.87	day	est.

3 Steady States and Initial Conditions

We estimate all initial conditions and steady states under the assumption that no pembrolizumab has/will be administered. We assume that the patient initially has stage IIIA or stage IIIB MSI-H/dMMR colorectal adenocarcinoma with metastasis to at least one lymph node.

3.1 Tumour Site Cell Steady States and Initial Conditions

Digital cytometry has proved itself to be a powerful technique in characterising immune cell populations from individual patients' bulk tissue transcriptomes without requiring physical cell isolation [264–268]. In particular, RNA-sequencing (RNA-seq) deconvolution of tumour gene expressions has been very useful in determining their immune profile and adjusting treatment accordingly.

Using the UCSC Xena web portal [269], RSEM normalised RNA-seq gene expression profiles of patients from the TCGA COAD and TCGA READ projects [43], featuring patients with colorectal adenocarcinomas. Corresponding clinical and biospecimen data were downloaded from the GDC portal [270] which includes tumour dimensions, necrotic cell percentage, AJCC TNM stage, and MSI sensor and MANTIS MSI statuses. We filtered for samples from primary samples and with non-empty necrosis

percentage data, from patients with AJCC stage III or stage IV CRC, and at least one of MANTIS score > 0.4 or MSIsensor score $> 3.5\%$, as these are the default thresholds for MSI-H [271]. We use the stage IIIC and stage IV samples to infer steady states, and the stage IIIA and stage IIIB samples to infer initial conditions. For all algorithms outlined in the sequel, we aggregate the estimates by taking the median of the relevant non-zero values elementwise, and then normalising such that their sums become 1.

To estimate immune cell population proportions in locally advanced MSI-H/dMMR CRC, we apply multiple algorithms and then synthesise their results to obtain estimates for all cell types in the model. We first use the ImmuCellAI algorithm [272] which estimates the abundance of 24 immune cell types from gene expression data and has also been shown to be highly accurate in predicting immunotherapy response. These immune cell types include 18 T cell subsets, including CD4+ T cells which incorporate T helper cells (namely Th1 cells, Th2 cells, Th17 cells, and T follicular helper cells), regulatory T cells (including natural Tregs (nTregs), induced Tregs (iTregs), and type 1 regulatory T cells (Tr1s)), naive CD4+ T cells (CD4_naive) and other CD4+ T cells (CD4_T). In addition, they include naive CD8+ T cells (CD8_T), cytotoxic T cells or CTLs (Tc), exhausted CD8+ T cells (Tex) cells, central memory T cells (Tcm), effector memory T cells (Tem), natural killer T cells (NKT), $\gamma\delta$ T cells (Tgd), and mucosal-associated invariant T cells (MAIT). ImmuCellAI also estimates the abundance of DCs, B cells, monocytes, macrophages, NK cells, and neutrophils. Direct correspondences between state variables in the model and ImmuCellAI cell types are shown in Table B.1. Additionally, the aggregated estimated cell proportions generated by ImmuCellAI for steady states and initial conditions, after normalisation, are shown in Table B.2 and Table B.3.

To determine the proportions of D_0 and D , K_0 and K , M_0 and M_1 and M_2 , we use the CIBERSORTx algorithm [264], due to its high accuracy [273]. We followed a similar approach to [42] and [44] and applied CIBERSORTx B-mode on the refined gene expression data, using the validated LM22 signature matrix [268], which gave relative immune cell proportions of 22 immune cell types using 547 signature genes derived from microarray data. Direct correspondences between state variables in the model and keys of the LM22 signature matrix are shown in Table B.4. The aggregated estimated cell proportions generated by CIBERSORTx for steady states and initial conditions, after normalisation, are shown in Table B.5 and Table B.6.

We integrated the relative proportions within cell types for DCs, NK cells, and macrophages outputted by CIBERSORTx into the ImmuCellAI abundance estimates. In studies of pancreatic ductal adenocarcinoma, the ratio of the median number of tumour-associated N1 and tumour-associated N2 neutrophils was 10.7 : 20 – 21 [274, 275]. From this, we assume that there is a 1 : 2 ratio of N1/N2 neutrophils in locally advanced MSI-H/dMMR CRC. We also assume that the ratio of N0 neutrophils to the total of N1 and N2 neutrophils is equal to the ratio of M0 macrophages to the total of M1 and M2 macrophages. That is, at steady state, $N_0 : N_1 + N_2 = 0.048864 : 0.281657$, and we set the initial condition such that $N_0 : N_1 + N_2 = 0.062173 : 0.161427$. We also note that the density of immune cells in a healthy adult colon is approximately 3.37×10^7 cell/g [276], which assuming a tissue density of 1.03 g/cm³, results in a total immune cell density of 3.47×10^7 cell/cm³. However, advanced cancer induces lymphadenopathy [277, 278], which [276] estimates results in an increase in the total number of lymphocytes of at most 10%. As such, we assume that there is a 10% increase in lymphocyte concentration in locally advanced MSI-H/dMMR CRC.

To determine the densities of CAFs, which are considered to be essentially all fibroblasts in the TME [60], we used MCP-counter [279]. MCP-counter uses a gene expression matrix to estimate the sample

relative abundance of eight immune and two stromal cell populations in the TME from gene expression data and is amongst the highest accuracy and specificity estimation methods available [280]. The aggregated estimated cell proportions generated by MCP-counter for steady states and initial conditions, after normalisation, are shown in Table B.7 and Table B.8.

To estimate CAF densities at steady state and to choose its initial condition, we assume that the ratio of all immune cells (that is cells excluding endothelial cells and fibroblasts) to fibroblasts given by MCP-counter is the ratio of immune cells to fibroblasts in the TME. Combining everything, the resultant steady-state approximations and initial conditions for the model are shown in Table 3 and Table 4.

Table 3: TS steady-state cell densities for the model, combining estimates derived from ImmuCellAI, CIBERSORTx, and MCP-counter. All values are in cell/cm³.

D_0	D	T_8	T_{ex}	T_1	T_2	T_r	C_F
1.70×10^6	6.67×10^5	1.81×10^5	1.44×10^5	1.08×10^5	1.44×10^5	1.81×10^5	9.33×10^6
N_0	N_1	N_2	M_0	M_1	M_2	K_0	K
6.62×10^5	1.27×10^6	2.54×10^6	3.69×10^5	3.77×10^5	1.75×10^6	1.39×10^6	4.06×10^6

Table 4: TS initial conditions for the model, combining estimates derived from ImmuCellAI, CIBERSORTx, and MCP-counter. All values are in cell/cm³.

D_0	D	T_8	T_{ex}	T_1	T_2	T_r	C_F
1.27×10^6	1.15×10^6	2.29×10^5	2.11×10^5	8.79×10^4	1.06×10^5	2.11×10^5	8.22×10^6
N_0	N_1	N_2	M_0	M_1	M_2	K_0	K
9.33×10^5	8.08×10^5	1.62×10^6	7.64×10^5	8.41×10^5	1.14×10^6	6.96×10^5	4.70×10^6

We follow [44], and at steady state assume that the density of cancer cells is approximately double that of the total number of immune cells (excluding fibroblasts). From the TCGA biospecimen data, the median necrotic cancer cell percentage for stage IIIA and stage IIIB MSI-H CRC samples is 10%, and 5% for stage IIIC and stage IV MSI-H CRC. As such, denoting TIC as the total immune cell density, TCD as the total cell density, and N_p as the necrotic cell percentage, we have that

$$C + N_c = 2 \times \text{TIC}, \quad (3.1)$$

$$\frac{N_c}{N_p} = \frac{C}{1 - N_p}, \quad C = 2 \times \text{TIC} \times (1 - N_p) \implies N_c = 2 \times \text{TIC} \times N_p. \quad (3.2)$$

Taking into account lymphadenopathy, and using data from [276], we assume that the total immune cell density in locally advanced MSI-H/dMMR CRC at steady state is approximately 3.67×10^7 cell/cm³. Thus, at steady state $C \approx 6.97 \times 10^7$ cell/cm³ and $N_c \approx 3.67 \times 10^6$ cell/cm³.

A retrospective cohort study by Burke et al., considered CRC patients at Leeds Teaching Hospitals NHS Trust over a 2-year interval, who received no treatment and who underwent CT twice more than 5 weeks apart. It was found that in patients whose M category changed from M0 to M1, the median interval between CTs was 155 days, and the median tumour doubling time was 172 days [281]. As such, we assume that it takes 155 days for C to reach its steady-state value. This corresponds to an initial condition for C being $C(0) = 3.54 \times 10^7$ cell/cm³ and thus $N_c(0) \approx 3.93 \times 10^6$ cell/cm³.

3.2 TDLN Cell Steady States and Initial Conditions

To determine initial conditions and steady-state values for $T_0^8, T_A^8, T_0^4, T_A^1, T_A^2, T_A^r$, we can use ImmuCellAI on the GSE26571 dataset from the NCBI Gene Expression Omnibus repository [282, 283]. This contains 9 samples of lymph node metastases from 7 patients with colon adenocarcinoma, with data from [284]. However, the dataset’s metadata does not contain AJCC TNM stages for patients. To estimate the TNM stages of the patients with lymph node metastases, noting that lymph node metastases guarantee a TNM stage of at least stage IIIA, we consider the samples of the primary tumour for these patients and apply the ImmuCellAI algorithm to estimate their immune cell abundances, ignoring Tem and Tem cell subtypes. Mappings between ImmuCellAI immune cell types and TDLN cell types in the model are shown in Table B.9.

We categorise patients as being in stage IIIA or stage IIIB if their lymph node metastases are well or moderately differentiated and categorise patients as being in stage IIIC or stage IV if their lymph node metastases are poorly differentiated, noting that poorer differentiation is correlated with more advanced disease staging in CRC [285]. As before, we use lymph node metastases from stage IIIC and stage IV patients to infer TDLN steady states, and the stage IIIA and stage IIIB samples to infer initial conditions. Aggregating the estimates, as before, and then normalising such that their sums become 1, results in the proportions as shown in Table B.10 and Table B.11.

The density of immune cells in the lymph nodes of an adult is approximately 1.8×10^9 cell/g [276], which assuming a tissue density of 1.03 g/cm³, results in a total immune cell density of 1.854×10^9 cell/cm³. Finally, we assume that in the TDLN, the number of activated CD8+ T cells having undergone n_{\max}^8 divisions is roughly half the number which have only undergone $n_{\max}^8 - 1$ divisions and so forth. Furthermore, we assume that initially, and at steady state, 10% of all Tregs are naive. Thus, we assume that for $i = 8, 1, 2$,

$$T_A^i = \frac{2^{n_{\max}^i}}{2^{n_{\max}^i+1} - 1} T_A^{i\text{LN}},$$

and that

$$T_0^r = \frac{T_A^{r\text{LN}}}{10}, \quad T_A^r = \frac{9}{10} \frac{2^{n_{\max}^r}}{2^{n_{\max}^r+1} - 1} T_A^{r\text{LN}},$$

where $T_A^{i\text{LN}}$ is the total number of activated T cells in the TDLN of the corresponding type.

Combining everything, the resultant steady-state approximations and initial conditions for the model are shown in Table 5 and Table 6.

Table 5: TDLN steady-state cell densities for the model, using estimates derived from ImmuCellAI. All values are in cell/cm³.

T_0^8	T_A^8	T_0^4	T_A^1	T_A^2	T_0^r	T_A^r
1.15×10^7	1.20×10^6	6.64×10^6	5.74×10^6	1.83×10^7	1.06×10^6	4.79×10^6

Table 6: TDLN initial conditions for the model, using estimates derived from ImmuCellAI. All values are in cell/cm³.

T_0^8	T_A^8	T_0^4	T_A^1	T_A^2	T_0^r	T_A^r
1.18×10^7	8.47×10^5	5.08×10^6	7.61×10^6	2.50×10^7	1.70×10^5	7.69×10^5

To estimate the steady states and initial conditions for D^{LN} , we consider (2.8) at steady state, which leads to

$$\frac{V_{\text{TS}}}{V_{\text{LN}}} \lambda_{DD^{\text{LN}}} e^{-d_D \tau_m} \bar{D} - d_D \bar{D}^{\text{LN}} = 0 \implies \bar{D}^{\text{LN}} = \frac{V_{\text{TS}} \lambda_{DD^{\text{LN}}} e^{-d_D \tau_m} \bar{D}}{V_{\text{LN}} d_D} = 8.26 \times 10^6 \text{ cell/cm}^3,$$

where we acquire the value of \bar{D} from Table 3. We set the initial condition for D^{LN} to be such that $D^{\text{LN}}(0)/\bar{D}^{\text{LN}} = D(0)/\bar{D} \implies D^{\text{LN}}(0) = 1.42 \times 10^7 \text{ cell/cm}^3$.

3.3 DAMP Steady States and Initial Conditions

We choose the DAMP steady states and initial conditions to be as in Table 7. Justification for the choice of these values is done in Appendix C.1.

Table 7: DAMP steady states and initial conditions for the model. All values are in units of g/cm^3 .

DAMP	Steady State	Initial Condition
H	1.33×10^{-8}	1.014×10^{-8}
A	3.55×10^{-4}	5.06×10^{-5}
S	4.50×10^{-8}	2.00×10^{-8}

3.4 Cytokine Steady States and Initial Conditions

We choose the cytokine steady states and initial conditions to be as in Table 8. Justification for the choice of these values is done in Appendix C.2.

Table 8: Cytokine steady states and initial conditions for the model. All values are in units of g/cm^3 .

Cytokine	Steady State	Initial Condition
I_2	2.00×10^{-9}	2.10×10^{-9}
I_γ	1.69×10^{-8}	1.52×10^{-8}
I_α	9.00×10^{-8}	5.30×10^{-8}
I_β	1.51×10^{-3}	1.35×10^{-3}
I_{12}	6.00×10^{-10}	6.25×10^{-10}
I_{10}	1.84×10^{-7}	1.15×10^{-7}
I_4	9.20×10^{-8}	5.00×10^{-8}
I_6	3.11×10^{-3}	3.64×10^{-3}
$I_{1\beta}$	1.92×10^{-7}	3.61×10^{-8}

3.5 Immune Checkpoint Protein Steady States and Initial Conditions

We choose the immune checkpoint protein steady states and initial conditions to be as in Table 9. Justification for the choice of these values is done in Appendix C.3.

Table 9: Immune checkpoint protein steady states and initial conditions for the model. All values are in units of molec/cm³.

Protein	Steady State	Initial Condition
P_D	5.66×10^9	5.83×10^9
P_D^{LN}	2.49×10^{10}	1.95×10^{10}
P_L	1.65×10^{11}	1.10×10^{11}
P_L^{LN}	2.37×10^{10}	1.86×10^{10}
Q	1.99×10^5	1.36×10^5
Q^{LN}	1.26×10^5	7.77×10^4
P_A	8.32×10^8	9.83×10^8
P_A^{LN}	2.45×10^{10}	1.68×10^{10}

4 Results

We now aim to optimise neoadjuvant pembrolizumab therapy in locally advanced MSI-H/dMMR CRC. For simplicity, we assume that pembrolizumab is given at a constant dosage and the spacing between consecutive pembrolizumab infusions is constant. We also assume that the patient has pembrolizumab at $t = 0$ days, and we consider a treatment regimen lasting for 12 weeks so that the time for the latest allowed infusion is $t = 84$ days, and simulate to 20 weeks = 140 days.

It is important to note that the administered dose is not equal to the corresponding change in concentration in either A_1 or A_1^{LN} . We assume linear pharmacokinetics, so that $\xi_j, \gamma_j = f_{\text{pembro}} \xi_j$ for some scaling factor f_{pembro} . To determine these, we use the formula

$$f_{\text{pembro}} = \frac{C_{\text{max,ss}}(\xi_{\text{pembro}}) - C_{\text{min,ss}}(\xi_{\text{pembro}})}{\xi_{\text{pembro}}}, \quad (4.1)$$

where $C_{\text{max,ss}}/C_{\text{min,ss}}$ corresponds to the maximum and minimum serum concentration of pembrolizumab at steady state after a dose, ξ_{pembro} , of pembrolizumab is administered, respectively.

For pembrolizumab, the mean $C_{\text{min,ss}}/C_{\text{max,ss}}$ was found to be approximately 32.6/85.8 $\mu\text{g}/\text{mL}$ and 22.4/147.7 $\mu\text{g}/\text{mL}$ for Treatment 1 and Treatment 2 respectively [286]. This results in $f_{\text{pembro}} \approx 2.90 \times 10^{-7}$ $\text{g}/\text{cm}^3 \text{ day}^{-1}/\text{mg}$ of pembrolizumab administered for all doses.

In our optimisation of pembrolizumab therapy, we consider the following three endpoints: tumour volume reduction (TVR), efficiency, and toxicity.

We define $V(t) = C(t) + N_c(t)$ as the total cancer concentration at time t without treatment, and define $V(\xi_{\text{pembro}}; \eta_{\text{pembro}}, t) = C(\xi_{\text{pembro}}; \eta_{\text{pembro}}, t) + N_c(\xi_{\text{pembro}}; \eta_{\text{pembro}}, t)$ as the total cancer concentration at time t with treatment with pembrolizumab doses of ξ_{pembro} at a dosing interval of η_{pembro} . We define the efficacy at t from this regimen to be

$$\text{efficacy}(\xi_{\text{pembro}}; \eta_{\text{pembro}}, t) := \frac{V(t) - V(\xi_{\text{pembro}}; \eta_{\text{pembro}}, t)}{V(t)} \times 100\%. \quad (4.2)$$

We also define the TVR similarly, as

$$\text{TVR}(\xi_{\text{pembro}}; \eta_{\text{pembro}}, t) := \frac{V(0) - V(\xi_{\text{pembro}}; \eta_{\text{pembro}}, t)}{V(0)} \times 100\%. \quad (4.3)$$

In particular, the efficacy represents the extent of tumour volume shrinkage throughout its growth course in comparison to no treatment, whereas the TVR reveals how much the absolute tumour volume has reduced since the commencement of treatment. We see that the TVR and efficacy are linearly related via the formula

$$\text{TVR}(\xi_{\text{pembro}}; \eta_{\text{pembro}}, t) = \left(1 - \frac{V(0)}{V(t)} + \frac{V(0) \text{efficacy}(\xi_{\text{pembro}}; \eta_{\text{pembro}}, t)}{V(t)} \right) \times 100\%, \quad (4.4)$$

so that an increase in treatment efficacy results in increased TVR, and vice-versa. As such, we calculate only the TVR and the corresponding treatment efficacy can be calculated via (4.4).

We can also consider the efficiency of the treatment regimen, with a dosing interval of η_{pembro} and dosage ξ_{pembro} given by

$$\text{efficiency}(\xi_{\text{pembro}}; \eta_{\text{pembro}}, t) := \frac{\text{TVR}(\xi_{\text{pembro}}; \eta_{\text{pembro}}, t)}{\xi_{\text{pembro}} (1 + \lfloor t/\eta_{\text{pembro}} \rfloor)}, \quad (4.5)$$

where $\xi_{\text{pembro}} (1 + \lfloor t/\eta_{\text{pembro}} \rfloor)$ is the total dose of pembrolizumab administered by time t . This corresponds to the ratio between the TVR percentage and the total dose of pembrolizumab administered.

Finally, we can define the toxicity of the treatment regimen, noting that large enough pembrolizumab concentrations can potentially cause hepatotoxicity and ocular toxicity [287, 288], as well as increase the probability of serious infections, and malignancies. Experiments show that dosages of pembrolizumab between 0.1 mg/kg and 10 mg/kg, given every 2 weeks, is safe and tolerable [289, 290]. We thus assume that the threshold for pembrolizumab toxicity is 10 mg/kg every 2 weeks, with higher doses being deemed toxic. To rigorise this notion, we define the toxicity of the treatment regimen, with dose interval η_{pembro} and dosage ξ_{pembro} , as

$$\text{toxicity}(\xi_{\text{pembro}}; \eta_{\text{pembro}}, t) := \max \left(\frac{\max_{s \in [0, t]} A_1(\xi_{\text{pembro}}; \eta_{\text{pembro}}, s)}{\max_{s \in [0, t]} A_1(800 \text{ mg}; 14 \text{ days}, s)}, \frac{\max_{s \in [0, t]} A_1^{\text{LN}}(\xi_{\text{pembro}}; \eta_{\text{pembro}}, s)}{\max_{s \in [0, t]} A_1^{\text{LN}}(800 \text{ mg}; 14 \text{ days}, s)} \right). \quad (4.6)$$

In particular, $A_1(\xi_{\text{pembro}}; \eta_{\text{pembro}}, s)$ and $A_1^{\text{LN}}(\xi_{\text{pembro}}; \eta_{\text{pembro}}, s)$ denote the concentrations of A_1 and A_1^{LN} at time s , with pembrolizumab doses of ξ_{pembro} at a dosing interval of η_{pembro} , respectively, noting that we assume a patient mass of 80 kg. In particular, the toxicity quantifies the ratio of the maximum pembrolizumab concentrations from the regimen to those of a 10 mg/kg dose given every 2 weeks, taking the highest value of this ratio between the TDLN and TS. A toxicity greater than 1 indicates a toxic and unsafe regimen, whereas a toxicity of 1 or less signifies a non-toxic and safe regimen, with lower toxicity values corresponding to safer treatments.

Denoting the dosing interval of pembrolizumab as η_{pembro} , we perform a sweep across the space $\eta_{\text{pembro}} \in \{1, 2, 3, 4, 6, 7, 12, 14, 21, 28, 42, 84, \infty\}$ days, where $\eta_{\text{pembro}} = \infty$ days denotes a single dose of treatment, given at $t = 0$ days. These values are integer factors of 84 days, and each η_{pembro} corresponds to a distinct number of doses administered. This approach ensures practicality whilst preventing any artefacts that could occur from selecting a treatment regimen that ends at a fixed time of 12 weeks. We consider 500 linearly spaced dosages in the domain $\xi_{\text{pembro}} \in [1 \text{ mg/kg}, 10 \text{ mg/kg}]$, corresponding to $\xi_{\text{pembro}} \in [80 \text{ mg}, 800 \text{ mg}]$, assuming a patient mass of 80 kg.

It is also beneficial for us to consider FDA-approved pembrolizumab regimens for the first-line treatment of metastatic MSI-H/dMMR CRC as a benchmark for comparison. There are 2 distinct treatment

regimens for pembrolizumab therapy that are approved by the FDA for metastatic MSI-H/dMMR CRC in adults [291]:

- Treatment 1: 200 mg of pembrolizumab administered by intravenous infusion over a duration of 30 minutes every 3 weeks until disease progression or unacceptable toxicity.
- Treatment 2: 400 mg of pembrolizumab administered by intravenous infusion over a duration of 30 minutes every 6 weeks until disease progression or unacceptable toxicity.

These correspond to the following parameter values in the model:

- Treatment 1: $\xi_j = 200$ mg, $\gamma_j = f_{\text{pembro}}\xi_j$, $t_j = 21(j - 1)$, $n = 5$,
- Treatment 2: $\xi_j = 400$ mg, $\gamma_j = f_{\text{pembro}}\xi_j$, $t_j = 42(j - 1)$, $n = 3$.

Furthermore, this corresponds to a dose of 2.5 mg/kg(5 mg/kg) of pembrolizumab being administered in Treatment 1(2), assuming a patient mass of 80 kg.

Heatmaps of TVR, efficiency, and toxicity at $t = 20$ weeks for these η_{pembro} and ξ_{pembro} values are shown in Fig 1. All simulations were done in MATLAB using the dde23 solver with the initial conditions stated in Section 3 and drug parameters as above.

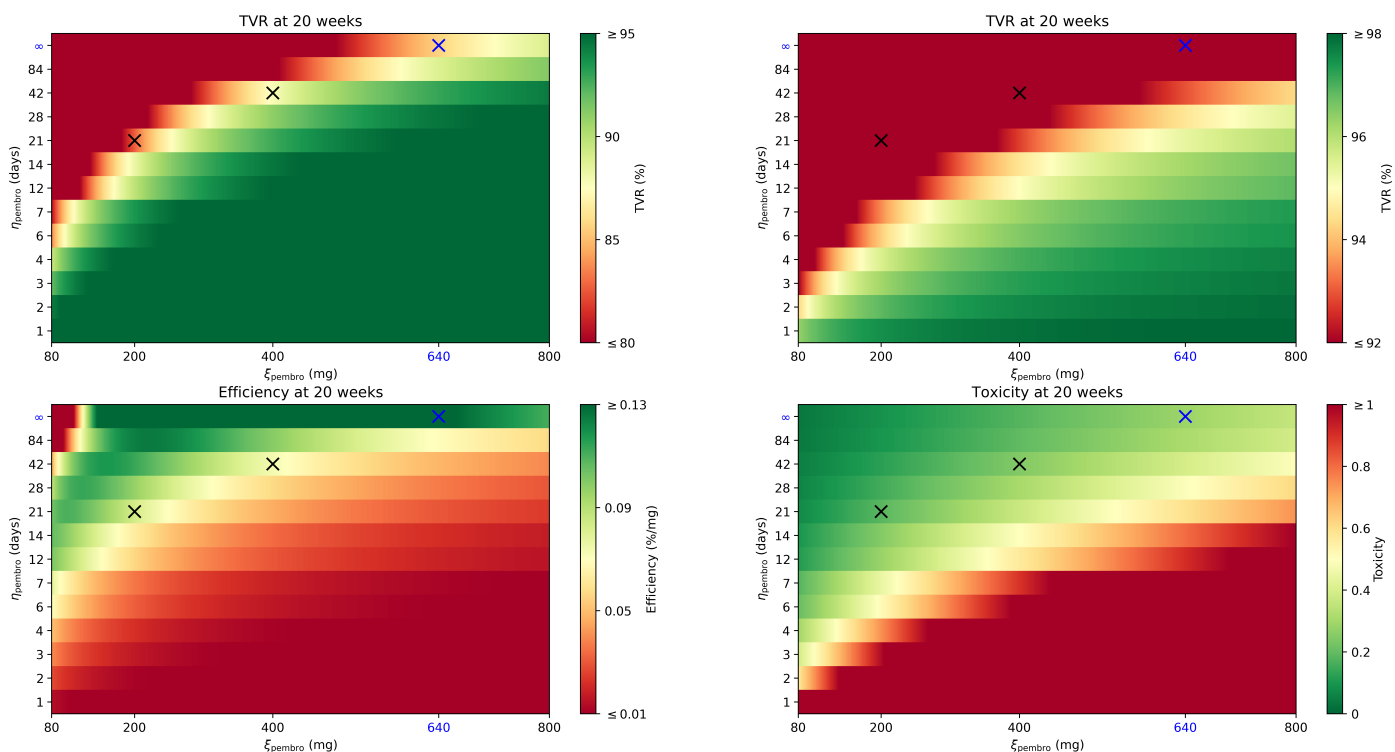


Fig 1: TVR (top left and top right), efficiency (bottom left), and toxicity (bottom right) at 20 weeks for η_{pembro} in the domain $\{1, 2, 3, 4, 6, 7, 12, 14, 21, 28, 42, 84, \infty\}$ days with 500 linearly spaced ξ_{pembro} dosages between 80 mg and 800 mg. The FDA-approved regimens (Treatment 1 and Treatment 2) for metastatic MSI-H/dMMR CRC are shown in black and the optimal treatment regimen for locally advanced MSI-H/dMMR CRC is shown in blue. We note that the bounds represented by the colour bar of the top-right figure differ from those in the top-left figure.

We can determine the optimal pembrolizumab therapy by considering the regimen that achieves an acceptable TVR at 20 weeks, whilst maximising treatment efficiency as much as possible and ensuring

a toxicity of less than 1. The TVR of Treatment 1 at 20 weeks was calculated to be 82.71%, and the TVR of Treatment 2 at 20 weeks was calculated to be 87.67%. As such, to ensure that the TVR of the optimal treatment is comparable to or greater than that of current FDA-approved pembrolizumab regimens, we set the threshold TVR to be 85.5%. We also consider constraints due to practicality, so that $\eta_{\text{pembro}}^{\text{opt}} \in \{7, 14, 21, 28, 42, 84, \infty\}$ days, so that the pembrolizumab dose intervals are an integer number of weeks. We also constrain that $\eta_{\text{pembro}}^{\text{opt}}$ is an integer multiple of 0.1 mg/kg, corresponding to an integer multiple of 8 mg. Denoting the space of $(\xi_{\text{pembro}}, \eta_{\text{pembro}})$ pairs that satisfy these criteria as $\mathcal{S}^{\text{prac}}$, the optimal pembrolizumab dosing and spacing, denoted $\xi_{\text{pembro}}^{\text{opt}}$ and $\eta_{\text{pembro}}^{\text{opt}}$, satisfy

$$(\xi_{\text{pembro}}^{\text{opt}}, \eta_{\text{pembro}}^{\text{opt}}) = \underset{\substack{\text{TVR}(\xi_{\text{pembro}}; \eta_{\text{pembro}}, 140) \geq 85.5\% \\ (\xi_{\text{pembro}}, \eta_{\text{pembro}}) \in \mathcal{S}^{\text{prac}} \\ \text{toxicity}(\xi_{\text{pembro}}; \eta_{\text{pembro}}, 140) \leq 1}}{\text{argmax}} \text{efficiency}(\xi_{\text{pembro}}; \eta_{\text{pembro}}, 140). \quad (4.7)$$

Solving (4.7), leads to the optimal therapy occurring when $\xi_{\text{pembro}}^{\text{opt}} = 640$ mg and $\eta_{\text{pembro}}^{\text{opt}} = \infty$ days. This corresponds to a single dose of 640 mg, corresponding to 8 mg/kg, and results in a TVR of 85.62%, an efficiency of $1.34 \times 10^{-1}\%$ /mg, and a toxicity of 2.87×10^{-1} at 20 weeks. Time traces for total cancer concentration ($C + N_c$) under optimal pembrolizumab therapy, compared to Treatments 1 and 2 and no treatment, are shown in Fig 2.

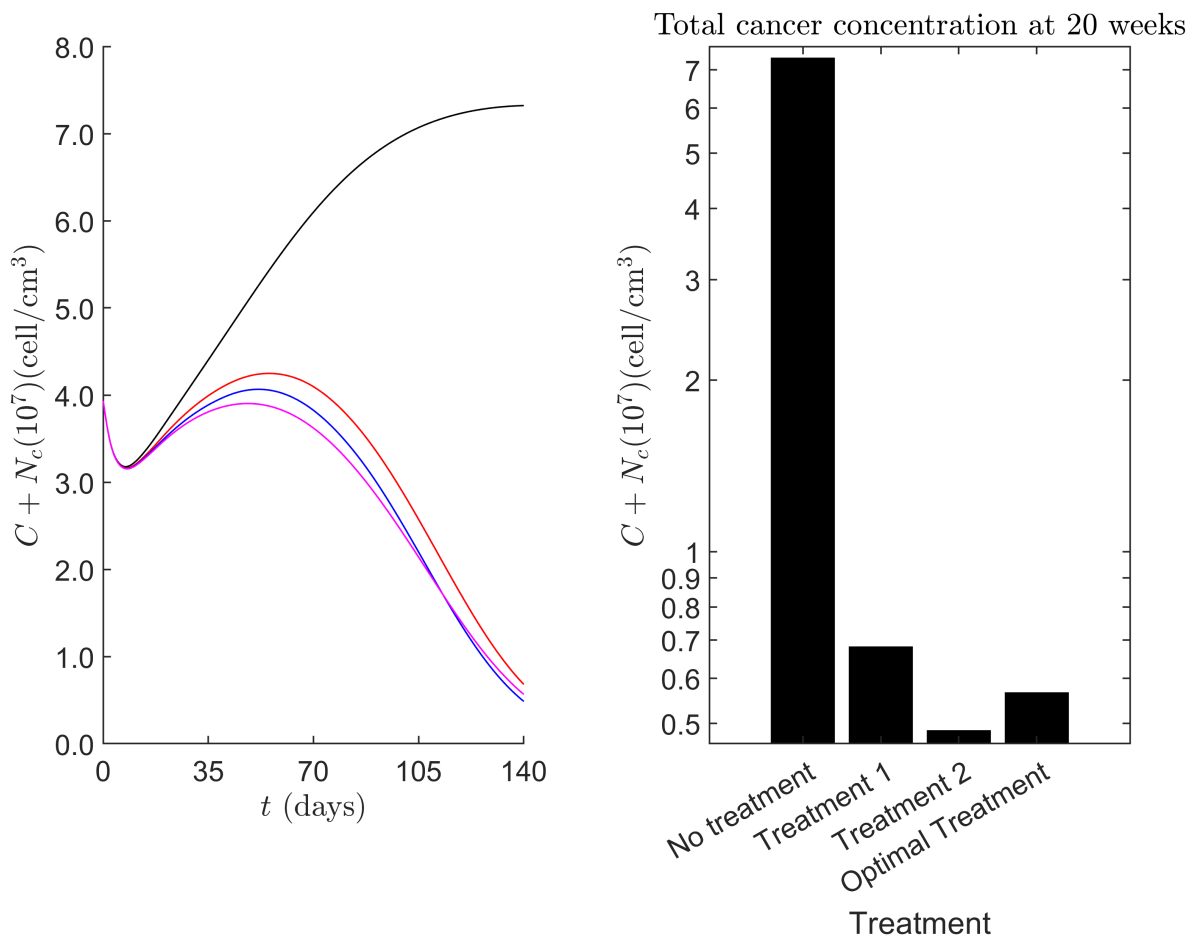


Fig 2: Left: time traces of total cancer concentration up to 20 weeks from commencement, with no treatment in black, Treatment 1 in red, Treatment 2 in blue, and the optimal pembrolizumab treatment regimen for locally advanced MSI-H/dMMR CRC in magenta. Right: concentration of $C + N_c$, 20 weeks after pembrolizumab treatment commencement.

We can also compare the effect of optimal pembrolizumab therapy, against Treatments 1 and 2, as well as no treatment, on the TME, with time traces of key variables shown in Fig 3.

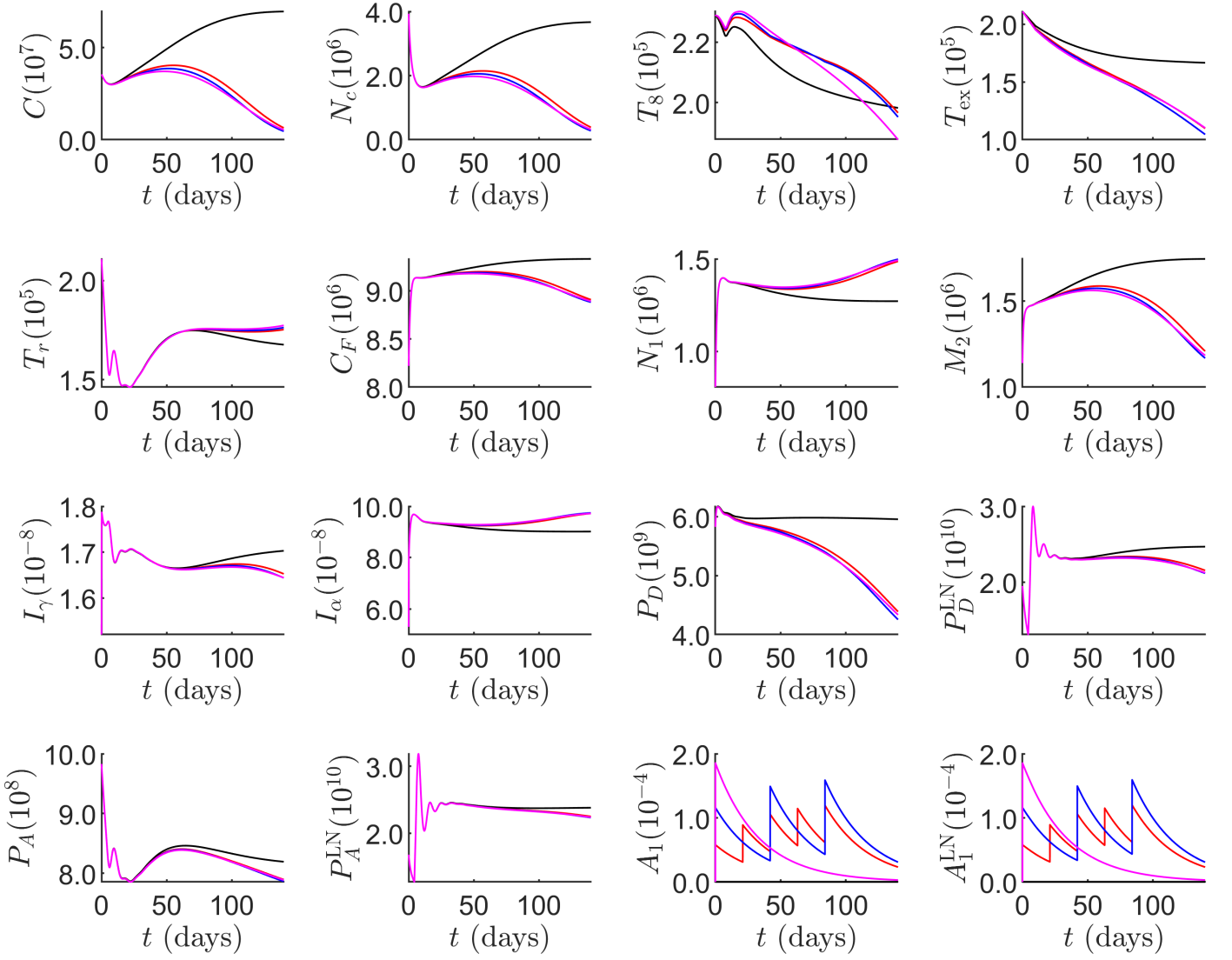


Fig 3: Time traces of notable variables in the model, with the units of the variables as in Table 1. Time traces with no treatment are in black, Treatment 1 in red, Treatment 2 in blue, and the optimal pembrolizumab treatment regimen for locally advanced MSI-H/dMMR CRC in magenta.

The results from Fig 1, Fig 2, and Fig 3 will be discussed in detail in Section 5.

5 Discussion

We can see from Fig 2 and Fig 3, that Treatments 1 and 2 are highly effective in eradicating cancer cells. Without treatment, the total cancer cell concentration (including necrotic cancer cells), at 20 weeks equals 7.32×10^7 cell/cm³, however, equals 6.80×10^6 cell/cm³, and 4.85×10^6 cell/cm³ with Treatments 1 and 2 respectively. This corresponds to an efficacy of 90.71% and 93.38% for Treatments 1 and 2, respectively. In particular, this leads to two immediate, but important, observations. We must note that when comparing pembrolizumab, we must ensure that we take into account that locally advanced MSI-H/dMMR CRC patients will have not been treated with chemotherapy/other therapies

and that these drugs are given as a first-line treatment. Firstly, higher doses at larger intervals are comparable but slightly more effective than smaller doses at shorter intervals, which is consistent with clinical and experimental observations for other cancers [36, 292]. It is difficult to compare our results to that of pre-existing clinical trials for locally advanced MSI-H/dMMR CRC due to the lack of time-series data, widely varying treatment regimens tested and the broad range of outcomes found. Focusing on Treatment 1, which appears to be the primary focus of ongoing clinical trials, a tumour volume reduction of 82.71% at 20 weeks, following the cessation of treatment at 12 weeks, is consistent with the extent of response observed. Therefore, we consider the model to be accurate; however, additional experimental data is needed for further verification. We also observed that slight variations in the initial conditions had minimal impact on model trajectories after a few days (not shown). Additionally, the first week of treatment induces transient behaviour, arising from the absence of interactions within the system for $t < 0$. Moreover, it takes a couple of months for pembrolizumab to begin showing effects and for tumour reductions to be observed, in agreement with experimental findings for CRC [18].

Furthermore, by analysing immune cell trajectories from Fig 3, offering potential explanations for behaviour in the TME and identifying key factors that contribute to maximising cancer reduction. One of the most important observations is that with pembrolizumab, the concentration of effector CD8+ T cells increases greatly compared to without treatment, with the exhausted CD8+ T cell concentration decreasing correspondingly. In particular, the concentration of exhausted CD8+ T cells without treatment at 20 weeks is 1.67×10^5 cell/cm³ compared to 1.10×10^5 cell/cm³, 1.05×10^5 cell/cm³, and 1.10×10^5 cell/cm³ with Treatments 1 and 2, and the optimal treatment respectively. This showcases that a) pembrolizumab increases the concentration of cytotoxic CD8+ T cells through re-invigorating exhausted CD8+ T cells, and b) the concentration of exhausted CD8+ T cells plays a major role in treatment efficacy, as a reduction in exhausted T cells results in decreased PD-1 concentrations and improved cancer eradication.

One important thing to note is that the effector CD8+ T cell population for the optimal regimen drops significantly after a couple of months, and is only 1.88×10^5 cell/cm³ at 20 weeks, despite having the largest effector CD8+ T cell population initially. This occurs since the pembrolizumab concentration at the TS and TDLN gradually declines after the initial infusion so that reinvigoration of exhausted CD8+ T cells diminishes after a few months. However, the optimal therapy eradicates the tumour most rapidly, reducing the viable and necrotic cancer cell population to very low levels, eventually resulting in decreased DAMP release and a reduced influx of effector CD8+ T cells from the TDLN. Despite this, a sufficient number of effector CD8+ T cells and other cytotoxic cells remain to sufficiently kill the remaining cancer. In particular, this significantly reduced cancer population explains why the number of exhausted CD8+ T cells during the optimal treatment is comparable to Treatments 1 and 2, as the extent of antigen exposure is substantially decreased.

Furthermore, with pembrolizumab inhibitor therapy, the concentration of pro-inflammatory immune species, such as N1 neutrophils and TNF increase in concentration relative to without treatment, whilst the concentration of immunosuppressive cell types such as M2 macrophages and CAFs decreases. The increased concentration of TNF is particularly noteworthy since it directly induces necroptosis of cancer cells, causing the release of DAMPs, which in turn induces DC maturation. Without treatment, TNF concentration at 20 weeks is 9.02×10^{-8} g/cm³, compared to 9.72×10^{-8} g/cm³, 9.74×10^{-8} g/cm³, and 9.72×10^{-8} g/cm³ with Treatments 1 and 2, and the optimal treatment respectively. This further shows that increased TNF concentration is correlated with enhanced cancer death and treatment efficacy and that inducing more pro-inflammatory immunogenicity in the TME is key for this to occur.

We can also analyse the impact of pembrolizumab therapy on the concentration of PD-1 in the TS and the TDLN, as well as the concentration of CTLA-4. As expected, pembrolizumab therapy massively decreases the concentration of PD-1 in the TS and the TDLN. At 20 weeks, the concentration of PD-1 in the TS and the TDLN without treatment is 5.96×10^9 cell/cm³ and 2.47×10^{10} cell/cm³, respectively. However, with the optimal treatment, and with Treatments 1 and 2, at 20 weeks the concentration of PD-1 in the TS is reduced by 27.26%, 26.35%, and 28.62% respectively, and its concentration in the TDLN reduces by 13.96%, 12.72%, and 14.27% respectively. Thus, we see that treatment efficacy and success are directly correlated with the extent of PD-1 concentration reduction. This makes sense since PD-1 inhibits T cell activation in the TDLN, inhibits the cytotoxicity of NK cells, and interacts with PD-L1 to form PD-1/PD-L1 which inhibits T cell proliferation. Interestingly, after a couple of months of PD-1 blockade, CTLA-4 concentrations in the TS and TDLN decrease, enhancing T cell activation and proliferation in the TDLN. However, this also pertains to Tregs, resulting in their increased concentration in the TDLN and at the TS, and slightly reduced IFN- γ levels, highlighting the need to consider the balance between PD-1 inhibition and Treg proliferation.

We now shift our focus to [Fig 1](#). We see that TVR increases as the dosing increases and spacing decreases, noting that the effects of acquired resistance to pembrolizumab are quite small since the treatment regimen has a duration of only 12 weeks. In particular, the TVRs of Treatment 1 and Treatment 2 are high, and the TVR of treatments does not change significantly near these regions.

Unsurprisingly, the regimens of FDA-approved treatments for metastatic MSI-H/dMMR CRC are quite efficient, with the efficiency of Treatment 1 being approximately $8.27 \times 10^{-2}\%$ /mg and the efficiency of Treatment 2 being approximately $7.31 \times 10^{-2}\%$ /mg. Whilst these treatments are amongst the most efficient practical ones, they pale in comparison to the global maximum efficiency of $2.13 \times 10^{-1}\%$ /mg, achieved by administering a single 255 mg dose of pembrolizumab. There is also a clear transition between efficient and inefficient treatments, marked by the rapid shift in efficiency as one deviates from local optima. In particular, treatment is inefficient if its TVR is low, regardless of the dosing and spacing (corresponding to the top left inefficient region in [Fig 1](#)), or if an excessive amount of pembrolizumab is administered, regardless of the TVR (corresponding to the bottom right inefficient region in [Fig 1](#)).

In the spirit of completeness, we verify that Treatments 1 and 2 are non-toxic, and compare their toxicity to that of the optimal regimen found. As expected, Treatments 1 and 2 are non-toxic, with toxicities of 1.85×10^{-1} and 2.46×10^{-1} , respectively, whilst the optimal regimen has a toxicity of 2.87×10^{-1} . Thus, we see that these treatments are all non-toxic, and the optimal regimen has comparable toxicity to FDA-approved regimens for metastatic MSI-H/dMMR CRC.

Striking a balance between TVR, efficiency, and toxicity is difficult, and the current FDA-approved regimens for metastatic MSI-H/dMMR CRC do this quite well in the case of locally advanced MSI-H/dMMR CRC. The optimal regimen of administering pembrolizumab as a single dose of 640 mg is also more efficient, leads to comparable or greater TVR, and is more cost-effective and convenient than current regimens, whilst again, maintaining practicality and safety. Moreover, lower single doses of pembrolizumab are effective, with a single dose of 400 mg (equivalent to 5 mg/kg) achieving a TVR of 74.05%, and a single dose of 560 mg (equivalent to 7 mg/kg) achieving a TVR of 83.10%. The associated toxicities are 1.79×10^{-1} and 2.51×10^{-1} , respectively, which are lower than or comparable to those of Treatments 1 and 2. Administering a single dose of pembrolizumab before surgery has proven highly effective for achieving long-term tumour eradication in a phase 1b clinical trial involving resectable stage III/IV melanoma [293]. In particular, 30% of patients experienced $> 90\%$ tumour

eradication, and all of these patients remained disease-free at a median follow-up of 25 months. Medium to high single-dose pembrolizumab demonstrates promising potential for successful and cost-effective treatment, with a phase II clinical trial to evaluate the efficacy and safety of a single-dose of 4 mg/kg of pembrolizumab in patients with stage I-III dMMR CRC currently underway [294].

It should be noted that the model has several limitations, many of which exist for simplicity, but the potential for addressing these issues serves as exciting avenues for future research.

- We ignored spatial effects in the model, however, their resolution can provide information about the distribution and clustering of different immune cell types in the TME and their clinical implications [295, 296].
- We assumed that the death rates were constant throughout the T cell proliferation program, however linear death rates, were shown to markedly improve the quality of fit of Deenick et al.'s model [297] to experimental data [298].
- We considered only the M1/M2 and N1/N2 macrophage and neutrophil dichotomies respectively, however, their plasticity motivates the description of their phenotypes as a continuum, giving them the ability to adapt their functions to achieve mixtures of M1/N1 and M2/N2 responses and functions [76, 299].
- In the optimisation of neoadjuvant pembrolizumab therapy, we restricted ourselves to treatments with constant dosing and spacing as is common in the literature, however varying dosages and dosing frequencies may result in improved regimens.
- We did not consider T cell avidity, the overall strength of a TCR-pMHC interaction, which governs whether a cancer cell will be successfully killed [54]. In particular, high-avidity T cells are necessary for lysing cancer cells and durable tumour eradication, whilst low-avidity T cells are ineffective, and may inhibit high-avidity T cells [300, 301].
- We also did not consider the influence of cytokines in the TDLN for T cell activation and proliferation, which are important in influencing effector T cell differentiation [302, 303].
- The definition of toxicity does not account for its potential origins in autoimmunity, which is a crucial component of certain adverse effects [287].

In this work, we have provided a framework for mathematically modelling many immune cell types in the TME, using experimental data to govern parameter estimation, and finally analysing and optimising neoadjuvant pembrolizumab therapy in MSI-H/dMMR CRC for efficacy and efficiency. We conclude that medium to high single-dose pembrolizumab is more efficient and demonstrates comparable or greater efficacy and TVR than current FDA-approved regimens for metastatic MSI-H/dMMR CRC, whilst maintaining practicality and safety. In addition, the versatility and power of the methods and equations herein can be easily adapted to attain a more comprehensive understanding of other cancers and improve healthcare as a result.

6 CRediT Authorship Contribution Statement

Georgio Hawi: conceptualisation, data curation, formal analysis, funding acquisition, investigation, methodology, project administration, resources, software, validation, visualisation, writing — original draft, writing — review & editing.

Peter S. Kim: conceptualisation, formal analysis, funding acquisition, investigation, methodology, project administration, resources, supervision, validation, visualisation, writing — original draft, writing — review & editing.

Peter P. Lee: conceptualisation, formal analysis, investigation, methodology, project administration, resources, supervision, validation, visualisation, writing — original draft, writing — review & editing.

7 Declaration of Competing Interests

The authors declare that they have no known competing financial interests or personal relationships that could have appeared to influence the work reported in this paper.

8 Data Availability

All data and procedures are available within the manuscript and its Supporting Information file.

9 Acknowledgements

This work was supported by an Australian Government Research Training Program Scholarship. PSK gratefully acknowledges support from the Australian Research Council Discovery Project (DP230100485).

10 Supporting Information

S1 File. Supporting Information: Optimisation of locally advanced MSI-H/dMMR colorectal cancer treatment with neoadjuvant pembrolizumab using data-driven delay integro-differential equations. Derivation of (2.45) (Section A in S1 File), digital cytometry calculations (Section B in S1 File), and parameter estimation (Section C in S1 File).

References

- [1] Klimeck L, Heisser T, Hoffmeister M, Brenner H. Colorectal cancer: A health and economic problem. *Best Practice & Research Clinical Gastroenterology*. 2023 Oct;66:101839. Available from: <http://dx.doi.org/10.1016/j.bpg.2023.101839>.
- [2] Biller LH, Schrag D. Diagnosis and Treatment of Metastatic Colorectal Cancer: A Review. *JAMA*. 2021 Feb;325(7):669. Available from: <http://dx.doi.org/10.1001/jama.2021.0106>.
- [3] Siegel RL, Giaquinto AN, Jemal A. Cancer statistics, 2024. *CA: A Cancer Journal for Clinicians*. 2024 Jan;74(1):12–49. Available from: <http://dx.doi.org/10.3322/caac.21820>.
- [4] Gausman V, Dornblaser D, Anand S, Hayes RB, O’Connell K, Du M, et al. Risk Factors Associated With Early-Onset Colorectal Cancer. *Clinical Gastroenterology and Hepatology*. 2020 Nov;18(12):2752-9.e2. Available from: <http://dx.doi.org/10.1016/j.cgh.2019.10.009>.
- [5] Sifaki-Pistolla D, Poimenaki V, Fotopoulou I, Saloustros E, Mavroudis D, Vamvakas L, et al. Significant Rise of Colorectal Cancer Incidence in Younger Adults and Strong Determinants: 30 Years Longitudinal Differences between under and over 50s. *Cancers*. 2022 Sep;14(19):4799. Available from: <http://dx.doi.org/10.3390/cancers14194799>.

- [6] Siegel RL, Wagle NS, Cercek A, Smith RA, Jemal A. Colorectal cancer statistics, 2023. *CA: A Cancer Journal for Clinicians*. 2023 Mar;73(3):233–254. Available from: <http://dx.doi.org/10.3322/caac.21772>.
- [7] Andrew AS, Parker S, Anderson JC, Rees JR, Robinson C, Riddle B, et al. Risk Factors for Diagnosis of Colorectal Cancer at a Late Stage: a Population-Based Study. *Journal of General Internal Medicine*. 2018 Oct;33(12):2100–2105. Available from: <http://dx.doi.org/10.1007/s11606-018-4648-7>.
- [8] Rawla P, Sunkara T, Barsouk A. Epidemiology of colorectal cancer: incidence, mortality, survival, and risk factors. *Gastroenterology Review*. 2019;14(2):89–103. Available from: <http://dx.doi.org/10.5114/pg.2018.81072>.
- [9] Atreya CE, Yaeger R, Chu E. Systemic Therapy for Metastatic Colorectal Cancer: From Current Standards to Future Molecular Targeted Approaches. *American Society of Clinical Oncology Educational Book*. 2017 May;(37):246–256. Available from: http://dx.doi.org/10.1200/EDBK_175679.
- [10] Moran RG. Leucovorin enhancement of the effects of the fluoropyrimidines on thymidylate synthase. *Cancer*. 1989;63(S6):1008-12. Available from: [http://dx.doi.org/10.1002/1097-0142\(19890315\)63:6+<1008::AID-CNCR2820631303>3.0.CO;2-Z](http://dx.doi.org/10.1002/1097-0142(19890315)63:6+<1008::AID-CNCR2820631303>3.0.CO;2-Z).
- [11] Mohelnikova-Duchonova B. FOLFOX/FOLFIRI pharmacogenetics: The call for a personalized approach in colorectal cancer therapy. *World Journal of Gastroenterology*. 2014;20(30):10316. Available from: <http://dx.doi.org/10.3748/wjg.v20.i30.10316>.
- [12] Gu J, Li Z, Zhou J, Sun Z, Bai C. Response prediction to oxaliplatin plus 5-fluorouracil chemotherapy in patients with colorectal cancer using a four-protein immunohistochemical model. *Oncology Letters*. 2019 Jun. Available from: <http://dx.doi.org/10.3892/ol.2019.10474>.
- [13] Shulman K, Barnett-Griness O, Friedman V, Greenson JK, Gruber SB, Lejbkowitz F, et al. Outcomes of Chemotherapy for Microsatellite Instable–High Metastatic Colorectal Cancers. *JCO Precision Oncology*. 2018 Nov;(2):1–10. Available from: <http://dx.doi.org/10.1200/P0.17.00253>.
- [14] Mulet-Margalef N, Linares J, Badia-Ramentol J, Jimeno M, Sanz Monte C, Manzano Mozo JL, et al. Challenges and Therapeutic Opportunities in the dMMR/MSI-H Colorectal Cancer Landscape. *Cancers*. 2023 Feb;15(4):1022. Available from: <http://dx.doi.org/10.3390/cancers15041022>.
- [15] Boland CR, Thibodeau SN, Hamilton SR, Sidransky D, Eshleman JR, Burt RW, et al. A National Cancer Institute Workshop on Microsatellite Instability for cancer detection and familial predisposition: development of international criteria for the determination of microsatellite instability in colorectal cancer. *Cancer Res*. 1998 Nov;58(22):5248-57. Available from: <https://pubmed.ncbi.nlm.nih.gov/9823339/>.
- [16] Sinicrope FA, Foster NR, Thibodeau SN, Marsoni S, Monges G, Labianca R, et al. DNA Mismatch Repair Status and Colon Cancer Recurrence and Survival in Clinical Trials of 5-Fluorouracil-Based Adjuvant Therapy. *JNCI Journal of the National Cancer Institute*. 2011 May;103(11):863–875. Available from: <http://dx.doi.org/10.1093/jnci/djr153>.

- [17] Venderbosch S, Nagtegaal ID, Maughan TS, Smith CG, Cheadle JP, Fisher D, et al. Mismatch Repair Status and BRAF Mutation Status in Metastatic Colorectal Cancer Patients: A Pooled Analysis of the CAIRO, CAIRO2, COIN, and FOCUS Studies. *Clinical Cancer Research*. 2014 Oct;20(20):5322–5330. Available from: <http://dx.doi.org/10.1158/1078-0432.CCR-14-0332>.
- [18] André T, Shiu KK, Kim TW, Jensen BV, Jensen LH, Punt C, et al. Pembrolizumab in Microsatellite–Instability–High Advanced Colorectal Cancer. *New England Journal of Medicine*. 2020 Dec;383(23):2207–2218. Available from: <http://dx.doi.org/10.1056/NEJMoa2017699>.
- [19] Llosa NJ, Cruise M, Tam A, Wicks EC, Hechenbleikner EM, Taube JM, et al. The Vigorous Immune Microenvironment of Microsatellite Instable Colon Cancer Is Balanced by Multiple Counter-Inhibitory Checkpoints. *Cancer Discovery*. 2015 Jan;5(1):43–51. Available from: <http://dx.doi.org/10.1158/2159-8290.CD-14-0863>.
- [20] Giannakis M, Mu XJ, Shukla SA, Qian ZR, Cohen O, Nishihara R, et al. Genomic Correlates of Immune-Cell Infiltrates in Colorectal Carcinoma. *Cell Reports*. 2016 Apr;15(4):857–865. Available from: <http://dx.doi.org/10.1016/j.celrep.2016.03.075>.
- [21] Ciardiello D, Vitiello PP, Cardone C, Martini G, Troiani T, Martinelli E, et al. Immunotherapy of colorectal cancer: Challenges for therapeutic efficacy. *Cancer Treatment Reviews*. 2019 Jun;76:22–32. Available from: <http://dx.doi.org/10.1016/j.ctrv.2019.04.003>.
- [22] Topalian SL, Hodi FS, Brahmer JR, Gettinger SN, Smith DC, McDermott DF, et al. Safety, Activity, and Immune Correlates of Anti–PD-1 Antibody in Cancer. *New England Journal of Medicine*. 2012 Jun;366(26):2443–2454. Available from: <http://dx.doi.org/10.1056/NEJMoa1200690>.
- [23] Buchbinder EI, Desai A. CTLA-4 and PD-1 Pathways: Similarities, Differences, and Implications of Their Inhibition. *American Journal of Clinical Oncology*. 2016 Feb;39(1):98–106. Available from: <http://dx.doi.org/10.1097/COC.000000000000239>.
- [24] Sarshekeh AM, Overman MJ, Kopetz S. Nivolumab in the Treatment of Microsatellite Instability High Metastatic Colorectal Cancer. *Future Oncology*. 2018 Feb;14(18):1869–1874. Available from: <http://dx.doi.org/10.2217/fon-2017-0696>.
- [25] Yaghoubi N, Soltani A, Ghazvini K, Hassanian SM, Hashemy SI. PD-1/ PD-L1 blockade as a novel treatment for colorectal cancer. *Biomedicine & Pharmacotherapy*. 2019 Feb;110:312–318. Available from: <http://dx.doi.org/10.1016/j.biopha.2018.11.105>.
- [26] Lin X, Kang K, Chen P, Zeng Z, Li G, Xiong W, et al. Regulatory mechanisms of PD-1/PD-L1 in cancers. *Molecular Cancer*. 2024 May;23(1). Available from: <http://dx.doi.org/10.1186/s12943-024-02023-w>.
- [27] Han Y, Liu D, Li L. PD-1/PD-L1 pathway: current researches in cancer. *American journal of cancer research*. 2020;10(3):727. Available from: <https://pmc.ncbi.nlm.nih.gov/articles/PMC7136921/>.
- [28] Oliveira AF, Bretes L, Furtado I. Review of PD-1/PD-L1 Inhibitors in Metastatic dMMR/MSI-H Colorectal Cancer. *Frontiers in Oncology*. 2019 May;9. Available from: <http://dx.doi.org/10.3389/fonc.2019.00396>.

- [29] Lee J, Ahn E, Kissick HT, Ahmed R. Reinvigorating Exhausted T Cells by Blockade of the PD-1 Pathway. *Forum on Immunopathological Diseases and Therapeutics*. 2015;6(1–2):7–17. Available from: <http://dx.doi.org/10.1615/ForumImmDisTher.2015014188>.
- [30] Zhang Y, Zhang Z. The history and advances in cancer immunotherapy: understanding the characteristics of tumor-infiltrating immune cells and their therapeutic implications. *Cellular & Molecular Immunology*. 2020 Jul;17(8):807–821. Available from: <http://dx.doi.org/10.1038/s41423-020-0488-6>.
- [31] Casak SJ, Marcus L, Fashoyin-Aje L, Mushti SL, Cheng J, Shen YL, et al. FDA Approval Summary: Pembrolizumab for the First-line Treatment of Patients with MSI-H/dMMR Advanced Unresectable or Metastatic Colorectal Carcinoma. *Clinical Cancer Research*. 2021 Apr;27(17):4680–4684. Available from: <http://dx.doi.org/10.1158/1078-0432.CCR-21-0557>.
- [32] Shiu KK, Jiang Y, Saunders M, Seligmann JF, Iveson T, Wilson RH, et al. NEOPRISM-CRC: Neoadjuvant pembrolizumab stratified to tumour mutation burden for high risk stage 2 or stage 3 deficient-MMR/MSI-high colorectal cancer. *Journal of Clinical Oncology*. 2024 Jun;42(17_suppl):LBA3504–LBA3504. Available from: http://dx.doi.org/10.1200/JCO.2024.42.17_suppl.LBA3504.
- [33] Ludford K, Ho WJ, Thomas JV, Raghav KPS, Murphy MB, Fleming ND, et al. Neoadjuvant Pembrolizumab in Localized Microsatellite Instability High/Deficient Mismatch Repair Solid Tumors. *Journal of Clinical Oncology*. 2023 Apr;41(12):2181–2190. Available from: <http://dx.doi.org/10.1200/JCO.22.01351>.
- [34] Centanni M, Moes DJAR, Trocóniz IF, Ciccolini J, van Hasselt JGC. Clinical Pharmacokinetics and Pharmacodynamics of Immune Checkpoint Inhibitors. *Clinical Pharmacokinetics*. 2019 Feb;58(7):835–857. Available from: <http://dx.doi.org/10.1007/s40262-019-00748-2>.
- [35] Le Louedec F, Leenhardt F, Marin C, Chatelut E, Evrard A, Ciccolini J. Cancer Immunotherapy Dosing: A Pharmacokinetic/Pharmacodynamic Perspective. *Vaccines*. 2020 Oct;8(4):632. Available from: <http://dx.doi.org/10.3390/vaccines8040632>.
- [36] Dubé-Pelletier M, Labbé C, Côté J, Pelletier-St-Pierre AA. Pembrolizumab Every 6 Weeks Versus Every 3 Weeks in Advanced Non-Small Cell Lung Cancer. *The Oncologist*. 2023 Jun;28(11):969–977. Available from: <http://dx.doi.org/10.1093/oncolo/oyad182>.
- [37] Lindauer A, Valiathan C, Mehta K, Sriram V, de Greef R, Ellassais-Schaap J, et al. Translational Pharmacokinetic/Pharmacodynamic Modeling of Tumor Growth Inhibition Supports Dose-Range Selection of the Anti-PD-1 Antibody Pembrolizumab: Translational Pharmacokinetic/Pharmacodynamic Modeling. *CPT: Pharmacometrics & Systems Pharmacology*. 2016 Nov;6(1):11–20. Available from: <http://dx.doi.org/10.1002/psp4.12130>.
- [38] Shang J, Huang L, Huang J, Ren X, Liu Y, Feng Y. Population pharmacokinetic models of anti-PD-1 mAbs in patients with multiple tumor types: A systematic review. *Frontiers in Immunology*. 2022 Aug;13. Available from: <http://dx.doi.org/10.3389/fimmu.2022.871372>.
- [39] Yan T, Yu L, Shangguan D, Li W, Liu N, Chen Y, et al. Advances in pharmacokinetics and pharmacodynamics of PD-1/PD-L1 inhibitors. *International Immunopharmacology*. 2023 Feb;115:109638. Available from: <http://dx.doi.org/10.1016/j.intimp.2022.109638>.

- [40] Wang Cy, Sheng Cc, Ma Gl, Xu D, Liu Xq, Wang Yy, et al. Population pharmacokinetics of the anti-PD-1 antibody camrelizumab in patients with multiple tumor types and model-informed dosing strategy. *Acta Pharmacologica Sinica*. 2020 Nov;42(8):1368–1375. Available from: <http://dx.doi.org/10.1038/s41401-020-00550-y>.
- [41] Puzskiel A, Bianconi G, Pasquiers B, Balakirouchenane D, Arrondeau J, Boudou-Rouquette P, et al. Extending the dosing intervals of nivolumab: model-based simulations in unselected cancer patients. *British Journal of Cancer*. 2024 Mar;130(11):1866–1874. Available from: <http://dx.doi.org/10.1038/s41416-024-02659-x>.
- [42] Kirshtein A, Akbarinejad S, Hao W, Le T, Su S, Aronow RA, et al. Data Driven Mathematical Model of Colon Cancer Progression. *Journal of Clinical Medicine*. 2020 Dec;9(12):3947. Available from: <http://dx.doi.org/10.3390/jcm9123947>.
- [43] Comprehensive molecular characterization of human colon and rectal cancer. *Nature*. 2012 Jul;487(7407):330–337. Available from: <http://dx.doi.org/10.1038/nature11252>.
- [44] Budithi A, Su S, Kirshtein A, Shahriyari L. Data Driven Mathematical Model of FOLFIRI Treatment for Colon Cancer. *Cancers*. 2021 May;13(11):2632. Available from: <http://dx.doi.org/10.3390/cancers13112632>.
- [45] Bozkurt F, Yousef A, Bilgil H, Baleanu D. A mathematical model with piecewise constant arguments of colorectal cancer with chemo-immunotherapy. *Chaos, Solitons & Fractals*. 2023 Mar;168:113207. Available from: <http://dx.doi.org/10.1016/j.chaos.2023.113207>.
- [46] dePillis LG, Savage H, Radunskaya AE. Mathematical Model of Colorectal Cancer with Monoclonal Antibody Treatments. arXiv; 2013. Available from: <https://arxiv.org/abs/1312.3023>.
- [47] Butner JD, Dogra P, Chung C, Pasqualini R, Arap W, Lowengrub J, et al. Mathematical modeling of cancer immunotherapy for personalized clinical translation. *Nature Computational Science*. 2022 Dec;2(12):785–796. Available from: <http://dx.doi.org/10.1038/s43588-022-00377-z>.
- [48] Lai X, Friedman A. Combination therapy of cancer with cancer vaccine and immune checkpoint inhibitors: A mathematical model. *PLOS ONE*. 2017 May;12(5):e0178479. Available from: <http://dx.doi.org/10.1371/journal.pone.0178479>.
- [49] Lai X, Friedman A. How to schedule VEGF and PD-1 inhibitors in combination cancer therapy? *BMC Systems Biology*. 2019 Mar;13(1). Available from: <http://dx.doi.org/10.1186/s12918-019-0706-y>.
- [50] Siewe N, Friedman A. TGF- β inhibition can overcome cancer primary resistance to PD-1 blockade: A mathematical model. *PLOS ONE*. 2021 Jun;16(6):e0252620. Available from: <http://dx.doi.org/10.1371/journal.pone.0252620>.
- [51] Siewe N, Friedman A. Cancer therapy with immune checkpoint inhibitor and CSF-1 blockade: A mathematical model. *Journal of Theoretical Biology*. 2023 Jan;556:111297. Available from: <http://dx.doi.org/10.1016/j.jtbi.2022.111297>.
- [52] Liao KL, Bai XF, Friedman A. IL-27 in combination with anti-PD-1 can be anti-cancer or pro-cancer. *Journal of Theoretical Biology*. 2024 Feb;579:111704. Available from: <http://dx.doi.org/10.1016/j.jtbi.2023.111704>.

- [53] Kumbhari A, Kim PS, Lee PP. Optimisation of anti-cancer peptide vaccines to preferentially elicit high-avidity T cells. *Journal of Theoretical Biology*. 2020 Feb;486:110067. Available from: <http://dx.doi.org/10.1016/j.jtbi.2019.110067>.
- [54] Kumbhari A, Egelston CA, Lee PP, Kim PS. Mature Dendritic Cells May Promote High-Avidity Tuning of Vaccine T Cell Responses. *Frontiers in Immunology*. 2020 Oct;11. Available from: <http://dx.doi.org/10.3389/fimmu.2020.584680>.
- [55] Plambeck M, Kazeroonian A, Loeffler D, Kretschmer L, Salinno C, Schroeder T, et al. Heritable changes in division speed accompany the diversification of single T cell fate. *Proceedings of the National Academy of Sciences*. 2022 Feb;119(9). Available from: <http://dx.doi.org/10.1073/pnas.2116260119>.
- [56] Del Prete A, Salvi V, Soriani A, Laffranchi M, Sozio F, Bosisio D, et al. Dendritic cell subsets in cancer immunity and tumor antigen sensing. *Cellular & Molecular Immunology*. 2023 Mar;20(5):432–447. Available from: <http://dx.doi.org/10.1038/s41423-023-00990-6>.
- [57] Blank CU, Haining WN, Held W, Hogan PG, Kallies A, Lugli E, et al. Defining ‘T cell exhaustion’. *Nature Reviews Immunology*. 2019 Sep;19(11):665–674. Available from: <http://dx.doi.org/10.1038/s41577-019-0221-9>.
- [58] Hedrick CC, Malanchi I. Neutrophils in cancer: heterogeneous and multifaceted. *Nature Reviews Immunology*. 2021 Jul;22(3):173–187. Available from: <http://dx.doi.org/10.1038/s41577-021-00571-6>.
- [59] Ustyanovska Avtenyuk N, Visser N, Bremer E, Wiersma VR. The Neutrophil: The Underdog That Packs a Punch in the Fight against Cancer. *International Journal of Molecular Sciences*. 2020 Oct;21(21):7820. Available from: <http://dx.doi.org/10.3390/ijms21217820>.
- [60] Zhang Y, Lv N, Li M, Liu M, Wu C. Cancer-associated fibroblasts: tumor defenders in radiation therapy. *Cell Death & Disease*. 2023 Aug;14(8). Available from: <http://dx.doi.org/10.1038/s41419-023-06060-z>.
- [61] Mao X, Xu J, Wang W, Liang C, Hua J, Liu J, et al. Crosstalk between cancer-associated fibroblasts and immune cells in the tumor microenvironment: new findings and future perspectives. *Molecular Cancer*. 2021 Oct;20(1). Available from: <http://dx.doi.org/10.1186/s12943-021-01428-1>.
- [62] Briukhovetska D, Dörr J, Endres S, Libby P, Dinarello CA, Kobold S. Interleukins in cancer: from biology to therapy. *Nature Reviews Cancer*. 2021 Jun;21(8):481–499. Available from: <http://dx.doi.org/10.1038/s41568-021-00363-z>.
- [63] Wu T, Dai Y. Tumor microenvironment and therapeutic response. *Cancer Letters*. 2017 Feb;387:61–68. Available from: <http://dx.doi.org/10.1016/j.canlet.2016.01.043>.
- [64] Shah K, Al-Haidari A, Sun J, Kazi JU. T cell receptor (TCR) signaling in health and disease. *Signal Transduction and Targeted Therapy*. 2021 Dec;6(1). Available from: <http://dx.doi.org/10.1038/s41392-021-00823-w>.
- [65] Sugiyarto G, Lau D, Hill SL, Arcia-Anaya D, Boulanger DSM, Parkes EE, et al. Reactivation of low avidity tumor-specific CD8+ T cells associates with immunotherapeutic efficacy of anti-PD-1. *Journal for ImmunoTherapy of Cancer*. 2023 Aug;11(8):e007114. Available from: <https://doi.org/10.1136/jitc-2023-007114>.

- [66] Maimela NR, Liu S, Zhang Y. Fates of CD8+ T cells in Tumor Microenvironment. *Computational and Structural Biotechnology Journal*. 2019;17:1–13. Available from: <http://dx.doi.org/10.1016/j.csbj.2018.11.004>.
- [67] Hoekstra ME, Vijver SV, Schumacher TN. Modulation of the tumor micro-environment by CD8+ T cell-derived cytokines. *Current Opinion in Immunology*. 2021 Apr;69:65–71. Available from: <http://dx.doi.org/10.1016/j.coi.2021.03.016>.
- [68] Caza T, Landas S. Functional and Phenotypic Plasticity of CD4+ T Cell Subsets. *BioMed Research International*. 2015;2015:1-13. Available from: <https://doi.org/10.1155/2015/521957>.
- [69] Nakayama T, Hirahara K, Onodera A, Endo Y, Hosokawa H, Shinoda K, et al. Th2 Cells in Health and Disease. *Annual Review of Immunology*. 2017 Apr;35(1):53-84. Available from: <https://doi.org/10.1146/annurev-immunol-051116-052350>.
- [70] Furiati SC, Catarino JS, Silva MV, Silva RF, Estevam RB, Teodoro RB, et al. Th1, Th17, and Treg Responses are Differently Modulated by TNF- α Inhibitors and Methotrexate in Psoriasis Patients. *Scientific Reports*. 2019 May;9(1). Available from: <https://doi.org/10.1038/s41598-019-43899-9>.
- [71] Jarnicki AG, Lysaght J, Todryk S, Mills KHG. Suppression of Antitumor Immunity by IL-10 and TGF- β -Producing T Cells Infiltrating the Growing Tumor: Influence of Tumor Environment on the Induction of CD4+ and CD8+ Regulatory T Cells. *The Journal of Immunology*. 2006 Jul;177(2):896–904. Available from: <http://dx.doi.org/10.4049/jimmunol.177.2.896>.
- [72] Turnis ME, Sawant DV, Szymczak-Workman AL, Andrews LP, Delgoffe GM, Yano H, et al. Interleukin-35 Limits Anti-Tumor Immunity. *Immunity*. 2016 Feb;44(2):316–329. Available from: <http://dx.doi.org/10.1016/j.immuni.2016.01.013>.
- [73] Cui G. TH9, TH17, and TH22 Cell Subsets and Their Main Cytokine Products in the Pathogenesis of Colorectal Cancer. *Frontiers in Oncology*. 2019 Oct;9. Available from: <http://dx.doi.org/10.3389/fonc.2019.01002>.
- [74] Hetta HF, Elkady A, Yahia R, Meshall AK, Saad MM, Mekky MA, et al. T follicular helper and T follicular regulatory cells in colorectal cancer: A complex interplay. *Journal of Immunological Methods*. 2020 May;480:112753. Available from: <http://dx.doi.org/10.1016/j.jim.2020.112753>.
- [75] Kerneur C, Cano CE, Olive D. Major pathways involved in macrophage polarization in cancer. *Frontiers in Immunology*. 2022 Oct;13. Available from: <http://dx.doi.org/10.3389/fimmu.2022.1026954>.
- [76] Mills C. M1 and M2 Macrophages: Oracles of Health and Disease. *Critical Reviews in Immunology*. 2012;32(6):463-88. Available from: <https://doi.org/10.1615/critrevimmunol.v32.i6.10>.
- [77] Viola A, Munari F, Sánchez-Rodríguez R, Scolaro T, Castegna A. The Metabolic Signature of Macrophage Responses. *Frontiers in Immunology*. 2019 Jul;10. Available from: <https://doi.org/10.3389/fimmu.2019.01462>.

- [78] Han X, Ding S, Jiang H, Liu G. Roles of Macrophages in the Development and Treatment of Gut Inflammation. *Frontiers in Cell and Developmental Biology*. 2021 Mar;9. Available from: <https://doi.org/10.3389/fcell.2021.625423>.
- [79] Mizuno R, Kawada K, Itatani Y, Ogawa R, Kiyasu Y, Sakai Y. The Role of Tumor-Associated Neutrophils in Colorectal Cancer. *International Journal of Molecular Sciences*. 2019 Jan;20(3):529. Available from: <http://dx.doi.org/10.3390/ijms20030529>.
- [80] Wang X, Qiu L, Li Z, Wang XY, Yi H. Understanding the Multifaceted Role of Neutrophils in Cancer and Autoimmune Diseases. *Frontiers in Immunology*. 2018 Nov;9. Available from: <http://dx.doi.org/10.3389/fimmu.2018.02456>.
- [81] Fridlender ZG, Sun J, Kim S, Kapoor V, Cheng G, Ling L, et al. Polarization of Tumor-Associated Neutrophil Phenotype by TGF- β : “N1” versus “N2” TAN. *Cancer Cell*. 2009 Sep;16(3):183–194. Available from: <http://dx.doi.org/10.1016/j.ccr.2009.06.017>.
- [82] Mihaila AC, Ciortan L, Macarie RD, Vadana M, Cecoltan S, Preda MB, et al. Transcriptional Profiling and Functional Analysis of N1/N2 Neutrophils Reveal an Immunomodulatory Effect of S100A9-Blockade on the Pro-Inflammatory N1 Subpopulation. *Frontiers in Immunology*. 2021 Aug;12. Available from: <http://dx.doi.org/10.3389/fimmu.2021.708770>.
- [83] Masucci MT, Minopoli M, Carriero MV. Tumor Associated Neutrophils. Their Role in Tumorigenesis, Metastasis, Prognosis and Therapy. *Frontiers in Oncology*. 2019 Nov;9. Available from: <http://dx.doi.org/10.3389/fonc.2019.01146>.
- [84] Xue J, Schmidt SV, Sander J, Draffehn A, Krebs W, Quester I, et al. Transcriptome-Based Network Analysis Reveals a Spectrum Model of Human Macrophage Activation. *Immunity*. 2014 Feb;40(2):274–88. Available from: <https://doi.org/10.1016/j.immuni.2014.01.006>.
- [85] Giese MA, Hind LE, Huttenlocher A. Neutrophil plasticity in the tumor microenvironment. *Blood*. 2019 May;133(20):2159–2167. Available from: <http://dx.doi.org/10.1182/blood-2018-11-844548>.
- [86] Raskov H, Orhan A, Christensen JP, Gögenur I. Cytotoxic CD8+ T cells in cancer and cancer immunotherapy. *British Journal of Cancer*. 2020 Sep;124(2):359–367. Available from: <http://dx.doi.org/10.1038/s41416-020-01048-4>.
- [87] Zhang C, Hu Y, Shi C. Targeting Natural Killer Cells for Tumor Immunotherapy. *Frontiers in Immunology*. 2020 Feb;11. Available from: <http://dx.doi.org/10.3389/fimmu.2020.00060>.
- [88] Knutson KL, Disis ML. Tumor antigen-specific T helper cells in cancer immunity and immunotherapy. *Cancer Immunology, Immunotherapy*. 2005 Jan;54(8):721–728. Available from: <http://dx.doi.org/10.1007/s00262-004-0653-2>.
- [89] Haabeth OAW, Tveita AA, Fauskanger M, Schjesvold F, Lorvik KB, Hofgaard PO, et al. How Do CD4+ T Cells Detect and Eliminate Tumor Cells That Either Lack or Express MHC Class II Molecules? *Frontiers in Immunology*. 2014 Apr;5. Available from: <http://dx.doi.org/10.3389/fimmu.2014.00174>.
- [90] Josephs SF, Ichim TE, Prince SM, Kesari S, Marincola FM, Escobedo AR, et al. Unleashing endogenous TNF- α as a cancer immunotherapeutic. *Journal of Translational Medicine*. 2018 Aug;16(1). Available from: <http://dx.doi.org/10.1186/s12967-018-1611-7>.

- [91] Wang X, Lin Y. Tumor necrosis factor and cancer, buddies or foes? *Acta Pharmacologica Sinica*. 2008 Nov;29(11):1275–1288. Available from: <http://dx.doi.org/10.1111/j.1745-7254.2008.00889.x>.
- [92] Jorgovanovic D, Song M, Wang L, Zhang Y. Roles of IFN- γ in tumor progression and regression: a review. *Biomarker Research*. 2020 Sep;8(1). Available from: <http://dx.doi.org/10.1186/s40364-020-00228-x>.
- [93] Castro F, Cardoso AP, Gonçalves RM, Serre K, Oliveira MJ. Interferon-Gamma at the Crossroads of Tumor Immune Surveillance or Evasion. *Frontiers in Immunology*. 2018 May;9. Available from: <http://dx.doi.org/10.3389/fimmu.2018.00847>.
- [94] Thomas DA, Massagué J. TGF- β directly targets cytotoxic T cell functions during tumor evasion of immune surveillance. *Cancer Cell*. 2005 Nov;8(5):369–380. Available from: <http://dx.doi.org/10.1016/j.ccr.2005.10.012>.
- [95] Juneja VR, McGuire KA, Manguso RT, LaFleur MW, Collins N, Haining WN, et al. PD-L1 on tumor cells is sufficient for immune evasion in immunogenic tumors and inhibits CD8 T cell cytotoxicity. *Journal of Experimental Medicine*. 2017 Mar;214(4):895–904. Available from: <http://dx.doi.org/10.1084/jem.20160801>.
- [96] Kang YJ, Jeung IC, Park A, Park YJ, Jung H, Kim TD, et al. An increased level of IL-6 suppresses NK cell activity in peritoneal fluid of patients with endometriosis via regulation of SHP-2 expression. *Human Reproduction*. 2014 Jul;29(10):2176–2189. Available from: <http://dx.doi.org/10.1093/humrep/deu172>.
- [97] Hsu J, Hodgins JJ, Marathe M, Nicolai CJ, Bourgeois-Daigneault MC, Trevino TN, et al. Contribution of NK cells to immunotherapy mediated by PD-1/PD-L1 blockade. *Journal of Clinical Investigation*. 2018 Sep;128(10):4654–4668. Available from: <http://dx.doi.org/10.1172/JCI99317>.
- [98] Fucikova J, Kepp O, Kasikova L, Petroni G, Yamazaki T, Liu P, et al. Detection of immunogenic cell death and its relevance for cancer therapy. *Cell Death & Disease*. 2020 Nov;11(11). Available from: <http://dx.doi.org/10.1038/s41419-020-03221-2>.
- [99] Ren Y, Cao L, Wang L, Zheng S, Zhang Q, Guo X, et al. Autophagic secretion of HMGB1 from cancer-associated fibroblasts promotes metastatic potential of non-small cell lung cancer cells via NF κ B signaling. *Cell Death & Disease*. 2021 Sep;12(10). Available from: <http://dx.doi.org/10.1038/s41419-021-04150-4>.
- [100] Martins I, Wang Y, Michaud M, Ma Y, Sukkurwala AQ, Shen S, et al. Molecular mechanisms of ATP secretion during immunogenic cell death. *Cell Death & Differentiation*. 2013 Jul;21(1):79–91. Available from: <http://dx.doi.org/10.1038/cdd.2013.75>.
- [101] Ahmed A, Tait SWG. Targeting immunogenic cell death in cancer. *Molecular Oncology*. 2020 Dec;14(12):2994–3006. Available from: <http://dx.doi.org/10.1002/1878-0261.12851>.
- [102] Morandi B, Mortara L, Chiossone L, Accolla RS, Mingari MC, Moretta L, et al. Dendritic Cell Editing by Activated Natural Killer Cells Results in a More Protective Cancer-Specific Immune Response. *PLoS ONE*. 2012 Jun;7(6):e39170. Available from: <http://dx.doi.org/10.1371/journal.pone.0039170>.

- [103] Vivier E, Tomasello E, Baratin M, Walzer T, Ugolini S. Functions of natural killer cells. *Nature Immunology*. 2008 Apr;9(5):503–510. Available from: <http://dx.doi.org/10.1038/ni1582>.
- [104] Ruhland MK, Roberts EW, Cai E, Mujal AM, Marchuk K, Beppler C, et al. Visualizing Synaptic Transfer of Tumor Antigens among Dendritic Cells. *Cancer Cell*. 2020 Jun;37(6):786–99.e5. Available from: <http://dx.doi.org/10.1016/j.ccell.2020.05.002>.
- [105] Choi G, Kim BS, Park YJ, Shim I, Chung Y. Clonal Expansion of Allergen-specific CD4+ T Cell in the Lung in the Absence of Lymph Nodes. *Immune Network*. 2017;17(3):163. Available from: <http://dx.doi.org/10.4110/in.2017.17.3.163>.
- [106] Brunner-Weinzierl MC, Rudd CE. CTLA-4 and PD-1 Control of T-Cell Motility and Migration: Implications for Tumor Immunotherapy. *Frontiers in Immunology*. 2018 Nov;9. Available from: <http://dx.doi.org/10.3389/fimmu.2018.02737>.
- [107] Mizuno R, Sugiura D, Shimizu K, Maruhashi T, Watada M, Okazaki Im, et al. PD-1 Primarily Targets TCR Signal in the Inhibition of Functional T Cell Activation. *Frontiers in Immunology*. 2019 Mar;10. Available from: <http://dx.doi.org/10.3389/fimmu.2019.00630>.
- [108] Harris NL, Watt V, Ronchese F, Le Gros G. Differential T Cell Function and Fate in Lymph Node and Nonlymphoid Tissues. *The Journal of Experimental Medicine*. 2002 Feb;195(3):317–326. Available from: <http://dx.doi.org/10.1084/jem.20011558>.
- [109] Catron DM, Rusch LK, Hataye J, Itano AA, Jenkins MK. CD4+ T cells that enter the draining lymph nodes after antigen injection participate in the primary response and become central-memory cells. *The Journal of Experimental Medicine*. 2006 Mar;203(4):1045–1054. Available from: <http://dx.doi.org/10.1084/jem.20051954>.
- [110] Riley JL. PD-1 signaling in primary T cells. *Immunological Reviews*. 2009 Apr;229(1):114–125. Available from: <http://dx.doi.org/10.1111/j.1600-065X.2009.00767.x>.
- [111] Rosenberg SA. IL-2: The First Effective Immunotherapy for Human Cancer. *The Journal of Immunology*. 2014 Jun;192(12):5451–5458. Available from: <http://dx.doi.org/10.4049/jimmunol.1490019>.
- [112] Jiang Y, Chen M, Nie H, Yuan Y. PD-1 and PD-L1 in cancer immunotherapy: clinical implications and future considerations. *Human Vaccines & Immunotherapeutics*. 2019 Mar;15(5):1111–1122. Available from: <http://dx.doi.org/10.1080/21645515.2019.1571892>.
- [113] Oft M. Immune regulation and cytotoxic T cell activation of IL-10 agonists – Preclinical and clinical experience. *Seminars in Immunology*. 2019 Aug;44:101325. Available from: <http://dx.doi.org/10.1016/j.smim.2019.101325>.
- [114] Qiu H, Hu X, Gao L, Chen L, Chen J, Yuan J, et al. Interleukin 10 enhanced CD8+ T cell activity and reduced CD8+ T cell apoptosis in patients with diffuse large B cell lymphoma. *Experimental Cell Research*. 2017 Nov;360(2):146–152. Available from: <http://dx.doi.org/10.1016/j.yexcr.2017.08.036>.
- [115] Lee KA, Shin KS, Kim GY, Song YC, Bae EA, Kim IK, et al. Characterization of age-associated exhausted CD8+ T cells defined by increased expression of Tim-3 and PD-1. *Aging Cell*. 2016 Jan;15(2):291–300. Available from: <http://dx.doi.org/10.1111/accel.12435>.

- [116] Shive CL, Freeman ML, Younes S, Kowal CM, Canaday DH, Rodriguez B, et al. Markers of T Cell Exhaustion and Senescence and Their Relationship to Plasma TGF- β Levels in Treated HIV+ Immune Non-responders. *Frontiers in Immunology*. 2021 Mar;12. Available from: <http://dx.doi.org/10.3389/fimmu.2021.638010>.
- [117] Pauken KE, Wherry EJ. Overcoming T cell exhaustion in infection and cancer. *Trends in Immunology*. 2015 Apr;36(4):265–276. Available from: <http://dx.doi.org/10.1016/j.it.2015.02.008>.
- [118] De Boer RJ, Perelson AS. Towards a general function describing T cell proliferation. *Journal of Theoretical Biology*. 1995 Aug;175(4):567–576. Available from: <http://dx.doi.org/10.1006/jtbi.1995.0165>.
- [119] Choudhry H, Helmi N, Abdulaal WH, Zeyadi M, Zamzami MA, Wu W, et al. Prospects of IL-2 in Cancer Immunotherapy. *BioMed Research International*. 2018;2018:1–7. Available from: <http://dx.doi.org/10.1155/2018/9056173>.
- [120] Marangoni F, Zhakyp A, Corsini M, Geels SN, Carrizosa E, Thelen M, et al. Expansion of tumor-associated Treg cells upon disruption of a CTLA-4-dependent feedback loop. *Cell*. 2021 Jul;184(15):3998–4015.e19. Available from: <http://dx.doi.org/10.1016/j.cell.2021.05.027>.
- [121] Fotsitzoudis C, Koulouridi A, Messaritakis I, Konstantinidis T, Gouvas N, Tsiaoussis J, et al. Cancer-Associated Fibroblasts: The Origin, Biological Characteristics and Role in Cancer—A Glance on Colorectal Cancer. *Cancers*. 2022 Sep;14(18):4394. Available from: <http://dx.doi.org/10.3390/cancers14184394>.
- [122] Kennel KB, Bozlar M, De Valk AF, Greten FR. Cancer-Associated Fibroblasts in Inflammation and Antitumor Immunity. *Clinical Cancer Research*. 2022 Nov;29(6):1009–1016. Available from: <http://dx.doi.org/10.1158/1078-0432.CCR-22-1031>.
- [123] Wu F, Yang J, Liu J, Wang Y, Mu J, Zeng Q, et al. Signaling pathways in cancer-associated fibroblasts and targeted therapy for cancer. *Signal Transduction and Targeted Therapy*. 2021 Jun;6(1). Available from: <http://dx.doi.org/10.1038/s41392-021-00641-0>.
- [124] Chen LC, Wang LJ, Tsang NM, Ojcius DM, Chen CC, OuYang CN, et al. Tumour inflammasome-derived IL-1 β recruits neutrophils and improves local recurrence-free survival in EBV-induced nasopharyngeal carcinoma. *EMBO Molecular Medicine*. 2012 Oct;4(12):1276–1293. Available from: <http://dx.doi.org/10.1002/emmm.201201569>.
- [125] Ellis TN, Beaman BL. Interferon- γ activation of polymorphonuclear neutrophil function. *Immunology*. 2004 Apr;112(1):2–12. Available from: <http://dx.doi.org/10.1111/j.1365-2567.2004.01849.x>.
- [126] Zou JM, Qin J, Li YC, Wang Y, Li D, Shu Y, et al. IL-35 induces N2 phenotype of neutrophils to promote tumor growth. *Oncotarget*. 2017 Apr;8(20):33501–33514. Available from: <http://dx.doi.org/10.18632/oncotarget.16819>.
- [127] Kroner A, Greenhalgh AD, Zarruk JG, Passos dos Santos R, Gaestel M, David S. TNF and Increased Intracellular Iron Alter Macrophage Polarization to a Detrimental M1 Phenotype in the Injured Spinal Cord. *Neuron*. 2014 Sep;83(5):1098–1116. Available from: <http://dx.doi.org/10.1016/j.neuron.2014.07.027>.

- [128] Kratochvill F, Neale G, Haverkamp JM, Van de Velde LA, Smith AM, Kawauchi D, et al. TNF Counterbalances the Emergence of M2 Tumor Macrophages. *Cell Reports*. 2015 Sep;12(11):1902–1914. Available from: <http://dx.doi.org/10.1016/j.celrep.2015.08.033>.
- [129] Nathan CF, Murray HW, Wiebe ME, Rubin BY. Identification of interferon-gamma as the lymphokine that activates human macrophage oxidative metabolism and antimicrobial activity. *The Journal of experimental medicine*. 1983 Sep;158(3):670–689. Available from: <http://dx.doi.org/10.1084/jem.158.3.670>.
- [130] Ivashkiv LB. IFN γ : signalling, epigenetics and roles in immunity, metabolism, disease and cancer immunotherapy. *Nature Reviews Immunology*. 2018 Jun;18(9):545–558. Available from: <http://dx.doi.org/10.1038/s41577-018-0029-z>.
- [131] Luzina IG, Keegan AD, Heller NM, Rook GAW, Shea-Donohue T, Atamas SP. Regulation of inflammation by interleukin-4: a review of “alternatives”. *Journal of Leukocyte Biology*. 2012 Oct;92(4):753–764. Available from: <http://dx.doi.org/10.1189/jlb.0412214>.
- [132] Stein M, Keshav S, Harris N, Gordon S. Interleukin 4 potently enhances murine macrophage mannose receptor activity: a marker of alternative immunologic macrophage activation. *The Journal of experimental medicine*. 1992 Jul;176(1):287–292. Available from: <http://dx.doi.org/10.1084/jem.176.1.287>.
- [133] Ambade A, Satishchandran A, Saha B, Gyongyosi B, Lowe P, Kodys K, et al. Hepatocellular carcinoma is accelerated by NASH involving M2 macrophage polarization mediated by hif-1 α induced IL-10. *OncoImmunology*. 2016 Sep;5(10):e1221557. Available from: <http://dx.doi.org/10.1080/2162402X.2016.1221557>.
- [134] Chen Y, Song Y, Du W, Gong L, Chang H, Zou Z. Tumor-associated macrophages: an accomplice in solid tumor progression. *Journal of Biomedical Science*. 2019 Oct;26(1). Available from: <http://dx.doi.org/10.1186/s12929-019-0568-z>.
- [135] Wei Y, Liang M, Xiong L, Su N, Gao X, Jiang Z. PD-L1 induces macrophage polarization toward the M2 phenotype via Erk/Akt/mTOR. *Experimental Cell Research*. 2021 May;402(2):112575. Available from: <http://dx.doi.org/10.1016/j.yexcr.2021.112575>.
- [136] Zhang F, Wang H, Wang X, Jiang G, Liu H, Zhang G, et al. TGF- β induces M2-like macrophage polarization via SNAIL-mediated suppression of a pro-inflammatory phenotype. *Oncotarget*. 2016 Jul;7(32):52294–52306. Available from: <http://dx.doi.org/10.18632/oncotarget.10561>.
- [137] Chanmee T, Ontong P, Konno K, Itano N. Tumor-Associated Macrophages as Major Players in the Tumor Microenvironment. *Cancers*. 2014 Aug;6(3):1670–1690. Available from: <http://dx.doi.org/10.3390/cancers6031670>.
- [138] Wu X, Lu W, Xu C, Jiang C, Zhuo Z, Wang R, et al. Macrophages Phenotype Regulated by IL-6 Are Associated with the Prognosis of Platinum-Resistant Serous Ovarian Cancer: Integrated Analysis of Clinical Trial and Omics. *Journal of Immunology Research*. 2023 Apr;2023:1–15. Available from: <http://dx.doi.org/10.1155/2023/6455704>.
- [139] Yu XL, Wu BT, Ma TT, Lin Y, Cheng F, Xiong HY, et al. Overexpression of IL-12 reverses the phenotype and function of M2 macrophages to M1 macrophages. *Int J Clin Exp Pathol*.

- 2016;9(9):8963-72. Available from: <https://e-century.us/files/ijcep/9/9/ijcep0035905.pdf>.
- [140] Ye J, Xie C, Wang C, Huang J, Yin Z, Heng BC, et al. Promoting musculoskeletal system soft tissue regeneration by biomaterial-mediated modulation of macrophage polarization. *Bioactive Materials*. 2021 Nov;6(11):4096–4109. Available from: <http://dx.doi.org/10.1016/j.bioactmat.2021.04.017>.
- [141] Konjević GM, Vuletić AM, Mirjačić Martinović KM, Larsen AK, Jurišić VB. The role of cytokines in the regulation of NK cells in the tumor environment. *Cytokine*. 2019 May;117:30–40. Available from: <http://dx.doi.org/10.1016/j.cyto.2019.02.001>.
- [142] Widowati W, K Jasaputra D, B Sumitro S, A Widodo M, Mozef T, Rizal R, et al. Effect of interleukins (IL-2, IL-15, IL-18) on receptors activation and cytotoxic activity of natural killer cells in breast cancer cell. *African Health Sciences*. 2020 Jul;20(2):822–832. Available from: <http://dx.doi.org/10.4314/ahs.v20i2.36>.
- [143] Ferlazzo G, Tsang ML, Moretta L, Melioli G, Steinman RM, Münz C. Human Dendritic Cells Activate Resting Natural Killer (NK) Cells and Are Recognized via the Nkp30 Receptor by Activated NK Cells. *The Journal of Experimental Medicine*. 2002 Feb;195(3):343–351. Available from: <http://dx.doi.org/10.1084/jem.20011149>.
- [144] Kish DD, Gorbachev AV, Fairchild RL. CD8⁺ T cells produce IL-2, which is required for CD4⁺CD25⁺ T cell regulation of effector CD8⁺ T cell development for contact hypersensitivity responses. *Journal of Leukocyte Biology*. 2005 Jul;78(3):725–735. Available from: <http://dx.doi.org/10.1189/jlb.0205069>.
- [145] D'Souza WN, Lefrançois L. Frontline: An in-depth evaluation of the production of IL-2 by antigen-specific CD8 T cells in vivo. *European Journal of Immunology*. 2004 Oct;34(11):2977–2985. Available from: <http://dx.doi.org/10.1002/eji.200425485>.
- [146] Hwang ES, Hong JH, Glimcher LH. IL-2 production in developing Th1 cells is regulated by heterodimerization of RelA and T-bet and requires T-bet serine residue 508. *The Journal of Experimental Medicine*. 2005 Nov;202(9):1289–1300. Available from: <http://dx.doi.org/10.1084/jem.20051044>.
- [147] Bhat P, Leggatt G, Waterhouse N, Frazer IH. Interferon- γ derived from cytotoxic lymphocytes directly enhances their motility and cytotoxicity. *Cell Death & Disease*. 2017 Jun;8(6):e2836–e2836. Available from: <http://dx.doi.org/10.1038/cddis.2017.67>.
- [148] Szabo SJ, Sullivan BM, Stemmann C, Satoskar AR, Sleckman BP, Glimcher LH. Distinct Effects of T-bet in TH1 Lineage Commitment and IFN- γ Production in CD4 and CD8 T Cells. *Science*. 2002 Jan;295(5553):338–342. Available from: <http://dx.doi.org/10.1126/science.1065543>.
- [149] Sojka DK, Fowell DJ. Regulatory T cells inhibit acute IFN- γ synthesis without blocking T-helper cell type 1 (Th1) differentiation via a compartmentalized requirement for IL-10. *Proceedings of the National Academy of Sciences*. 2011 Oct;108(45):18336–18341. Available from: <http://dx.doi.org/10.1073/pnas.1110566108>.
- [150] Cui F, Qu D, Sun R, Zhang M, Nan K. NK cell-produced IFN- γ regulates cell growth and apoptosis of colorectal cancer by regulating IL-15. *Experimental and Therapeutic Medicine*. 2019 Dec. Available from: <http://dx.doi.org/10.3892/etm.2019.8343>.

- [151] Stojanovic A, Fiegler N, Brunner-Weinzierl M, Cerwenka A. CTLA-4 Is Expressed by Activated Mouse NK Cells and Inhibits NK Cell IFN- γ Production in Response to Mature Dendritic Cells. *The Journal of Immunology*. 2014 May;192(9):4184–4191. Available from: <http://dx.doi.org/10.4049/jimmunol.1302091>.
- [152] Mehta AK, Gracias DT, Croft M. TNF activity and T cells. *Cytokine*. 2018 Jan;101:14–18. Available from: <http://dx.doi.org/10.1016/j.cyto.2016.08.003>.
- [153] Basu A, Ramamoorthi G, Albert G, Gallen C, Beyer A, Snyder C, et al. Differentiation and Regulation of TH Cells: A Balancing Act for Cancer Immunotherapy. *Frontiers in Immunology*. 2021 May;12. Available from: <http://dx.doi.org/10.3389/fimmu.2021.669474>.
- [154] Zhang J, Patel MB, Griffiths R, Mao A, Song Ys, Karlovich NS, et al. Tumor Necrosis Factor- α Produced in the Kidney Contributes to Angiotensin II-dependent Hypertension. *Hypertension*. 2014 Dec;64(6):1275–1281. Available from: <http://dx.doi.org/10.1161/HYPERTENSIONAHA.114.03863>.
- [155] Chen S, Saeed AFUH, Liu Q, Jiang Q, Xu H, Xiao GG, et al. Macrophages in immunoregulation and therapeutics. *Signal Transduction and Targeted Therapy*. 2023 May;8(1). Available from: <http://dx.doi.org/10.1038/s41392-023-01452-1>.
- [156] Fauriat C, Long EO, Ljunggren HG, Bryceson YT. Regulation of human NK-cell cytokine and chemokine production by target cell recognition. *Blood*. 2010 Mar;115(11):2167–2176. Available from: <http://dx.doi.org/10.1182/blood-2009-08-238469>.
- [157] Wang R, Jaw JJ, Stutzman NC, Zou Z, Sun PD. Natural killer cell-produced IFN- γ and TNF- α induce target cell cytolysis through up-regulation of ICAM-1. *Journal of Leukocyte Biology*. 2011 Nov;91(2):299–309. Available from: <http://dx.doi.org/10.1189/jlb.0611308>.
- [158] Massagué J. TGF β in Cancer. *Cell*. 2008 Jul;134(2):215–230. Available from: <http://dx.doi.org/10.1016/j.cell.2008.07.001>.
- [159] Tang Q, Bluestone JA. The Foxp3⁺ regulatory T cell: a jack of all trades, master of regulation. *Nature Immunology*. 2008 Feb;9(3):239–244. Available from: <http://dx.doi.org/10.1038/ni1572>.
- [160] Shaul ME, Levy L, Sun J, Mishalian I, Singhal S, Kapoor V, et al. Tumor-associated neutrophils display a distinct N1 profile following TGF β modulation: A transcriptomics analysis of pro- vs. antitumor TANs. *OncoImmunology*. 2016 Sep;5(11):e1232221. Available from: <http://dx.doi.org/10.1080/2162402X.2016.1232221>.
- [161] Zheng XF, Hong YX, Feng GJ, Zhang GF, Rogers H, Lewis MAO, et al. Lipopolysaccharide-Induced M2 to M1 Macrophage Transformation for IL-12p70 Production Is Blocked by *Candida albicans* Mediated Up-Regulation of EB13 Expression. *PLoS ONE*. 2013 May;8(5):e63967. Available from: <http://dx.doi.org/10.1371/journal.pone.0063967>.
- [162] Rahim SS, Khan N, Boddupalli CS, Hasnain SE, Mukhopadhyay S. Interleukin-10 (IL-10) mediated suppression of IL-12 production in RAW 264.7 cells also involves c-rel transcription factor. *Immunology*. 2005 Feb;114(3):313–321. Available from: <http://dx.doi.org/10.1111/j.1365-2567.2005.02107.x>.

- [163] de Waal Malefyt R, Abrams J, Bennett B, Figdor CG, de Vries JE. Interleukin 10(IL-10) inhibits cytokine synthesis by human monocytes: an autoregulatory role of IL-10 produced by monocytes. *The Journal of experimental medicine*. 1991 Nov;174(5):1209–1220. Available from: <http://dx.doi.org/10.1084/jem.174.5.1209>.
- [164] la Sala A, Ferrari D, Corinti S, Cavani A, Di Virgilio F, Girolomoni G. Extracellular ATP Induces a Distorted Maturation of Dendritic Cells and Inhibits Their Capacity to Initiate Th1 Responses. *The Journal of Immunology*. 2001 Feb;166(3):1611–1617. Available from: <http://dx.doi.org/10.4049/jimmunol.166.3.1611>.
- [165] Itakura E, Huang RR, Wen DR, Paul E, Wünsch PH, Cochran AJ. IL-10 expression by primary tumor cells correlates with melanoma progression from radial to vertical growth phase and development of metastatic competence. *Modern Pathology*. 2011 Jun;24(6):801–809. Available from: <http://dx.doi.org/10.1038/modpathol.2011.5>.
- [166] Krüger-Krasagakes S, Krasagakis K, Garbe C, Schmitt E, Hüls C, Blankenstein T, et al. Expression of interleukin 10 in human melanoma. *British Journal of Cancer*. 1994 Dec;70(6):1182–1185. Available from: <http://dx.doi.org/10.1038/bjc.1994.469>.
- [167] Del Prete G, De Carli M, Almerigogna F, Giudizi MG, Biagiotti R, Romagnani S. Human IL-10 is produced by both type 1 helper (Th1) and type 2 helper (Th2) T cell clones and inhibits their antigen-specific proliferation and cytokine production. *Journal of immunology (Baltimore, Md: 1950)*. 1993;150(2):353-60. Available from: <https://pubmed.ncbi.nlm.nih.gov/8419468/>.
- [168] Fiorentino DF, Bond MW, Mosmann TR. Two types of mouse T helper cell. IV. Th2 clones secrete a factor that inhibits cytokine production by Th1 clones. *The Journal of experimental medicine*. 1989 Dec;170(6):2081–2095. Available from: <http://dx.doi.org/10.1084/jem.170.6.2081>.
- [169] Chen L, Shi Y, Zhu X, Guo W, Zhang M, Che Y, et al. IL-10 secreted by cancer-associated macrophages regulates proliferation and invasion in gastric cancer cells via c-Met/STAT3 signaling. *Oncology Reports*. 2019 Jun. Available from: <http://dx.doi.org/10.3892/or.2019.7206>.
- [170] Qi L, Yu H, Zhang Y, Zhao D, Lv P, Zhong Y, et al. IL-10 secreted by M2 macrophage promoted tumorigenesis through interaction with JAK2 in glioma. *Oncotarget*. 2016 Sep;7(44):71673–71685. Available from: <http://dx.doi.org/10.18632/oncotarget.12317>.
- [171] Moore KW, de Waal Malefyt R, Coffman RL, O’Garra A. Interleukin-10 and the Interleukin-10 Receptor. *Annual Review of Immunology*. 2001 Apr;19(1):683–765. Available from: <http://dx.doi.org/10.1146/annurev.immunol.19.1.683>.
- [172] Tsuji-Takayama K, Suzuki M, Yamamoto M, Harashima A, Okochi A, Otani T, et al. The Production of IL-10 by Human Regulatory T Cells Is Enhanced by IL-2 through a STAT5-Responsive Intronic Enhancer in the IL-10 Locus. *The Journal of Immunology*. 2008 Sep;181(6):3897–3905. Available from: <http://dx.doi.org/10.4049/jimmunol.181.6.3897>.
- [173] Malek TR, Castro I. Interleukin-2 Receptor Signaling: At the Interface between Tolerance and Immunity. *Immunity*. 2010 Aug;33(2):153–165. Available from: <http://dx.doi.org/10.1016/j.immuni.2010.08.004>.

- [174] Gadani SP, Cronk JC, Norris GT, Kipnis J. IL-4 in the Brain: A Cytokine To Remember. *The Journal of Immunology*. 2012 Nov;189(9):4213–4219. Available from: <http://dx.doi.org/10.4049/jimmunol.1202246>.
- [175] Xu YD, Cheng M, Shang PP, Yang YQ. Role of IL-6 in dendritic cell functions. *Journal of Leukocyte Biology*. 2021 Aug;111(3):695–709. Available from: <http://dx.doi.org/10.1002/JLB.3MR0621-616RR>.
- [176] Wu X, Tao P, Zhou Q, Li J, Yu Z, Wang X, et al. IL-6 secreted by cancer-associated fibroblasts promotes epithelial-mesenchymal transition and metastasis of gastric cancer via JAK2/STAT3 signaling pathway. *Oncotarget*. 2017 Feb;8(13):20741–20750. Available from: <http://dx.doi.org/10.18632/oncotarget.15119>.
- [177] Sansores-España LD, Melgar-Rodríguez S, Vernal R, Carrillo-Ávila BA, Martínez-Aguilar VM, Díaz-Zúñiga J. Neutrophil N1 and N2 Subsets and Their Possible Association with Periodontitis: A Scoping Review. *International Journal of Molecular Sciences*. 2022 Oct;23(20):12068. Available from: <http://dx.doi.org/10.3390/ijms232012068>.
- [178] Orecchioni M, Ghosheh Y, Pramod AB, Ley K. Macrophage Polarization: Different Gene Signatures in M1(LPS+) vs. Classically and M2(LPS-) vs. Alternatively Activated Macrophages. *Frontiers in Immunology*. 2019 May;10. Available from: <http://dx.doi.org/10.3389/fimmu.2019.01084>.
- [179] Ainscough JS, Frank Gerberick G, Zahedi-Nejad M, Lopez-Castejon G, Brough D, Kimber I, et al. Dendritic Cell IL-1 α and IL-1 β Are Polyubiquitinated and Degraded by the Proteasome. *Journal of Biological Chemistry*. 2014 Dec;289(51):35582–35592. Available from: <http://dx.doi.org/10.1074/jbc.M114.595686>.
- [180] Dinarello CA. Immunological and Inflammatory Functions of the Interleukin-1 Family. *Annual Review of Immunology*. 2009 Apr;27(1):519–550. Available from: <http://dx.doi.org/10.1146/annurev.immunol.021908.132612>.
- [181] Saito H, Kuroda H, Matsunaga T, Osaki T, Ikeguchi M. Increased PD-1 expression on CD4+ and CD8+ T cells is involved in immune evasion in gastric cancer. *Journal of Surgical Oncology*. 2012 Nov;107(5):517–522. Available from: <http://dx.doi.org/10.1002/jso.23281>.
- [182] Wu X, Zhang H, Xing Q, Cui J, Li J, Li Y, et al. PD-1+ CD8+ T cells are exhausted in tumours and functional in draining lymph nodes of colorectal cancer patients. *British Journal of Cancer*. 2014 Aug;111(7):1391–1399. Available from: <http://dx.doi.org/10.1038/bjc.2014.416>.
- [183] Jiang Y, Li Y, Zhu B. T-cell exhaustion in the tumor microenvironment. *Cell Death & Disease*. 2015 Jun;6(6):e1792–e1792. Available from: <http://dx.doi.org/10.1038/cddis.2015.162>.
- [184] Luz-Crawford P, Noël D, Fernandez X, Khoury M, Figueroa F, Carrión F, et al. Mesenchymal Stem Cells Repress Th17 Molecular Program through the PD-1 Pathway. *PLoS ONE*. 2012 Sep;7(9):e45272. Available from: <http://dx.doi.org/10.1371/journal.pone.0045272>.
- [185] Giancchetti E, Fierabracci A. Inhibitory Receptors and Pathways of Lymphocytes: The Role of PD-1 in Treg Development and Their Involvement in Autoimmunity Onset and Cancer Progression. *Frontiers in Immunology*. 2018 Oct;9. Available from: <http://dx.doi.org/10.3389/fimmu.2018.02374>.

- [186] Kono Y, Saito H, Miyauchi W, Shimizu S, Murakami Y, Shishido Y, et al. Increased PD-1-positive macrophages in the tissue of gastric cancer are closely associated with poor prognosis in gastric cancer patients. *BMC Cancer*. 2020 Mar;20(1). Available from: <http://dx.doi.org/10.1186/s12885-020-6629-6>.
- [187] Gordon SR, Maute RL, Dulken BW, Hutter G, George BM, McCracken MN, et al. PD-1 expression by tumour-associated macrophages inhibits phagocytosis and tumour immunity. *Nature*. 2017 May;545(7655):495–499. Available from: <http://dx.doi.org/10.1038/nature22396>.
- [188] Lei Q, Wang D, Sun K, Wang L, Zhang Y. Resistance Mechanisms of Anti-PD1/PDL1 Therapy in Solid Tumors. *Frontiers in Cell and Developmental Biology*. 2020 Jul;8. Available from: <http://dx.doi.org/10.3389/fcell.2020.00672>.
- [189] Koyama S, Akbay EA, Li YY, Herter-Sprue GS, Buczkowski KA, Richards WG, et al. Adaptive resistance to therapeutic PD-1 blockade is associated with upregulation of alternative immune checkpoints. *Nature Communications*. 2016 Feb;7(1). Available from: <http://dx.doi.org/10.1038/ncomms10501>.
- [190] Jenkins RW, Barbie DA, Flaherty KT. Mechanisms of resistance to immune checkpoint inhibitors. *British Journal of Cancer*. 2018 Jan;118(1):9–16. Available from: <http://dx.doi.org/10.1038/bjc.2017.434>.
- [191] Zheng Y, Fang YC, Li J. PD-L1 expression levels on tumor cells affect their immunosuppressive activity. *Oncology Letters*. 2019 Sep. Available from: <http://dx.doi.org/10.3892/ol.2019.10903>.
- [192] Oh SA, Wu DC, Cheung J, Navarro A, Xiong H, Cubas R, et al. PD-L1 expression by dendritic cells is a key regulator of T-cell immunity in cancer. *Nature Cancer*. 2020 Jun;1(7):681–691. Available from: <http://dx.doi.org/10.1038/s43018-020-0075-x>.
- [193] Zheng Y, Han L, Chen Z, Li Y, Zhou B, Hu R, et al. PD-L1+CD8+ T cells enrichment in lung cancer exerted regulatory function and tumor-promoting tolerance. *iScience*. 2022 Feb;25(2):103785. Available from: <http://dx.doi.org/10.1016/j.isci.2022.103785>.
- [194] Kowanetz M, Zou W, Gettinger SN, Koeppen H, Kockx M, Schmid P, et al. Differential regulation of PD-L1 expression by immune and tumor cells in NSCLC and the response to treatment with atezolizumab (anti-PD-L1). *Proceedings of the National Academy of Sciences*. 2018 Oct;115(43). Available from: <http://dx.doi.org/10.1073/pnas.1802166115>.
- [195] Chen L. Co-inhibitory molecules of the B7–CD28 family in the control of T-cell immunity. *Nature Reviews Immunology*. 2004 May;4(5):336–347. Available from: <http://dx.doi.org/10.1038/nri1349>.
- [196] Teramoto K, Igarashi T, Kataoka Y, Ishida M, Hanaoka J, Sumimoto H, et al. Clinical significance of PD-L1-positive cancer-associated fibroblasts in pN0M0 non-small cell lung cancer. *Lung Cancer*. 2019 Nov;137:56–63. Available from: <http://dx.doi.org/10.1016/j.lungcan.2019.09.013>.
- [197] Yoshikawa K, Ishida M, Yanai H, Tsuta K, Sekimoto M, Sugie T. Prognostic significance of PD-L1-positive cancer-associated fibroblasts in patients with triple-negative breast cancer. *BMC Cancer*. 2021 Mar;21(1). Available from: <http://dx.doi.org/10.1186/s12885-021-07970-x>.

- [198] Pei L, Liu Y, Liu L, Gao S, Gao X, Feng Y, et al. Roles of cancer-associated fibroblasts (CAFs) in anti-PD-1/PD-L1 immunotherapy for solid cancers. *Molecular Cancer*. 2023 Feb;22(1). Available from: <http://dx.doi.org/10.1186/s12943-023-01731-z>.
- [199] Zhu Z, Zhang H, Chen B, Liu X, Zhang S, Zong Z, et al. PD-L1-Mediated Immunosuppression in Glioblastoma Is Associated With the Infiltration and M2-Polarization of Tumor-Associated Macrophages. *Frontiers in Immunology*. 2020 Nov;11. Available from: <http://dx.doi.org/10.3389/fimmu.2020.588552>.
- [200] Yajuk O, Baron M, Toker S, Zelter T, Fainsod-Levi T, Granot Z. The PD-L1/PD-1 Axis Blocks Neutrophil Cytotoxicity in Cancer. *Cells*. 2021 Jun;10(6):1510. Available from: <http://dx.doi.org/10.3390/cells10061510>.
- [201] Khou S, Popa A, Luci C, Bihl F, Meghraoui-Kheddar A, Bourdely P, et al. Tumor-Associated Neutrophils Dampen Adaptive Immunity and Promote Cutaneous Squamous Cell Carcinoma Development. *Cancers*. 2020 Jul;12(7):1860. Available from: <http://dx.doi.org/10.3390/cancers12071860>.
- [202] Lin DYw, Tanaka Y, Iwasaki M, Gittis AG, Su HP, Mikami B, et al. The PD-1/PD-L1 complex resembles the antigen-binding Fv domains of antibodies and T cell receptors. *Proceedings of the National Academy of Sciences*. 2008 Feb;105(8):3011–3016. Available from: <http://dx.doi.org/10.1073/pnas.0712278105>.
- [203] Maute RL, Gordon SR, Mayer AT, McCracken MN, Natarajan A, Ring NG, et al. Engineering high-affinity PD-1 variants for optimized immunotherapy and immuno-PET imaging. *Proceedings of the National Academy of Sciences*. 2015 Nov;112(47). Available from: <http://dx.doi.org/10.1073/pnas.1519623112>.
- [204] Rowshanravan B, Halliday N, Sansom DM. CTLA-4: a moving target in immunotherapy. *Blood*. 2018 Jan;131(1):58–67. Available from: <http://dx.doi.org/10.1182/blood-2017-06-741033>.
- [205] Ha D, Tanaka A, Kibayashi T, Tanemura A, Sugiyama D, Wing JB, et al. Differential control of human Treg and effector T cells in tumor immunity by Fc-engineered anti-CTLA-4 antibody. *Proceedings of the National Academy of Sciences*. 2018 Dec;116(2):609–618. Available from: <http://dx.doi.org/10.1073/pnas.1812186116>.
- [206] Alegre ML, Shiels H, Thompson CB, Gajewski TF. Expression and Function of CTLA-4 in Th1 and Th2 Cells. *The Journal of Immunology*. 1998 Oct;161(7):3347–3356. Available from: <http://dx.doi.org/10.4049/jimmunol.161.7.3347>.
- [207] Jain N, Nguyen H, Chambers C, Kang J. Dual function of CTLA-4 in regulatory T cells and conventional T cells to prevent multiorgan autoimmunity. *Proceedings of the National Academy of Sciences*. 2010 Jan;107(4):1524–1528. Available from: <http://dx.doi.org/10.1073/pnas.0910341107>.
- [208] Takahashi T, Tagami T, Yamazaki S, Uede T, Shimizu J, Sakaguchi N, et al. Immunologic Self-Tolerance Maintained by Cd25+ Cd4+ Regulatory T Cells Constitutively Expressing Cytotoxic T Lymphocyte-Associated Antigen 4. *The Journal of Experimental Medicine*. 2000 Jul;192(2):303–310. Available from: <http://dx.doi.org/10.1084/jem.192.2.303>.

- [209] Potdar PD, Chaudhary S. Molecular characterization of cancer-associated fibroblasts isolated from human colorectal cancer as a major stromal cell component promoting metastasis. *Journal of Unexplored Medical Data*. 2017 Feb;2(1). Available from: <http://dx.doi.org/10.20517/2572-8180.2016.10>.
- [210] Sharp SP, Avram D, Stain SC, Lee EC. Local and systemic Th17 immune response associated with advanced stage colon cancer. *Journal of Surgical Research*. 2017 Feb;208:180–186. Available from: <http://dx.doi.org/10.1016/j.jss.2016.09.038>.
- [211] Calu V, Ionescu A, Stanca L, Geicu OI, Iordache F, Pisoschi AM, et al. Key biomarkers within the colorectal cancer related inflammatory microenvironment. *Scientific Reports*. 2021 Apr;11(1). Available from: <http://dx.doi.org/10.1038/s41598-021-86941-5>.
- [212] Zhang W, An F, Xia M, Zhan Q, Tian W, Jiao Y. Increased HMGB1 expression correlates with higher expression of c-IAP2 and pERK in colorectal cancer. *Medicine*. 2019 Jan;98(3):e14069. Available from: <http://dx.doi.org/10.1097/MD.0000000000014069>.
- [213] Pellegatti P, Raffaghello L, Bianchi G, Piccardi F, Pistoia V, Di Virgilio F. Increased Level of Extracellular ATP at Tumor Sites: In Vivo Imaging with Plasma Membrane Luciferase. *PLoS ONE*. 2008 Jul;3(7):e2599. Available from: <http://dx.doi.org/10.1371/journal.pone.0002599>.
- [214] Di Virgilio F, Adinolfi E. Extracellular purines, purinergic receptors and tumor growth. *Oncogene*. 2016 Jun;36(3):293–303. Available from: <http://dx.doi.org/10.1038/onc.2016.206>.
- [215] Cao Y, Chen E, Wang X, Song J, Zhang H, Chen X. An emerging master inducer and regulator for epithelial-mesenchymal transition and tumor metastasis: extracellular and intracellular ATP and its molecular functions and therapeutic potential. *Cancer Cell International*. 2023 Feb;23(1). Available from: <http://dx.doi.org/10.1186/s12935-023-02859-0>.
- [216] Abdullah TM, Whatmore J, Bremer E, Slibinskas R, Michalak M, Eggleton P. Endoplasmic reticulum stress-induced release and binding of calreticulin from human ovarian cancer cells. *Cancer Immunology, Immunotherapy*. 2021 Nov;71(7):1655–1669. Available from: <http://dx.doi.org/10.1007/s00262-021-03072-6>.
- [217] Autenshlyus AI, Arkhipov SA, Kunts TA, Marinkin IO, Mikhailova ES, Karpukhina XV, et al. Cytokine profiles of tumor supernatants in invasive ductal cancer and fibroadenoma of the breast and its relationship with VEGF-A expression in the tumors. *International Journal of Immunopathology and Pharmacology*. 2017 Jan;30(1):83–88. Available from: <http://dx.doi.org/10.1177/0394632016681306>.
- [218] Wang J, Xu K, Wu J, Luo C, Li Y, Wu X, et al. The changes of Th17 cells and the related cytokines in the progression of human colorectal cancers. *BMC Cancer*. 2012 Sep;12(1). Available from: <http://dx.doi.org/10.1186/1471-2407-12-418>.
- [219] Bersano J, Lashuk K, Edinger A, Schueler J. A Subset of Colon Cancer Cell Lines Displays a Cytokine Profile Linked to Angiogenesis, EMT and Invasion Which Is Modulated by the Culture Conditions In Vitro. *Cells*. 2023 Oct;12(21):2539. Available from: <http://dx.doi.org/10.3390/cells12212539>.

- [220] Park JY, Kim SH, Lee SM, Lee JS, Han JK. CT volumetric measurement of colorectal cancer helps predict tumor staging and prognosis. *PLOS ONE*. 2017 Jun;12(6):e0178522. Available from: <http://dx.doi.org/10.1371/journal.pone.0178522>.
- [221] Rössler O, Betge J, Harbaum L, Mrak K, Tschmelitsch J, Langner C. Tumor size, tumor location, and antitumor inflammatory response are associated with lymph node size in colorectal cancer patients. *Modern Pathology*. 2017 Jun;30(6):897–904. Available from: <http://dx.doi.org/10.1038/modpathol.2016.227>.
- [222] Zandarashvili L, Sahu D, Lee K, Lee YS, Singh P, Rajarathnam K, et al. Real-time Kinetics of High-mobility Group Box 1 (HMGB1) Oxidation in Extracellular Fluids Studied by in Situ Protein NMR Spectroscopy. *Journal of Biological Chemistry*. 2013 Apr;288(17):11621–11627. Available from: <http://dx.doi.org/10.1074/jbc.M113.449942>.
- [223] Nandigama R, Padmasekar M, Wartenberg M, Sauer H. Feed Forward Cycle of Hypotonic Stress-induced ATP Release, Purinergic Receptor Activation, and Growth Stimulation of Prostate Cancer Cells. *Journal of Biological Chemistry*. 2006 Mar;281(9):5686–5693. Available from: <http://dx.doi.org/10.1074/jbc.M510452200>.
- [224] Goicoechea SM, Murphy-Ullrich JE. In: *Cell Surface Calreticulin: Role in Signaling Thrombospondin Anti-Adhesive Activity*. Springer US; 2003. p. 193–204. Available from: http://dx.doi.org/10.1007/978-1-4419-9258-1_18.
- [225] Zhang Y, Thangam R, You SH, Sultonova RD, Venu A, Min JJ, et al. Engineering Calreticulin-Targeting Monobodies to Detect Immunogenic Cell Death in Cancer Chemotherapy. *Cancers*. 2021 Jun;13(11):2801. Available from: <http://dx.doi.org/10.3390/cancers13112801>.
- [226] Ruedl C, Koebel P, Bachmann M, Hess M, Karjalainen K. Anatomical Origin of Dendritic Cells Determines Their Life Span in Peripheral Lymph Nodes. *The Journal of Immunology*. 2000 Nov;165(9):4910–4916. Available from: <http://dx.doi.org/10.4049/jimmunol.165.9.4910>.
- [227] Kamath AT, Henri S, Battye F, Tough DF, Shortman K. Developmental kinetics and lifespan of dendritic cells in mouse lymphoid organs. *Blood*. 2002 Sep;100(5):1734–1741. Available from: http://dx.doi.org/10.1182/blood.V100.5.1734.h81702001734_1734_1741.
- [228] Takada K, Jameson SC. Self-class I MHC molecules support survival of naive CD8 T cells, but depress their functional sensitivity through regulation of CD8 expression levels. *Journal of Experimental Medicine*. 2009 Sep;206(10):2253–2269. Available from: <http://dx.doi.org/10.1084/jem.20082553>.
- [229] Hellerstein M, Hanley MB, Cesar D, Siler S, Papageorgopoulos C, Wieder E, et al. Directly measured kinetics of circulating T lymphocytes in normal and HIV-1-infected humans. *Nature Medicine*. 1999 Jan;5(1):83–89. Available from: <http://dx.doi.org/10.1038/4772>.
- [230] Vukmanovic-Stejic M, Zhang Y, Cook JE, Fletcher JM, McQuaid A, Masters JE, et al. Human CD4+ CD25hi Foxp3+ regulatory T cells are derived by rapid turnover of memory populations in vivo. *Journal of Clinical Investigation*. 2006 Sep;116(9):2423–2433. Available from: <http://dx.doi.org/10.1172/JCI28941>.
- [231] Louzoun Y, Xue C, Lesinski GB, Friedman A. A mathematical model for pancreatic cancer growth and treatments. *Journal of Theoretical Biology*. 2014 Jun;351:74–82. Available from: <http://dx.doi.org/10.1016/j.jtbi.2014.02.028>.

- [232] Coffelt SB, Wellenstein MD, de Visser KE. Neutrophils in cancer: neutral no more. *Nature Reviews Cancer*. 2016 Jun;16(7):431–446. Available from: <http://dx.doi.org/10.1038/nrc.2016.52>.
- [233] Ocana A, Nieto-Jiménez C, Pandiella A, Templeton AJ. Neutrophils in cancer: prognostic role and therapeutic strategies. *Molecular Cancer*. 2017 Aug;16(1). Available from: <http://dx.doi.org/10.1186/s12943-017-0707-7>.
- [234] Patel AA, Zhang Y, Fullerton JN, Boelen L, Rongvaux A, Maini AA, et al. The fate and lifespan of human monocyte subsets in steady state and systemic inflammation. *Journal of Experimental Medicine*. 2017 Jun;214(7):1913–1923. Available from: <http://dx.doi.org/10.1084/jem.20170355>.
- [235] Wu SY, Fu T, Jiang YZ, Shao ZM. Natural killer cells in cancer biology and therapy. *Molecular Cancer*. 2020 Aug;19(1). Available from: <http://dx.doi.org/10.1186/s12943-020-01238-x>.
- [236] Lowry LE, Zehring WA. Potentiation of Natural Killer Cells for Cancer Immunotherapy: A Review of Literature. *Frontiers in Immunology*. 2017 Sep;8. Available from: <http://dx.doi.org/10.3389/fimmu.2017.01061>.
- [237] Lotze MT, Matory YL, Ettinghausen SE, Rayner AA, Sharrow SO, Seipp CA, et al. In vivo administration of purified human interleukin 2. II. Half life, immunologic effects, and expansion of peripheral lymphoid cells in vivo with recombinant IL 2. *The Journal of Immunology*. 1985 Oct;135(4):2865–2875. Available from: <http://dx.doi.org/10.4049/jimmunol.135.4.2865>.
- [238] Lotze MT, Matory YL, Ettinghausen SE, Rayner AA, Sharrow SO, Seipp CA, et al. In vivo administration of purified human interleukin 2. II. Half life, immunologic effects, and expansion of peripheral lymphoid cells in vivo with recombinant IL 2. *The Journal of Immunology*. 1985 Oct;135(4):2865–2875. Available from: <http://dx.doi.org/10.4049/jimmunol.135.4.2865>.
- [239] Balachandran S, Adams GP. Interferon- γ -Induced Necrosis: An Antitumor Biotherapeutic Perspective. *Journal of Interferon & Cytokine Research*. 2013 Apr;33(4):171–180. Available from: <http://dx.doi.org/10.1089/jir.2012.0087>.
- [240] Ma Y, Zhao S, Shen S, Fang S, Ye Z, Shi Z, et al. A novel recombinant slow-release TNF α -derived peptide effectively inhibits tumor growth and angiogenesis. *Scientific Reports*. 2015 Sep;5(1). Available from: <http://dx.doi.org/10.1038/srep13595>.
- [241] Oliver J, Bland L, Oettinger C, Arduino M, McAllister S, Aguero S, et al. Cytokine kinetics in an in vitro whole blood model following an endotoxin challenge. *Lymphokine and cytokine research*. 1993 April;12(2):115–120. Available from: <https://pubmed.ncbi.nlm.nih.gov/8324076/>.
- [242] Tirado-Rodríguez B, Ortega E, Segura-Medina P, Huerta-Yepez S. TGF- β : An Important Mediator of Allergic Disease and a Molecule with Dual Activity in Cancer Development. *Journal of Immunology Research*. 2014;2014:1–15. Available from: <http://dx.doi.org/10.1155/2014/318481>.
- [243] Jung K, Ha JH, Kim JE, Kim JA, Kim YJ, Kim CH, et al. Heterodimeric Fc-fused IL12 shows potent antitumor activity by generating memory CD8⁺ T cells. *OncoImmunology*. 2018 Mar;7(7):e1438800. Available from: <http://dx.doi.org/10.1080/2162402X.2018.1438800>.

- [244] Huhn RD, Radwanski E, Gallo J, Afrime MB, Sabo R, Gonyo G, et al. Pharmacodynamics of subcutaneous recombinant human interleukin-10 in healthy volunteers. *Clinical Pharmacology & Therapeutics*. 1997 Aug;62(2):171–180. Available from: [http://dx.doi.org/10.1016/S0009-9236\(97\)90065-5](http://dx.doi.org/10.1016/S0009-9236(97)90065-5).
- [245] Prendiville J, Thatcher N, Lind M, McIntosh R, Ghosh A, Stern P, et al. Recombinant human interleukin-4 (rhu IL-4) administered by the intravenous and subcutaneous routes in patients with advanced cancer—A phase I toxicity study and pharmacokinetic analysis. *European Journal of Cancer*. 1993 Jan;29(12):1700–1707. Available from: [http://dx.doi.org/10.1016/0959-8049\(93\)90108-r](http://dx.doi.org/10.1016/0959-8049(93)90108-r).
- [246] Wirtz DC, Heller KD, Miltner O, Zilkens KW, Wolff JM. Interleukin-6: a potential inflammatory marker after total joint replacement. *International Orthopaedics*. 2000 Oct;24(4):194–196. Available from: <http://dx.doi.org/10.1007/s002640000136>.
- [247] Lachmann HJ, Lowe P, Felix SD, Rordorf C, Leslie K, Madhoo S, et al. In vivo regulation of interleukin 1 β in patients with cryopyrin-associated periodic syndromes. *Journal of Experimental Medicine*. 2009 Apr;206(5):1029–1036. Available from: <http://dx.doi.org/10.1084/jem.20082481>.
- [248] Longoria TC, Tewari KS. Evaluation of the pharmacokinetics and metabolism of pembrolizumab in the treatment of melanoma. *Expert Opinion on Drug Metabolism & Toxicology*. 2016 Aug;12(10):1247–1253. Available from: <http://dx.doi.org/10.1080/17425255.2016.1216976>.
- [249] Dang TO, Ogunniyi A, Barbee MS, Drilon A. Pembrolizumab for the treatment of PD-L1 positive advanced or metastatic non-small cell lung cancer. *Expert Review of Anticancer Therapy*. 2015 Dec;16(1):13–20. Available from: <http://dx.doi.org/10.1586/14737140.2016.1123626>.
- [250] Cheng X, Veverka V, Radhakrishnan A, Waters LC, Muskett FW, Morgan SH, et al. Structure and Interactions of the Human Programmed Cell Death 1 Receptor. *Journal of Biological Chemistry*. 2013 Apr;288(17):11771–11785. Available from: <http://dx.doi.org/10.1074/jbc.M112.448126>.
- [251] Pluim D, Ros W, Miedema IHC, Beijnen JH, Schellens JHM. Multiparameter Flow Cytometry Assay for Quantification of Immune Cell Subsets, PD-1 Expression Levels and PD-1 Receptor Occupancy by Nivolumab and Pembrolizumab. *Cytometry Part A*. 2019 Aug;95(10):1053–1065. Available from: <http://dx.doi.org/10.1002/cyto.a.23873>.
- [252] Saito A, Tojo M, Kumagai Y, Ohzawa H, Yamaguchi H, Miyato H, et al. Flow cytometry detection of cell type-specific expression of programmed death receptor ligand-1 (PD-L1) in colorectal cancer specimens. *Heliyon*. 2021 Jan;7(1):e05880. Available from: <http://dx.doi.org/10.1016/j.heliyon.2020.e05880>.
- [253] Moreira TG, Mangani D, Cox LM, Leibowitz J, Lobo ELC, Oliveira MA, et al. PD-L1+ and XCR1+ dendritic cells are region-specific regulators of gut homeostasis. *Nature Communications*. 2021 Aug;12(1). Available from: <http://dx.doi.org/10.1038/s41467-021-25115-3>.
- [254] Lai X, Friedman A. Mathematical modeling of cancer treatment with radiation and PD-L1 inhibitor. *Science China Mathematics*. 2020 Feb;63(3):465–484. Available from: <http://dx.doi.org/10.1007/s11425-019-1648-6>.

- [255] Catron DM, Itano AA, Pape KA, Mueller DL, Jenkins MK. Visualizing the First 50 Hr of the Primary Immune Response to a Soluble Antigen. *Immunity*. 2004 Sep;21(3):341–347. Available from: <http://dx.doi.org/10.1016/j.immuni.2004.08.007>.
- [256] Kinjyo I, Qin J, Tan SY, Wellard CJ, Mrass P, Ritchie W, et al. Real-time tracking of cell cycle progression during CD8+ effector and memory T-cell differentiation. *Nature Communications*. 2015 Feb;6(1). Available from: <http://dx.doi.org/10.1038/ncomms7301>.
- [257] Kaech SM, Ahmed R. Memory CD8+ T cell differentiation: initial antigen encounter triggers a developmental program in naïve cells. *Nature Immunology*. 2001 May;2(5):415–422. Available from: <http://dx.doi.org/10.1038/87720>.
- [258] Masopust D, Murali-Krishna K, Ahmed R. Quantitating the Magnitude of the Lymphocytic Choriomeningitis Virus-Specific CD8 T-Cell Response: It Is Even Bigger than We Thought. *Journal of Virology*. 2007 Feb;81(4):2002–2011. Available from: <http://dx.doi.org/10.1128/jvi.01459-06>.
- [259] McLane LM, Abdel-Hakeem MS, Wherry EJ. CD8 T Cell Exhaustion During Chronic Viral Infection and Cancer. *Annual Review of Immunology*. 2019 Apr;37(1):457–495. Available from: <http://dx.doi.org/10.1146/annurev-immunol-041015-055318>.
- [260] Jolley-Gibbs DM, Lepak NM, Yen M, Swain SL. Two Distinct Stages in the Transition from Naive CD4 T Cells to Effectors, Early Antigen-Dependent and Late Cytokine-Driven Expansion and Differentiation. *The Journal of Immunology*. 2000 Nov;165(9):5017–5026. Available from: <http://dx.doi.org/10.4049/jimmunol.165.9.5017>.
- [261] Kaech SM, Wherry EJ, Ahmed R. Effector and memory T-cell differentiation: implications for vaccine development. *Nature Reviews Immunology*. 2002 Apr;2(4):251–262. Available from: <http://dx.doi.org/10.1038/nri778>.
- [262] Homann D, Teyton L, Oldstone MBA. Differential regulation of antiviral T-cell immunity results in stable CD8+ but declining CD4+ T-cell memory. *Nature Medicine*. 2001 Aug;7(8):913–919. Available from: <http://dx.doi.org/10.1038/90950>.
- [263] Darrasse-Jèze G, Bergot AS, Durgeau A, Billiard F, Salomon BL, Cohen JL, et al. Tumor emergence is sensed by self-specific CD44hi memory Tregs that create a dominant tolerogenic environment for tumors in mice. *Journal of Clinical Investigation*. 2009 Aug. Available from: <http://dx.doi.org/10.1172/JCI36628>.
- [264] Newman AM, Steen CB, Liu CL, Gentles AJ, Chaudhuri AA, Scherer F, et al. Determining cell type abundance and expression from bulk tissues with digital cytometry. *Nature Biotechnology*. 2019 May;37(7):773–782. Available from: <http://dx.doi.org/10.1038/s41587-019-0114-2>.
- [265] Le T, Aronow RA, Kirshtein A, Shahriyari L. A review of digital cytometry methods: estimating the relative abundance of cell types in a bulk of cells. *Briefings in Bioinformatics*. 2020 Oct;22(4). Available from: <http://dx.doi.org/10.1093/bib/bbaa219>.
- [266] Gong T, Hartmann N, Kohane IS, Brinkmann V, Staedtler F, Letzkus M, et al. Optimal Deconvolution of Transcriptional Profiling Data Using Quadratic Programming with Application to Complex Clinical Blood Samples. *PLoS ONE*. 2011 Nov;6(11):e27156. Available from: <http://dx.doi.org/10.1371/journal.pone.0027156>.

- [267] Liebner DA, Huang K, Parvin JD. MMAD: microarray microdissection with analysis of differences is a computational tool for deconvoluting cell type-specific contributions from tissue samples. *Bioinformatics*. 2013 Oct;30(5):682–689. Available from: <http://dx.doi.org/10.1093/bioinformatics/btt566>.
- [268] Newman AM, Liu CL, Green MR, Gentles AJ, Feng W, Xu Y, et al. Robust enumeration of cell subsets from tissue expression profiles. *Nature Methods*. 2015 Mar;12(5):453–457. Available from: <http://dx.doi.org/10.1038/nmeth.3337>.
- [269] Goldman MJ, Craft B, Hastie M, Repečka K, McDade F, Kamath A, et al. Visualizing and interpreting cancer genomics data via the Xena platform. *Nature Biotechnology*. 2020 May;38(6):675–678. Available from: <http://dx.doi.org/10.1038/s41587-020-0546-8>.
- [270] Grossman RL, Heath AP, Ferretti V, Varmus HE, Lowy DR, Kibbe WA, et al. Toward a Shared Vision for Cancer Genomic Data. *New England Journal of Medicine*. 2016 Sep;375(12):1109–1112. Available from: <http://dx.doi.org/10.1056/NEJMp1607591>.
- [271] Kautto EA, Bonneville R, Miya J, Yu L, Krook MA, Reeser JW, et al. Performance evaluation for rapid detection of pan-cancer microsatellite instability with MANTIS. *Oncotarget*. 2016 Dec;8(5):7452–7463. Available from: <http://dx.doi.org/10.18632/oncotarget.13918>.
- [272] Miao YR, Zhang Q, Lei Q, Luo M, Xie GY, Wang H, et al. ImmuCellAI: A Unique Method for Comprehensive T-Cell Subsets Abundance Prediction and its Application in Cancer Immunotherapy. *Advanced Science*. 2020 Feb;7(7). Available from: <http://dx.doi.org/10.1002/adv.201902880>.
- [273] Sutton GJ, Poppe D, Simmons RK, Walsh K, Nawaz U, Lister R, et al. Comprehensive evaluation of deconvolution methods for human brain gene expression. *Nature Communications*. 2022 Mar;13(1). Available from: <http://dx.doi.org/10.1038/s41467-022-28655-4>.
- [274] Chen Q, Yin H, Liu S, Shoucair S, Ding N, Ji Y, et al. Prognostic value of tumor-associated N1/N2 neutrophil plasticity in patients following radical resection of pancreas ductal adenocarcinoma. *Journal for ImmunoTherapy of Cancer*. 2022 Dec;10(12):e005798. Available from: <http://dx.doi.org/10.1136/jitc-2022-005798>.
- [275] Yin H, Gao S, Chen Q, Liu S, Shoucair S, Ji Y, et al. Tumor-associated N1 and N2 neutrophils predict prognosis in patients with resected pancreatic ductal adenocarcinoma: A preliminary study. *MedComm*. 2022 Nov;3(4). Available from: <http://dx.doi.org/10.1002/mco2.183>.
- [276] Sender R, Weiss Y, Navon Y, Milo I, Azulay N, Keren L, et al. The total mass, number, and distribution of immune cells in the human body. *Proceedings of the National Academy of Sciences*. 2023 Oct;120(44). Available from: <http://dx.doi.org/10.1073/pnas.2308511120>.
- [277] Maini R, Nagalli S. *Lymphadenopathy*. StatPearls Publishing, Treasure Island (FL); 2023. Available from: <https://www.ncbi.nlm.nih.gov/books/NBK558918/>.
- [278] West H, Jin J. Lymph Nodes and Lymphadenopathy in Cancer. *JAMA Oncology*. 2016 Jul;2(7):971. Available from: <http://dx.doi.org/10.1001/jamaoncol.2015.3509>.
- [279] Becht E, Giraldo NA, Lacroix L, Buttard B, Elarouci N, Petitprez F, et al. Estimating the population abundance of tissue-infiltrating immune and stromal cell populations using gene expression. *Genome Biology*. 2016 Oct;17(1). Available from: <http://dx.doi.org/10.1186/s13059-016-1070-5>.

- [280] Sturm G, Finotello F, Petitprez F, Zhang JD, Baumbach J, Fridman WH, et al. Comprehensive evaluation of transcriptome-based cell-type quantification methods for immunoncology. *Bioinformatics*. 2019 Jul;35(14):i436–i445. Available from: <http://dx.doi.org/10.1093/bioinformatics/btz363>.
- [281] Burke JR, Brown P, Quyn A, Lambie H, Tolan D, Sagar P. Tumour growth rate of carcinoma of the colon and rectum: retrospective cohort study. *BJS Open*. 2020 Sep;4(6):1200–1207. Available from: <http://dx.doi.org/10.1002/bjs5.50355>.
- [282] Clough E, Barrett T. In: *The Gene Expression Omnibus Database*. Springer New York; 2016. p. 93–110. Available from: http://dx.doi.org/10.1007/978-1-4939-3578-9_5.
- [283] Barrett T, Wilhite SE, Ledoux P, Evangelista C, Kim IF, Tomashevsky M, et al. NCBI GEO: archive for functional genomics data sets—update. *Nucleic Acids Research*. 2012 Nov;41(D1):D991–D995. Available from: <http://dx.doi.org/10.1093/nar/gks1193>.
- [284] Leydold SM, Seewald M, Stratowa C, Kaserer K, Sommergruber W, Kraut N, et al. Peroxiredoxin-4 is Over-Expressed in Colon Cancer and its Down-Regulation Leads to Apoptosis. *Cancer Growth and Metastasis*. 2011 Jan;4:CGM.S6584. Available from: <http://dx.doi.org/10.4137/CGM.S6584>.
- [285] Derwinger K, Kodeda K, Bexe-Lindskog E, Taflin H. Tumour differentiation grade is associated with TNM staging and the risk of node metastasis in colorectal cancer. *Acta Oncologica*. 2009 Dec;49(1):57–62. Available from: <http://dx.doi.org/10.3109/02841860903334411>.
- [286] Lala M, Li TR, de Alwis DP, Sinha V, Mayawala K, Yamamoto N, et al. A six-weekly dosing schedule for pembrolizumab in patients with cancer based on evaluation using modelling and simulation. *European Journal of Cancer*. 2020 May;131:68–75. Available from: <http://dx.doi.org/10.1016/j.ejca.2020.02.016>.
- [287] Wang DY, Johnson DB, Davis EJ. Toxicities Associated With PD-1/PD-L1 Blockade. *The Cancer Journal*. 2018 Jan;24(1):36–40. Available from: <http://dx.doi.org/10.1097/PP0.000000000000296>.
- [288] Martins F, Sofiya L, Sykiotis GP, Lamine F, Maillard M, Fraga M, et al. Adverse effects of immune-checkpoint inhibitors: epidemiology, management and surveillance. *Nature Reviews Clinical Oncology*. 2019 May;16(9):563–580. Available from: <http://dx.doi.org/10.1038/s41571-019-0218-0>.
- [289] Robert C, Schachter J, Long GV, Arance A, Grob JJ, Mortier L, et al. Pembrolizumab versus Ipilimumab in Advanced Melanoma. *New England Journal of Medicine*. 2015 Jun;372(26):2521–2532. Available from: <http://dx.doi.org/10.1056/NEJMoa1503093>.
- [290] Chatterjee M, Turner DC, Felip E, Lena H, Cappuzzo F, Horn L, et al. Systematic evaluation of pembrolizumab dosing in patients with advanced non-small-cell lung cancer. *Annals of Oncology*. 2016 Jul;27(7):1291–1298. Available from: <http://dx.doi.org/10.1093/annonc/mdw174>.
- [291] Merck. KEYTRUDA (pembrolizumab) injection Label; 2021. Available from: https://www.accessdata.fda.gov/drugsatfda_docs/label/2021/125514s0961b1.pdf.

- [292] Simeone E, Mallardo D, Giannarelli D, Festino L, Vanella V, Trojaniello C, et al. Correlation of nivolumab 480 mg Q4W with better survival than other nivolumab monotherapy schedule in metastatic melanoma patients. *Journal of Clinical Oncology*. 2020 May;38(15_suppl):e22008–e22008. Available from: http://dx.doi.org/10.1200/JCO.2020.38.15_suppl.e22008.
- [293] Huang AC, Orlowski RJ, Xu X, Mick R, George SM, Yan PK, et al. A single dose of neoadjuvant PD-1 blockade predicts clinical outcomes in resectable melanoma. *Nature Medicine*. 2019 Feb;25(3):454–461. Available from: <http://dx.doi.org/10.1038/s41591-019-0357-y>.
- [294] Justesen TF, Gögenur I, Tarpgaard LS, Pfeiffer P, Qvortrup C. Evaluating the efficacy and safety of neoadjuvant pembrolizumab in patients with stage I–III MMR-deficient colon cancer: a national, multicentre, prospective, single-arm, phase II study protocol. *BMJ Open*. 2023 Jun;13(6):e073372. Available from: <http://dx.doi.org/10.1136/bmjopen-2023-073372>.
- [295] Barua S, Fang P, Sharma A, Fujimoto J, Wistuba I, Rao AUK, et al. Spatial interaction of tumor cells and regulatory T cells correlates with survival in non-small cell lung cancer. *Lung Cancer*. 2018 Mar;117:73–79. Available from: <http://dx.doi.org/10.1016/j.lungcan.2018.01.022>.
- [296] Maley CC, Koelble K, Natrajan R, Aktipis A, Yuan Y. An ecological measure of immune-cancer colocalization as a prognostic factor for breast cancer. *Breast Cancer Research*. 2015 Sep;17(1). Available from: <http://dx.doi.org/10.1186/s13058-015-0638-4>.
- [297] Deenick EK, Gett AV, Hodgkin PD. Stochastic Model of T Cell Proliferation: A Calculus Revealing IL-2 Regulation of Precursor Frequencies, Cell Cycle Time, and Survival. *The Journal of Immunology*. 2003 May;170(10):4963–4972. Available from: <http://dx.doi.org/10.4049/jimmunol.170.10.4963>.
- [298] De Boer RJ, Ganusov VV, Milutinović D, Hodgkin PD, Perelson AS. Estimating Lymphocyte Division and Death Rates from CFSE Data. *Bulletin of Mathematical Biology*. 2006 May;68(5):1011–1031. Available from: <http://dx.doi.org/10.1007/s11538-006-9094-8>.
- [299] Hsu BE, Shen Y, Siegel PM. Neutrophils: Orchestrators of the Malignant Phenotype. *Frontiers in Immunology*. 2020 Aug;11. Available from: <http://dx.doi.org/10.3389/fimmu.2020.01778>.
- [300] Kumbhari A, Rose D, Lee PP, Kim PS. A minimal model of T cell avidity may identify subtherapeutic vaccine schedules. *Mathematical Biosciences*. 2021 Apr;334:108556. Available from: <https://doi.org/10.1016/j.mbs.2021.108556>.
- [301] Chung B, Stuge TB, Murad JP, Beilhack G, Andersen E, Armstrong BD, et al. Antigen-Specific Inhibition of High-Avidity T Cell Target Lysis by Low-Avidity T Cells via Trogocytosis. *Cell Reports*. 2014 Aug;8(3):871–82. Available from: <https://doi.org/10.1016/j.celrep.2014.06.052>.
- [302] Curtsinger JM, Schmidt CS, Mondino A, Lins DC, Kedl RM, Jenkins MK, et al. Inflammatory Cytokines Provide a Third Signal for Activation of Naive CD4⁺ and CD8⁺ T Cells. *The Journal of Immunology*. 1999 Mar;162(6):3256–3262. Available from: <http://dx.doi.org/10.4049/jimmunol.162.6.3256>.
- [303] Raphael I, Nalawade S, Eagar TN, Forsthuber TG. T cell subsets and their signature cytokines in autoimmune and inflammatory diseases. *Cytokine*. 2015 Jul;74(1):5–17. Available from: <http://dx.doi.org/10.1016/j.cyto.2014.09.011>.

Supporting Information: Optimisation of locally advanced MSI-H/dMMR colorectal cancer treatment with neoadjuvant pembrolizumab using data-driven delay integro-differential equations

Georgio Hawi^{1, *}, Peter S. Kim^{1, †}, and Peter P. Lee^{2, †}

¹School of Mathematics and Statistics, University of Sydney, Sydney, Australia

²Department of Immuno-Oncology, Beckman Research Institute, City of Hope, Duarte, California, USA

*Corresponding author: georgio.hawi@sydney.edu.au

†These authors contributed comparably to this work

A Derivation of (2.45)

The derivation of (2.45) follows similarly to that in [1–3], which we include here for completeness. If no pembrolizumab is present, then P_D simply follows the equation

$$\begin{aligned} P_D &= \rho_{P_D^8} T_8 + \rho_{P_D^{\text{ex}}} T_{\text{ex}} + \rho_{P_D^1} T_1 + \rho_{P_D^r} T_r + \rho_{P_D^{M_2}} M_2 \\ &= \rho_{P_D^1} \left(\frac{\rho_{P_D^8}}{\rho_{P_D^1}} T_8 + \frac{\rho_{P_D^{\text{ex}}}}{\rho_{P_D^1}} T_{\text{ex}} + T_1 + \frac{\rho_{P_D^r}}{\rho_{P_D^1}} T_r + \frac{\rho_{P_D^{M_2}}}{\rho_{P_D^1}} M_2 \right), \end{aligned}$$

so that

$$\frac{dP_D}{dt} = \rho_{P_D^1} \left(\frac{\rho_{P_D^8}}{\rho_{P_D^1}} \frac{dT_8}{dt} + \frac{\rho_{P_D^{\text{ex}}}}{\rho_{P_D^1}} \frac{T_{\text{ex}}}{dt} + \frac{dT_1}{dt} + \frac{\rho_{P_D^r}}{\rho_{P_D^1}} \frac{dT_r}{dt} + \frac{\rho_{P_D^{M_2}}}{\rho_{P_D^1}} \frac{dM_2}{dt} \right),$$

where $\rho_{P_D^1}$ is constant. However, when pembrolizumab is injected, PD-1 on these PD-1 expressing cells can bind to it, causing their depletion [4] and in turn changing the number of PD-1 molecules expressed on each cell. We assume, however, that the ratio of the number of PD-1 molecules expressed on each cell stays invariant. Thus, we can replace $\rho_{P_D^1}$ above with

$P_D / \left(\frac{\rho_{P_D^8}}{\rho_{P_D^1}} T_8 + \frac{\rho_{P_D^{\text{ex}}}}{\rho_{P_D^1}} T_{\text{ex}} + T_1 + \frac{\rho_{P_D^r}}{\rho_{P_D^1}} T_r + \frac{\rho_{P_D^{M_2}}}{\rho_{P_D^1}} M_2 \right)$ so that dP_D/dt is given by, taking resistance and the depletion into account,

$$\frac{dP_D}{dt} = \frac{P_D}{\frac{\rho_{P_D^8}}{\rho_{P_D^1}} T_8 + \frac{\rho_{P_D^{\text{ex}}}}{\rho_{P_D^1}} T_{\text{ex}} + T_1 + \frac{\rho_{P_D^r}}{\rho_{P_D^1}} T_r + \frac{\rho_{P_D^{M_2}}}{\rho_{P_D^1}} M_2} \left(\frac{\rho_{P_D^8}}{\rho_{P_D^1}} \frac{dT_8}{dt} + \frac{\rho_{P_D^{\text{ex}}}}{\rho_{P_D^1}} \frac{T_{\text{ex}}}{dt} + \frac{dT_1}{dt} + \frac{\rho_{P_D^r}}{\rho_{P_D^1}} \frac{dT_r}{dt} + \frac{\rho_{P_D^{M_2}}}{\rho_{P_D^1}} \frac{dM_2}{dt} \right)$$

$$\begin{aligned}
& - \frac{d_{P_D A_1} P_D A_1}{1 + \int_0^t A_1(s) ds / K_{P_D A_1}} \\
& = P_D \frac{\left(\rho_{P_D^8} \frac{dT_8}{dt} + \rho_{P_D^{\text{ex}}} \frac{dT_{\text{ex}}}{dt} \rho_{P_D^1} \frac{dT_1}{dt} + \rho_{P_D^r} \frac{dT_r}{dt} + \rho_{P_D^{M_2}} \frac{dM_2}{dt} \right)}{\rho_{P_D^8} T_8 + \rho_{P_D^{\text{ex}}} T_{\text{ex}} + \rho_{P_D^1} T_1 + \rho_{P_D^r} T_r + \rho_{P_D^{M_2}} M_2} - \frac{d_{P_D A_1} P_D A_1}{1 + \int_0^t A_1(s) ds / K_{P_D A_1}},
\end{aligned}$$

which is the same as (2.45).

B Digital Cytometry Calculations

B.1 Tumour Site Cell Steady States and Initial Conditions

Nine ImmuCellAI cell types have a direct correspondence to state variables in the model which we outline in Table B.1.

Table B.1: Mappings between state variables of the model and ImmuCellAI immune cell types.

State Variable	ImmuCellAI Cell Type
T_8	Tc
T_{ex}	Tex
T_r	nTreg
D_0, D	DC
T_1	Th1
T_2	Th2
M_0, M_1, M_2	Macrophage
K_0, K	NK
N_0, N_1, N_2	Neutrophil

Aggregated estimated cell proportions generated by ImmuCellAI for steady states and initial conditions, after normalisation, are shown in Table B.2 and Table B.3.

Table B.2: TS steady-state cell proportions for the model, derived using RNA-sequencing deconvolution via ImmuCellAI. Values for italicised cell types are used in estimating TS cell populations in the model. Values for italicised cell types are used in estimating TS cell populations in the model.

Cell Type	Proportion	Cell Type	Proportion
<i>DC</i>	0.068085	<i>nTreg</i>	0.004728
B_cell	0.099291	iTreg	0.004728
Monocyte	0.090780	<i>Th1</i>	0.002837
<i>Macrophage</i>	0.071868	<i>Th2</i>	0.003783
<i>NK</i>	0.142790	Th17	0.002837
<i>Neutrophil</i>	0.129078	Tfh	0.006619
CD4_T	0.060520	CD8_naive	0.003783
CD8_T	0.075650	<i>Tc</i>	0.004728
NKT	0.119149	<i>Tex</i>	0.003783
Tgd	0.085106	MAIT	0.005674
CD4_naive	0.000946	Tcm	0.002837
Tr1	0.006619	Tem	0.003783

Table B.3: Proportions of TS initial conditions for the model, derived using RNA-sequencing deconvolution via ImmuCellAI. Values for italicised cell types are used in estimating TS cell populations in the model.

Cell Type	Proportion	Cell Type	Proportion
<i>DC</i>	0.069553	<i>nTreg</i>	0.005527
B_cell	0.086596	iTreg	0.003685
Monocyte	0.062644	<i>Th1</i>	0.002303
<i>Macrophage</i>	0.079226	<i>Th2</i>	0.002764
<i>NK</i>	0.141409	Th17	0.002764
<i>Neutrophil</i>	0.096730	Tfh	0.008752
CD4_T	0.069553	CD8_naive	0.004146
CD8_T	0.091663	<i>Tc</i>	0.005988
NKT	0.118839	<i>Tex</i>	0.005527
Tgd	0.126209	MAIT	0.005527
CD4_naive	0.000921	Tcm	0.002303
Tr1	0.007370	Tem	0

Seven keys from the LM22 signature matrix have a direct correspondence to state variables in the model which we outline in [Table B.4](#).

Table B.4: Mappings between state variables of the model and keys of the LM22 signature matrix.

State Variable	LM22 key
D_0	Dendritic cells resting
D	Dendritic cells activated
M_0	Macrophages M0
M_1	Macrophages M1
M_2	Macrophages M2
K_0	NK cells resting
K	NK cells activated

The aggregated estimated cell proportions generated by CIBERSORTx for steady states and initial conditions, after normalisation, are shown in [Table B.5](#) and [Table B.6](#).

Table B.5: TS steady-state cell proportions for the model, derived using RNA-sequencing deconvolution via CIBERSORTx. Values for italicised cell types are used in estimating TS cell populations in the model.

Cell Type	Proportion	Cell Type	Proportion
B cells naive	0.029081	<i>NK cells activated</i>	0.085127
B cells memory	0.027170	Monocytes	0.021546
Plasma cells	0.003780	<i>Macrophages M0</i>	0.048864
T cells CD8	0.175206	<i>Macrophages M1</i>	0.049936
T cells CD4 naive	0.024736	<i>Macrophages M2</i>	0.231721
T cells CD4 memory resting	0.106671	<i>Dendritic cells resting</i>	0.012129
T cells CD4 memory activated	0.029082	<i>Dendritic cells activated</i>	0.004769
T cells follicular helper	0.004535	Mast cells resting	0.017985
T cells regulatory (Tregs)	0.025139	Mast cells activated	0.053773
T cells gamma delta	0	Eosinophils	0.008408
<i>NK cells resting</i>	0.029259	Neutrophils	0.011085

Table B.6: Proportions for TS initial conditions for the model, derived using RNA-sequencing deconvolution via CIBERSORTx. Values for italicised cell types are used in estimating TS cell populations in the model.

Cell Type	Proportion	Cell Type	Proportion
B cells naive	0.017903	<i>NK cells activated</i>	0.064016
B cells memory	0.010573	Monocytes	0.026564
Plasma cells	0.001255	<i>Macrophages M0</i>	0.062173
T cells CD8	0.223294	<i>Macrophages M1</i>	0.068401
T cells CD4 naive	0	<i>Macrophages M2</i>	0.093026
T cells CD4 memory resting	0.114576	<i>Dendritic cells resting</i>	0.014823
T cells CD4 memory activated	0.057725	<i>Dendritic cells activated</i>	0.013436
T cells follicular helper	0.007747	Mast cells resting	0.054464
T cells regulatory (Tregs)	0.021777	Mast cells activated	0.113885
T cells gamma delta	0	Eosinophils	0.007285
<i>NK cells resting</i>	0.009484	Neutrophils	0.017593

The aggregated estimated cell proportions generated by MCP-counter for steady states and initial conditions, after normalisation, are shown in [Table B.7](#) and [Table B.8](#).

Table B.7: TS steady-state cell proportions for the model, derived using RNA-sequencing deconvolution via MCP-counter. Values for italicised cell types are used in estimating TS cell populations in the model.

Cell Type	Proportion	Cell Type	Proportion
CD3 T cells	0.094371	Monocytic lineage	0.086805
CD8 T cells	0.039625	Myeloid dendritic cells	0.053923
Cytotoxic lymphocytes	0.059169	Neutrophils	0.081216
B lineage	0.131949	Endothelial cells	0.104214
NK cells	0.012771	<i>Fibroblasts</i>	0.335956

Table B.8: Proportions for TS initial conditions for the model, derived using RNA-sequencing deconvolution via MCP-counter. Values for italicised cell types are used in estimating TS cell populations in the model.

Cell Type	Proportion	Cell Type	Proportion
CD3 T cells	0.099410	Monocytic lineage	0.099047
CD8 T cells	0.031353	Myeloid dendritic cells	0.074070
Cytotoxic lymphocytes	0.066416	Neutrophils	0.070405
B lineage	0.127136	Endothelial cells	0.092450
NK cells	0.015155	<i>Fibroblasts</i>	0.324559

B.2 TDLN Cell Steady States and Initial Conditions

Mappings between ImmuCellAI immune cell types and TDLN cell types in the model are shown in [Table B.9](#).

Table B.9: Mappings between TDLN cell types in the model and ImmuCellAI immune cell types.

State Variable	ImmuCellAI Cell Type
T_0^8	CD8_naive
T_A^{8LN}	Tc
T_0^4	CD4_naive
T_A^{1LN}	Th1
T_A^{2LN}	Th2
T_0^r	nTreg
T_A^{rLN}	nTreg

Aggregated estimated cell proportions generated by ImmuCellAI for steady states and initial conditions, after normalisation, are shown in [Table B.10](#) and [Table B.11](#).

Table B.10: TDLN steady-state cell proportions for the model, derived using RNA-sequencing deconvolution via ImmuCellAI. Values for italicised cell types are used in estimating TS cell populations in the model.

Cell Type	Proportion	Cell Type	Proportion
DC	0.133416	<i>nTreg</i>	0.005695
B_cell	0.137854	iTreg	0.002553
Monocyte	0.057306	<i>Th1</i>	0.006186
Macrophage	0.039766	<i>Th2</i>	0.019699
NK	0.027758	Th17	0.006268
Neutrophil	0.083950	Tfh	0.003535
CD4_T	0.139621	<i>CD8_naive</i>	0.006186
CD8_T	0.061858	Tc	0.001293
NKT	0.152219	Tex	0.004418
Tgd	0.104264	MAIT	0.001724
<i>CD4_naive</i>	0.003582	Tr1	0.000851

Table B.11: Proportions of TDLN initial conditions for the model, derived using RNA-sequencing deconvolution via ImmuCellAI. Values for italicised cell types are used in estimating TS cell populations in the model.

Cell Type	Proportion	Cell Type	Proportion
DC	0.162562	<i>nTreg</i>	0.000915
B_cell	0.109441	iTreg	0.003667
Monocyte	0.040678	<i>Th1</i>	0.008197
Macrophage	0.069026	<i>Th2</i>	0.026928
NK	0.037126	Th17	0.004563
Neutrophil	0.082688	Tfh	0.002295
CD4_T	0.135822	<i>CD8_naive</i>	0.006384
CD8_T	0.063604	<i>Tc</i>	0.000914
NKT	0.128791	Tex	0.003672
Tgd	0.107255	MAIT	0.001820
<i>CD4_naive</i>	0.002739	Tr1	0.000915

C Parameter Estimation

We estimate all parameters, where possible, under the assumption that no pembrolizumab has/will be administered. The exception to this is the parameters directly related to pembrolizumab treatment for which the assumptions are explicitly stated during estimation. We also denote 1 d to be 1 day, 1 h to be 1 hour, 1 m to be 1 minute, and 1 s to be 1 second.

C.1 DAMP Steady States and Initial Conditions

Like cytokines, we note that $1 \text{ cm}^3 = 1 \text{ mL}$ for all DAMP measurements.

C.1.1 Estimates for H

In [5], a study of blood samples from 144 patients with CRC was conducted, with the serum HMGB1 levels of patients with distant metastasis being $13.32 \pm 6.12 \mu\text{g/L}$, which was significantly higher than those with only lymphatic metastasis at $10.14 \pm 4.38 \mu\text{g/L}$. We assume that the serum concentrations and tissue concentrations of HMGB1 are similar, so we take the initial condition of H to be $1.014 \times 10^{-8} \text{ g/cm}^3$ and the steady state to be $1.33 \times 10^{-8} \text{ g/cm}^3$.

C.1.2 Estimates for A

Extracellular ATP is present in high concentrations in the TME, and in the TME and metastases, extracellular ATP concentration can reach several hundred μM [6]. In particular, concentrations of extracellular ATP in the TME range between 100–700 μM [7], which is $10^3 - 10^4$ times higher than in healthy tissue [8]. Since extracellular ATP is produced by necrotic cancer cells, which have a larger population at steady state compared to initially, we assume that there is more extracellular ATP at steady state. As such, we take the initial condition for A to be equal to 100 μM and a steady state equal to 700 μM , corresponding to $6.02 \times 10^{16} \text{ molec/cm}^3$ and $4.22 \times 10^{17} \text{ molec/cm}^3$, respectively. Recalling that ATP has a molecular mass of approximately 507.181 Da = $8.419 \times 10^{-22} \text{ g}$ [9], this corresponds to an initial condition of $5.06 \times 10^{-5} \text{ g/cm}^3$ and a steady state of $3.55 \times 10^{-4} \text{ g/cm}^3$.

C.1.3 Estimates for S

In epithelial ovarian cancer (EOC), calreticulin concentrations when no drugs are introduced were approximately $2 \times 10^{-2} \pm 2.5 \times 10^{-2} \mu\text{g/mL}$ [10]. Since surface calreticulin is produced by necrotic cancer cells, which have a larger population at steady state compared to initially, we assume that there is more surface calreticulin at steady state. We assume that calreticulin concentrations in EOC are similar to that of MSI-H/dMMR CRC, so we assume an initial condition for S of $2 \times 10^{-8} \text{ g/cm}^3$ and a steady state of $4.5 \times 10^{-8} \text{ g/cm}^3$.

C.2 Cytokine Steady States and Initial Conditions

To estimate cytokine steady states and initial conditions, we look at the respective experimental tissue concentration data, noting that this is more accurate than the more widely available serum/plasma concentration data. Nonetheless, we use serum/plasma concentration data, where relevant, to guide estimates if the corresponding tissue concentration data is limited. We note that $1 \text{ cm}^3 = 1 \text{ mL}$ for all cytokine measurements.

C.2.1 Estimates for I_2

The tissue concentration of IL-2 in CRC is very low and was found to be below the lower limit of quantification in various experiments [11, 12]. In tumour supernatants of invasive ductal cancer the median IL-2 concentration was found 2.1 pg/mL with the interquartile range being 2.0 pg/mL – 4.9 pg/mL [13]. We assume similar concentrations of IL-2 in the tissue of CRC patients.

Taking into account the well-documented anti-tumour properties of IL-2 [14, 15] and decreased IL-2 serum concentration in metastatic CRC patients compared to those without distant metastasis [16], we assume that I_2 has a steady state value of $2.00 \times 10^{-9} \text{ g/cm}^3$, and we set the initial condition to be $2.1 \times 10^{-9} \text{ g/cm}^3$.

C.2.2 Estimates for I_γ

It was found in [11] that the median tissue concentration of IFN- γ in CRC patients was 15.2 pg/mL, with the upper quartile concentration being approximately 16.9 pg/mL. It was found in [17] that the serum concentration of IFN- γ in stage IV CRC patients (median $\approx 20.75 \text{ pg/mL}$) is significantly higher than that of stage I-III patients (median $\approx 1 \text{ pg/mL}$). We thus set the steady state of I_γ to $1.69 \times 10^{-8} \text{ g/cm}^3$, with an initial condition of $1.52 \times 10^{-8} \text{ g/cm}^3$.

C.2.3 Estimates for I_α

It was found in [17] that in advanced CRC patients, i.e those with stage III or stage IV disease, the mean TNF tissue concentration was $\approx 53 \text{ pg/mL}$, with the concentration one standard deviation above the mean being approximately 90 pg/mL. Furthermore, the serum TNF concentration in stage IV CRC patients (median 20.3 pg/mL) is significantly higher than in stage III CRC patients (median 16.0 pg/mL) [18]. We thus set the steady state of I_α to $9.00 \times 10^{-8} \text{ g/cm}^3$, with an initial condition of $5.30 \times 10^{-8} \text{ g/cm}^3$.

C.2.4 Estimates for I_β

It was found in [19] that in advanced CRC patients, i.e those with stage III or stage IV disease, the mean TGF- β tissue concentration was 1311.5 pg/mg, with the concentration one standard deviation

above the mean being 1469.1 pg/mg. Assuming a tissue density of 1.03 g/mL, these correspond to tissue concentrations of 1.35×10^6 pg/mL and 1.51×10^6 pg/mL, respectively. Furthermore, the serum TGF- β concentration in stage IV CRC patients (mean 55 pg/mL) is significantly higher than in stage III CRC patients (mean 45 pg/mL) [20]. We thus set the steady state of I_β to 1.51×10^{-3} g/cm³, with an initial condition of 1.35×10^{-3} g/cm³.

C.2.5 Estimates for I_{12}

The tissue concentration of IL-12 in CRC is very low, and was found to be below the lower limit of quantification in various experiments [11, 12]. In CRC cells in 3D spheroid cultures, the mean IL-12 concentration from cell supernatants was found to be ≈ 0.6 pg/mL, with the concentration one standard deviation above the mean being ≈ 0.625 pg/mL [21]. Furthermore, the serum IL-12 concentration in metastatic CRC patients is lower than in patients without distant metastasis [16]. We thus set the steady state of I_{12} to 6.00×10^{-10} g/cm³, with an initial condition of 6.25×10^{-10} g/cm³.

C.2.6 Estimates for I_{10}

It was found in [17] that in advanced CRC patients, i.e those with stage III or stage IV disease, the mean TNF tissue concentration was 115 pg/mL, with the concentration one standard deviation above the mean being approximately 184 pg/mL. Furthermore, the serum IL-10 concentration in stage IV CRC patients (mean 36.02 pg/mL) is significantly higher than in stage III CRC patients (mean 17.07 pg/mL) [22]. We thus set the steady state of I_{10} to 1.84×10^{-7} g/cm³, with an initial condition of 1.15×10^{-7} g/cm³.

C.2.7 Estimates for I_4

It was found in [17] that in advanced CRC patients, i.e those with stage III or stage IV disease, the mean TNF tissue concentration was ≈ 92 pg/mL, with the concentration one standard deviation above the mean being approximately 150 pg/mL. Furthermore, the serum IL-4 concentration in metastatic CRC patients is higher than in patients without distant metastasis [16]. We thus set the steady state of I_4 to 9.20×10^{-8} g/cm³, with an initial condition of 5.0×10^{-8} g/cm³.

C.2.8 Estimates for I_6

It was found in [19] that in advanced CRC patients, i.e those with stage III or stage IV disease, the mean IL-6 tissue concentration was 3026.2 pg/mg, with the concentration one standard deviation above the mean being 3532.9 pg/mg. Assuming a tissue density of 1.03 g/mL, these correspond to tissue concentrations of 3.11×10^6 pg/mL and 3.64×10^6 pg/mL, respectively. Furthermore, the tissue IL-6 concentration in early CRC patients (mean 3026.2 pg/mg) is significantly higher than in advanced CRC patients (mean 45 pg/mg) [19]. We thus set the steady state of I_6 to 3.11×10^{-3} g/cm³, with an initial condition of 3.64×10^{-3} g/cm³.

C.2.9 Estimates for $I_{1\beta}$

It was found in [11], that the median tissue concentration of IL-1 β in CRC patients was 36.1 pg/mL, with the upper quartile concentration being approximately 191.7 pg/mL. It was found in [18], that the serum concentration of IL-1 β in stage IV CRC patients (median 2.28 pg/mL) is significantly higher than that of stage III patients (median ≈ 1.63 pg/mL). We thus set the steady state of $I_{1\beta}$ to 1.92×10^{-7} g/cm³, with an initial condition of 3.61×10^{-8} g/cm³.

C.3 Immune Checkpoint Protein Steady States and Initial Conditions

C.3.1 PD-1 Steady States and Initial Conditions

To find many of the parameters for P_D , we use the baseline data collected in [23] on 5 advanced cancer patients, before their pembrolizumab infusions. The net number of PD-1 molecules on the surface of CD4+ T cells was 2053 molec/cell, and so we set $\rho_{P_D^1} = \rho_{P_D^r} = 2.05 \times 10^3$ molec/cell. The net number of PD-1 molecules on the surface of CD8+ T cells was 2761 molec/cell, and so we set $\rho_{P_D^s} = 2.76 \times 10^3$ molec/cell. However, PD-1 is significantly more expressed on exhausted CD8+ T cells compared to effector CD8+ T cells [24]. We estimate that there is a 5-fold increase in PD-1 expression on exhausted CD8+ T cells, so we set $\rho_{P_D^s} = 1.38 \times 10^4$ molec/cell. The net number of PD-1 molecules on the surface of non-classical monocytes T cells was 1474 molec/cell, and assume that this is the same as that for M2 macrophages, and so we set $\rho_{P_D^{M2}} = 1.47 \times 10^3$ molec/cell.

This corresponds to

$$\begin{aligned}\overline{P_D} &= \rho_{P_D^s} \overline{T_8} + \rho_{P_D^{\text{ex}}} \overline{T_{\text{ex}}} + \rho_{P_D^1} \overline{T_1} + \rho_{P_D^r} \overline{T_r} + \rho_{P_D^{M2}} \overline{M_2} = 5.66 \times 10^9 \text{ molec/cm}^3, \\ P_D(0) &= \rho_{P_D^s} T_8(0) + \rho_{P_D^{\text{ex}}} T_{\text{ex}}(0) + \rho_{P_D^1} T_1(0) + \rho_{P_D^r} T_r(0) + \rho_{P_D^{M2}} M_2(0) = 5.83 \times 10^9 \text{ molec/cm}^3, \\ \overline{P_D^{\text{LN}}} &= \rho_{P_D^s} \overline{T_A^8} + \rho_{P_D^1} \overline{T_A^1} + \rho_{P_D^r} \overline{T_A^r} = 2.49 \times 10^{10} \text{ molec/cm}^3, \\ P_D^{\text{LN}}(0) &= \rho_{P_D^s} T_A^8(0) + \rho_{P_D^1} T_A^1(0) + \rho_{P_D^r} T_A^r(0) = 1.95 \times 10^{10} \text{ molec/cm}^3.\end{aligned}$$

C.3.2 PD-L1 Steady States and Initial Conditions

It was found in [25], that the PD-L1 expression on activated CD3+ PD-L1+ T cells was 9282 molec/cell, whilst the PD-L1 expression on mature DCs was 80,372 molec/cell. However, amongst advanced CRC patients, only 22.4% of CD4+ T cells were PD-L1+, and only 16.1% of CD8+ T cells were PD-L1+ [26]. Moreover, only 22% of colonic DCs were PD-L1+ in [27]. We thus assume that $\rho_{P_L^1} = \rho_{P_L^r} = 2.08 \times 10^3$ molec/cell, $\rho_{P_L^s} = 1.49 \times 10^3$ molec/cell, and $\rho_{P_L^D} = 1.77 \times 10^4$ molec/cell.

It was estimated in [28] and [1], that the ratio of net PD-L1 molecules on M2 macrophages to that of activated CD4+ and CD8+ T cells is 0.01. We assume this too, so that $\rho_{P_L^{M2}}/0.01 = (\rho_{P_L^1} + \rho_{P_L^s})/2 \implies \rho_{P_L^{M2}} = 1.79 \times 10^3$ molec/cell. Furthermore, we assume that the ratio $\rho_{P_L^{M2}} : \rho_{P_L^C} : \rho_{P_L^{CF}} : \rho_{P_L^{N1}} : \rho_{P_L^{N2}}$ reflects the percentage of PD-L1+ M2 macrophages, PD-L1+ tumour cells, PD-L1+ CAFs, PD-L1+ N1 neutrophils, and PD-L1+ N2 neutrophils, respectively. Amongst advanced CRC patients, only 33.4% of tumour cells were PD-L1+, 56.0% of CD90+ stromal cells were PD-L1+, and 35.6% of CD11b+ myeloid cells were PD-L1+ [26]. We assume that the percentage of PD-L1+ M2 macrophages, N1 neutrophils and N2 neutrophils is equal to the percentage of PD-L1+ CD11b+ myeloid cells, and that the percentage of PD-L1+ CAFs is equal to the percentage of CD90+ stromal cells. Assuming that $\rho_{P_L^{N1}} = \rho_{P_L^{N2}}$, we have that $\rho_{P_L^{M2}}/35.6\% = \rho_{P_L^C}/33.4\% = \rho_{P_L^{CF}}/56.0\% = \rho_{P_L^{N1}}/35.6\% = \rho_{P_L^{N2}}/35.6\%$. Thus, we have that $\rho_{P_L^{N1}} = \rho_{P_L^{N2}} = 1.79 \times 10^3$ molec/cell, $\rho_{P_L^C} = 1.67 \times 10^3$ molec/cell, and $\rho_{P_L^{CF}} = 2.81 \times 10^3$ molec/cell.

This corresponds to

$$\begin{aligned}\overline{P_L} &= \rho_{P_L^C} \overline{C} + \rho_{P_L^D} \overline{D} + \rho_{P_L^s} \overline{T_8} + \rho_{P_L^1} \overline{T_1} + \rho_{P_L^r} \overline{T_r} + \rho_{P_L^{CF}} \overline{C_F} + \rho_{P_L^{M2}} \overline{M_2} + \rho_{P_L^{N1}} \overline{N_1} + \rho_{P_L^{N2}} \overline{N_2} = 1.65 \times 10^{11} \text{ molec/cm}^3, \\ P_L(0) &= \rho_{P_L^C} C(0) + \rho_{P_L^D} D(0) + \rho_{P_L^s} T_8(0) + \rho_{P_L^1} T_1(0) + \rho_{P_L^r} T_r(0) + \rho_{P_L^{CF}} C_F(0) + \rho_{P_L^{M2}} M_2(0) + \rho_{P_L^{N1}} N_1(0) + \rho_{P_L^{N2}} N_2(0) \\ &= 1.10 \times 10^{11} \text{ molec/cm}^3,\end{aligned}$$

$$\begin{aligned}\overline{P_L^{\text{LN}}} &= \rho_{P_L^s} \overline{T_A^8} + \rho_{P_L^1} \overline{T_A^1} + \rho_{P_L^r} \overline{T_A^r} = 2.37 \times 10^{10} \text{ molec/cm}^3, \\ P_L^{\text{LN}}(0) &= \rho_{P_L^s} T_A^8(0) + \rho_{P_L^1} T_A^1(0) + \rho_{P_L^r} T_A^r(0) = 1.86 \times 10^{10} \text{ molec/cm}^3.\end{aligned}$$

C.3.3 PD-1/PD-L1 Steady States and Initial Conditions

Looking at (2.50) and (2.51), we have that

$$\begin{aligned}\overline{Q} &= \frac{\alpha_{P_D P_L}}{d_Q} \overline{P_D P_L} = 1.99 \times 10^5 \text{ molec/cm}^3, \\ Q(0) &= \frac{\alpha_{P_D P_L}}{d_Q} P_D(0) P_L(0) = 1.36 \times 10^5 \text{ molec/cm}^3, \\ \overline{Q^{\text{LN}}} &= \frac{\alpha_{P_D P_L}}{d_Q} \overline{P_D^{\text{LN}} P_L^{\text{LN}}} = 1.26 \times 10^5 \text{ molec/cm}^3, \\ Q^{\text{LN}}(0) &= \frac{\alpha_{P_D P_L}}{d_Q} P_D^{\text{LN}}(0) P_L^{\text{LN}}(0) = 7.77 \times 10^4 \text{ molec/cm}^3,\end{aligned}$$

where $\alpha_{P_D P_L}$ and d_Q are estimated in [Degradation Rates](#).

C.3.4 CTLA-4 Steady States and Initial Conditions

It is known that Tregs constitutively express CTLA-4, unlike effector cells where CTLA-4 production is induced following antigen activation [29], with its activity not being inhibited by the CTLA-4/B7 complex, unlike that for activated CD4+ T helper cells and CD8+ T cells [30, 31]. Moreover, we know that CTLA-4 is expressed more on exhausted CD8+ T cells than their effector counterparts [32]. Additionally, in [33] a median of 1.95% of CD4+ T cells expressed CTLA-4 on their surface, whilst a median of 2.4% of CD8+ T cells expressed CTLA-4 on their surface in health. Assuming that this ratio stays the same in CRC, and combining everything, we assume that $\rho_{P_A^2}/1.95 = \rho_{P_A^s}/2.4 = \rho_{P_A^{\text{ex}}}/(2.4 \times 1.2) = \rho_{P_A^r}/(5 \times 1.95)$.

We assume that at steady state, effector CD8+ T cells express 4 times more PD-1 than CTLA-4. Thus, $\rho_{P_A^s} = \rho_{P_D^s}/4 = 6.90 \times 10^2 \text{ molec/cm}^3$, and so we have that $\rho_{P_A^2} = 5.61 \times 10^2 \text{ molec/cm}^3$, $\rho_{P_A^{\text{ex}}} = 8.28 \times 10^2 \text{ molec/cm}^3$, and $\rho_{P_A^r} = 2.79 \times 10^3 \text{ molec/cm}^3$.

This corresponds to

$$\begin{aligned}\overline{P_A} &= \rho_{P_A^s} \overline{T_8} + \rho_{P_A^{\text{ex}}} \overline{T_{\text{ex}}} + \rho_{P_A^2} \overline{T_2} + \rho_{P_A^r} \overline{T_r} = 8.32 \times 10^8 \text{ molec/cm}^3, \\ P_A(0) &= \rho_{P_A^s} T_8(0) + \rho_{P_A^{\text{ex}}} T_{\text{ex}}(0) + \rho_{P_A^2} T_2(0) + \rho_{P_A^r} T_r(0) = 9.83 \times 10^8 \text{ molec/cm}^3, \\ \overline{P_A^{\text{LN}}} &= \rho_{P_A^s} \overline{T_A^8} + \rho_{P_A^2} \overline{T_A^2} + \rho_{P_A^r} \overline{T_A^r} = 2.45 \times 10^{10} \text{ molec/cm}^3, \\ P_A^{\text{LN}}(0) &= \rho_{P_A^s} T_A^8(0) + \rho_{P_A^r} T_A^r + \rho_{P_A^2} T_A^2(0) = 1.68 \times 10^{10} \text{ molec/cm}^3.\end{aligned}$$

C.4 Drug Steady States

C.4.1 Pembrolizumab Steady States

The value of the geometric mean C_{avg} of pembrolizumab in serum at steady state varied minimally regardless of whether pembrolizumab was administered at 200 mg every 3 weeks, or 400 mg every 6 weeks [34]. This was equal to approximately 50.8 $\mu\text{g/mL}$, and we assume this to be the same in tissue, so we take $\overline{A_1} = 5.08 \times 10^{-5} \text{ g/cm}^3$.

C.5 Half-Saturation Constants

We recall that for some species X , K_X is denoted the half-saturation constant of X in a term of the form

$$\frac{X}{K_X + X}.$$

For simplicity, we assume that if \bar{X} denotes the steady state value of X , then

$$\frac{\bar{X}}{K_X + \bar{X}} = \frac{1}{2} \implies K_X = \bar{X}. \quad (\text{C.1})$$

This implies that

$$\begin{aligned} K_{KD_0} &= \bar{D}_0 = 1.70 \times 10^6 \text{ cell/cm}^3, \\ K_{KD} &= \bar{D} = 6.67 \times 10^5 \text{ cell/cm}^3, \\ K_{DH} &= \bar{H} = 1.33 \times 10^{-8} \text{ g/cm}^3, \\ K_{DA} &= \bar{A} = 3.55 \times 10^{-4} \text{ g/cm}^3, \\ K_{DS} &= \bar{S} = 4.50 \times 10^{-8} \text{ g/cm}^3, \\ K_{T_8 I_2} &= K_{T_1 I_2} = K_{K I_2} = K_{I_{10} I_2} = \bar{I}_2 = 2.00 \times 10^{-9} \text{ g/cm}^3, \\ K_{C I_\gamma} &= K_{N_1 I_\gamma} = K_{M_1 I_\gamma} = K_{M I_\gamma} = \bar{I}_\gamma = 1.69 \times 10^{-8} \text{ g/cm}^3, \\ K_{C I_\alpha} &= K_{M_1 I_\alpha} = K_{M I_\alpha} = \bar{I}_\alpha = 9.00 \times 10^{-8} \text{ g/cm}^3, \\ K_{C_F I_\beta} &= K_{N_2 I_\beta} = K_{M I_\beta} = \bar{I}_\beta = 1.51 \times 10^{-3} \text{ g/cm}^3, \\ K_{M I_{12}} &= K_{K I_{12}} = \bar{I}_{12} = 6.00 \times 10^{-10} \text{ g/cm}^3, \\ K_{M_2 I_{10}} &= \bar{I}_{10} = 1.84 \times 10^{-7} \text{ g/cm}^3, \\ K_{M_2 I_4} &= \bar{I}_4 = 9.20 \times 10^{-8} \text{ g/cm}^3, \\ K_{N_2 I_6} &= K_{M I_6} = \bar{I}_6 = 3.11 \times 10^{-3} \text{ g/cm}^3, \\ K_{C_F I_{1\beta}} &= K_{N_1 I_{1\beta}} = \bar{I}_{1\beta} = 1.92 \times 10^{-7} \text{ g/cm}^3, \\ K_{M_2 P_L} &= \bar{P}_L = 1.65 \times 10^{11} \text{ molec/cm}^3, \\ K_{T_{\text{ex}A_1}} &= \bar{A}_1 = 5.08 \times 10^{-5} \text{ cm}^3/\text{g} \\ K_{T_8 C} &= \bar{C} \tau_l = 6.97 \times 10^8 \text{ (cell/cm}^3) \text{ day.} \end{aligned}$$

C.6 Inhibition Constants

We recall that for some species X , K_X is denoted the inhibition constant of X in a term of the form

$$\frac{1}{1 + X/K_X}.$$

For simplicity, we assume that if \bar{X} denotes the steady state value of X , then

$$\frac{1}{1 + \bar{X}/K_X} = \frac{1}{2} \implies K_X = \bar{X}. \quad (\text{C.2})$$

This implies that

$$\begin{aligned}
K_{I_\gamma T_r} &= \overline{T_r} = 1.81 \times 10^5 \text{ cell/cm}^3, \\
K_{I_{12}A} &= \overline{A} = 3.55 \times 10^{-4} \text{ g/cm}^3, \\
K_{CI_\beta} &= \overline{I_\beta} = 1.51 \times 10^{-3} \text{ g/cm}^3, \\
K_{T_8 I_{10}} &= K_{T_{\text{ex}} I_{10}} = K_{I_{12} I_{10}} = \overline{I_{10}} = 1.84 \times 10^{-7} \text{ g/cm}^3, \\
K_{CI_6} &= \overline{I_6} = 3.11 \times 10^{-3} \text{ g/cm}^3, \\
K_{CP_D} &= \overline{P_D} = 5.66 \times 10^9 \text{ molec/cm}^3, \\
K_{CP_L} &= \overline{P_L} = 1.65 \times 10^{11} \text{ molec/cm}^3, \\
K_{T_8 Q} &= K_{T_1 Q} = \overline{Q} = 1.99 \times 10^5 \text{ molec/cm}^3, \\
K_{I_\gamma P_A} &= \overline{P_A} = 8.32 \times 10^8 \text{ molec/cm}^3, \\
K_{T_0^8 P_D^{\text{LN}}} &= \tau_8^{\text{act}} \overline{P_D^{\text{LN}}} = 4.98 \times 10^{10} \text{ (molec/cm}^3\text{) day}, \\
K_{T_0^8 P_A^{\text{LN}}} &= \tau_8^{\text{act}} \overline{P_A^{\text{LN}}} = 4.90 \times 10^{10} \text{ (molec/cm}^3\text{) day}, \\
K_{T_A^8 Q^{\text{LN}}} &= \tau_{T_A^8} \overline{Q^{\text{LN}}} = 6.14 \times 10^5 \text{ (molec/cm}^3\text{) day}, \\
K_{T_A^8 P_A^{\text{LN}}} &= \tau_{T_A^8} \overline{P_A^{\text{LN}}} = 1.19 \times 10^9 \text{ (molec/cm}^3\text{) day}, \\
K_{T_0^4 P_D^{\text{LN}}} &= \tau_4^{\text{act}} \overline{P_D^{\text{LN}}} = 3.74 \times 10^{10} \text{ (molec/cm}^3\text{) day}, \\
K_{T_0^4 P_A^{\text{LN}}} &= \tau_4^{\text{act}} \overline{P_A^{\text{LN}}} = 3.68 \times 10^{10} \text{ (molec/cm}^3\text{) day}, \\
K_{T_A^1 Q^{\text{LN}}} &= \tau_{T_A^1} \overline{Q^{\text{LN}}} = 5.20 \times 10^5 \text{ (molec/cm}^3\text{) day}, \\
K_{T_A^1 P_A^{\text{LN}}} &= \tau_{T_A^1} \overline{P_A^{\text{LN}}} = 1.01 \times 10^{11} \text{ (molec/cm}^3\text{) day}, \\
K_{T_A^2 Q^{\text{LN}}} &= \tau_{T_A^2} \overline{Q^{\text{LN}}} = 5.20 \times 10^5 \text{ (molec/cm}^3\text{) day}, \\
K_{T_A^2 P_A^{\text{LN}}} &= \tau_{T_A^2} \overline{P_A^{\text{LN}}} = 1.01 \times 10^{11} \text{ (molec/cm}^3\text{) day}, \\
K_{T_0^r P_D^{\text{LN}}} &= \tau_r^{\text{act}} \overline{P_D^{\text{LN}}} = 3.74 \times 10^{10} \text{ (molec/cm}^3\text{) day}, \\
K_{T_0^r P_A^{\text{LN}}} &= \tau_r^{\text{act}} \overline{P_A^{\text{LN}}} = 3.68 \times 10^{10} \text{ (molec/cm}^3\text{) day}, \\
K_{T_A^r Q^{\text{LN}}} &= \tau_{T_A^r} \overline{Q^{\text{LN}}} = 3.62 \times 10^5 \text{ (molec/cm}^3\text{) day}, \\
K_{T_A^r P_A^{\text{LN}}} &= \tau_{T_A^r} \overline{P_A^{\text{LN}}} = 7.03 \times 10^{10} \text{ (molec/cm}^3\text{) day}.
\end{aligned}$$

C.7 Degradation Rates

We recall the formula that the degradation rate of some species X , is given by

$$d_X = \frac{\ln 2}{t_{1/2}^X} \quad (\text{C.3})$$

where $t_{1/2}^X$ is the elimination half-life of X .

C.7.1 Estimate for d_H

The half-life of HMGB1 was found to be approximately 3 hours in the context of prostate cancer [35]. We assume a similar value for MSI-H/dMMR CRC and so

$$d_H = \frac{\ln 2}{3 \text{ h}} = 5.55 \text{ d}^{-1}.$$

C.7.2 Estimate for d_A

The half-life for extracellular ATP released by prostate cancer cells is approximately 5 minutes [36]. We assume a similar value for MSI-H/dMMR CRC and so

$$d_A = \frac{\ln 2}{5 \text{ m}} = 2.00 \times 10^2 \text{ d}^{-1}.$$

C.7.3 Estimate for d_S

Surface calreticulin has a half-life of approximately 12 hours [37, 38]. Thus, we have that

$$d_S = \frac{\ln 2}{12 \text{ h}} = 1.39 \text{ d}^{-1}.$$

C.7.4 Estimate for d_{D_0}

The time taken for immature DCs to degrade is estimated to be 28 days in mice [39]. We assume that this is similarly the case for humans so that this corresponds to

$$d_{D_0} = \frac{1}{28 \text{ d}} = 3.60 \times 10^{-2} \text{ d}^{-1}.$$

C.7.5 Estimate for d_D

Mature DCs have a half-life of 1.5 – 2.9 days in mice [40]. We assume that this is similarly the case for humans, and take $t_{1/2}^D = 2.2 \text{ d}$ so that

$$d_D = \frac{\ln 2}{2.2 \text{ d}} = 0.32 \text{ d}^{-1}.$$

C.7.6 Estimate for $d_{T_0^8}$

The half-life of naive CD8+ T cells in the lymph node was estimated to be 21.5 days in [41] so that

$$d_{T_0^8} = \frac{\ln 2}{21.5 \text{ d}} = 3.22 \times 10^{-2} \text{ d}^{-1}.$$

C.7.7 Estimate for d_{T_8} and $d_{T_{\text{ex}}}$

It was measured in [42] that the mean degradation rate of circulating CD8+ T cells in HIV seronegative patients was 0.009 d^{-1} . We assume that this is the case for MSI-H/dMMR CRC, and so we set $d_{T_8} = d_{T_{\text{ex}}} = 0.009 \text{ d}^{-1}$.

C.7.8 Estimate for $d_{T_0^4}$

The half-life of naive CD4+ T cells in the lymph node was estimated to be 17.2 days in [41] so that

$$d_{T_0^4} = \frac{\ln 2}{17.2 \text{ d}} = 4.03 \times 10^{-2} \text{ d}^{-1}.$$

C.7.9 Estimate for d_{T_1}

It was measured in [42] that the mean degradation rate of circulating CD4+ T cells in HIV seronegative patients was 0.008 d^{-1} . We assume that this is the case for Th1 cells in MSI-H/dMMR CRC, and so we set $d_{T_1} = 0.008 \text{ d}^{-1}$.

C.7.10 Estimate for d_{T_2}

It was measured in [42] that the mean degradation rate of circulating CD4+ T cells in HIV seronegative patients was 0.008 d^{-1} . We assume that this is the case for Th2 cells in MSI-H/dMMR CRC, and so we set $d_{T_2} = 0.008 \text{ d}^{-1}$.

C.7.11 Estimate for d_{T_r}

The degradation rate of naive Tregs in the lymph node was estimated to be $2.2 \times 10^{-3} \text{ d}^{-1}$ in [43], and we assume that the degradation rate in MSI-H CRC is similar so that

$$d_{T_r} = 2.2 \times 10^{-3} \text{ d}^{-1}.$$

C.7.12 Estimate for d_{T_r}

The mean half-life of Tregs in healthy adults was measured to be approximately 11 days in [44]. We assume that this is similarly the case for MSI-H/dMMR CRC, and so that this corresponds to

$$d_{T_r} = \frac{\ln 2}{11 \text{ d}} = 6.30 \times 10^{-2} \text{ d}^{-1}.$$

C.7.13 Estimate for d_{C_F}

The half-life of pancreatic stellate cells, one of the most studied subtypes of CAFs in pancreatic cancer, varies between 2 – 5 days [45]. We assume that the half-life of CAFs in CRC is similar, taking it to be 3.5 days, so that

$$d_{C_F} = \frac{\ln 2}{3.5 \text{ d}} = 1.98 \times 10^{-1} \text{ d}^{-1}.$$

C.7.14 Estimate for $d_{N_0}, d_{N_1}, d_{N_2}$

The lifespan of neutrophils in a cancer setting is approximately 17 hours [46, 47]. We assume that the half-lives of naive neutrophils, N1, and N2 neutrophils are all equal to 17 hours, so that

$$d_{N_0} = d_{N_1} = d_{N_2} = \frac{\ln 2}{17 \text{ h}} = 0.98 \text{ d}^{-1}.$$

C.7.15 Estimate for d_{M_0}

The lifespan for naive macrophages was found in humans to be approximately 1.37 days on average [48]. This corresponds to

$$d_{M_0} = \frac{1}{1.38 \text{ d}} = 0.72 \text{ d}^{-1}.$$

C.7.16 Estimate for d_{M_1}

The lifespan for M1 macrophages was found in humans to be approximately 1.01 days on average [48]. This corresponds to

$$d_{M_0} = \frac{1}{1.01 \text{ d}} = 0.99 \text{ d}^{-1}.$$

C.7.17 Estimate for d_{M_2}

The lifespan for M2 macrophages was found in humans to be approximately 7.41 days on average [48]. This corresponds to

$$d_{M_0} = \frac{1}{7.41 \text{ d}} = 1.35 \times 10^{-1} \text{ d}^{-1}.$$

C.7.18 Estimate for d_{K_0} and d_K

The half-life of human NK cells varies between 1 – 2 weeks [49–51]. We assume that the half-lives of naive and activated NK cells are both equal to 10 days, so that

$$d_{K_0} = d_K = \frac{\ln 2}{10 \text{ d}} = 7 \times 10^{-2} \text{ d}^{-1}.$$

C.7.19 Estimate for d_{I_2}

The half-life of IL-2 varies between 5 – 7 minutes [52, 53]. We take $t_{1/2}^{I_2} = 6.9 \text{ m}$ so that

$$d_{I_2} = \frac{\ln 2}{6.9 \text{ m}} = 1.44 \times 10^2 \text{ d}^{-1}.$$

C.7.20 Estimate for d_{I_γ}

The half-life of IFN- γ varies between 25 – 35 minutes [54]. We take $t_{1/2}^{I_\gamma}$ to be 30 minutes so that

$$d_{I_2} = \frac{\ln 2}{30 \text{ m}} = 3.33 \times 10^1 \text{ d}^{-1}.$$

C.7.21 Estimate for d_{I_α}

The half-life of TNF varies between 15 – 30 minutes [55, 56]. We take $t_{1/2}^{I_\alpha}$ to be 18.2 minutes, so that

$$d_{I_\alpha} = \frac{\ln 2}{18.2 \text{ m}} = 5.48 \times 10^1 \text{ d}^{-1}.$$

C.7.22 Estimate for d_{I_β}

The half-life of active TGF- β is approximately 2 – 3 minutes [57]. We take $t_{1/2}^{I_\beta} = 2.5$ m, so that

$$d_{I_\beta} = \frac{\ln 2}{2.5 \text{ m}} = 3.99 \times 10^2 \text{ d}^{-1}.$$

C.7.23 Estimate for $d_{I_{12}}$

The half-life of IL-12 varies between 5.3 – 10.3 hours [58]. We take $t_{1/2}^{I_{12}} = 7.8$ h, so that

$$d_{I_\beta} = \frac{\ln 2}{7.8 \text{ h}} = 2.13 \text{ d}^{-1}.$$

C.7.24 Estimate for $d_{I_{10}}$

The half-life of IL-10 varies between 2.7 – 4.5 hours [59]. We take $t_{1/2}^{I_{10}} = 2.7$ h so that

$$d_{I_\beta} = \frac{\ln 2}{2.7 \text{ h}} = 6.16 \text{ d}^{-1}.$$

C.7.25 Estimate for d_{I_4}

The half-life of uncomplexed IL-4 is very short, being approximately 19 minutes [60]. We take $t_{1/2}^{I_4} = 19$ m so that

$$d_{I_4} = \frac{\ln 2}{45 \text{ m}} = 5.25 \times 10^1 \text{ d}^{-1}.$$

C.7.26 Estimate for d_{I_6}

The half-life of IL-6 varies between 103 minutes in meningococcal septic shock [61] and 15 hours during acute inflammation [62]. We assume that in MSI-H/dMMR CRC, $t_{1/2}^{I_6} = 15$ hours so that

$$\frac{\ln 2}{15 \text{ h}} = 1.11 \text{ d}^{-1}.$$

C.7.27 Estimate for $d_{I_{1\beta}}$

The half-life of IL-1 β is approximately 3.5 hours [63], so that

$$\frac{\ln 2}{3.5 \text{ h}} = 4.75 \text{ d}^{-1}.$$

C.7.28 Estimate for d_{A_1}

The half-life of pembrolizumab varies between 22 – 27 days [64–66]. We take it to be 26 days so that

$$d_{A_1} = \frac{\ln 2}{26 \text{ d}} = 2.67 \times 10^{-2} \text{ d}^{-1}.$$

C.7.29 Estimate for $d_{P_D A_1}$ and $K_{P_D A_1}$

We assume at steady state, that 10% of pembrolizumab is used in blocking PD-1, while the remaining 90% degrades naturally. Considering (2.52), we have that

$$\frac{d_{P_D A_1} \overline{P_D A_1}}{10\%} = \frac{d_{A_1} \overline{A_1}}{90\%} \implies d_{P_D A_1} = \frac{d_{A_1}}{9P_D} = 5.24 \times 10^{-13} \text{ (molec/cm}^3\text{)}^{-1} \text{ day}^{-1}.$$

We assume that the extent of inhibition of PD-1 depletion by pembrolizumab is proportional to the level of acquired resistance. We now estimate $K_{P_D A_1}$. It was calculated in [67], that the acquired resistance rate of 10mg/kg pembrolizumab dosing every 2 weeks for dMMR cancers, as done in [68], was approximately 11%, at a median of 13 months after treatment commencement. Assuming that there are 395 days in 13 months and a patient mass of 80 kg, we thus have that

$$\frac{1}{1 + \int_0^{395} A_1(s) ds / K_{P_D A_1}} = 0.89 \implies K_{P_D A_1} = \frac{89}{11 \int_0^{395} A_1(s) ds},$$

with parameter values of $\xi_j = 800\text{mg}$, $\gamma_j = f_{\text{pembro}} \xi_j$, $t_j = 14(j-1)$, $n = 28$. We now approximate $\int_0^{395} A_1(s) ds$ for this regimen. We assume for simplicity, throughout the whole treatment that 10% of pembrolizumab is depleted due to blocking PD-1, and 90% degrades naturally, ignoring acquired resistance for this approximation. Thus, we have that

$$\frac{d_{P_D A_1} P_D A_1}{10\%} = \frac{d_{A_1} A_1}{90\%} \implies \frac{dA_1}{dt} = \sum_{j=1}^{28} 800 f_{\text{pembro}} \delta(t - 14(j-1)) - \frac{10}{9} d_{A_1} A_1.$$

Numerically solving this using the ode15s integrator leads to $\int_0^{395} A_1(s) \approx 7.83 \times 10^{-3} \text{ (g/cm}^3\text{) day}$, so that $K_{P_D A_1} = 6.33 \times 10^{-2} \text{ (g/cm}^3\text{) day}$.

C.7.30 Estimate for $d_{P_D^{\text{LN}} A_1^{\text{LN}}}$ and $K_{P_D^{\text{LN}} A_1^{\text{LN}}}$

We assume at steady state, that 10% of pembrolizumab is used in blocking PD-1, while the remaining 90% degrades naturally. Considering (2.53) in the case of pembrolizumab, we have that

$$\frac{d_{P_D^{\text{LN}} A_1^{\text{LN}}} \overline{P_D^{\text{LN}} A_1^{\text{LN}}}}{10\%} = \frac{d_{A_1} \overline{A_1^{\text{LN}}}}{90\%} \implies d_{P_D^{\text{LN}} A_1^{\text{LN}}} = \frac{d_{A_1}}{9P_D^{\text{LN}}} = 1.19 \times 10^{-13} \text{ (molec/cm}^3\text{)}^{-1} \text{ day}^{-1}.$$

We now estimate $K_{P_D^{\text{LN}} A_1^{\text{LN}}}$, making identical assumptions to those used to estimate $K_{P_D A_1}$. Like before, we have that

$$\frac{1}{1 + \int_0^{395} A_1^{\text{LN}}(s) ds / K_{P_D^{\text{LN}} A_1^{\text{LN}}}} = 0.89 \implies K_{P_D^{\text{LN}} A_1^{\text{LN}}} = \frac{89}{11 \int_0^{395} A_1^{\text{LN}}(s) ds},$$

and that

$$\frac{d_{P_D^{\text{LN}} A_1^{\text{LN}}} P_D^{\text{LN}} A_1^{\text{LN}}}{10\%} = \frac{d_{A_1} A_1^{\text{LN}}}{90\%} \implies \frac{dA_1^{\text{LN}}}{dt} = \sum_{j=1}^{28} 800 f_{\text{pembro}} \delta(t - 14(j-1)) - \frac{10}{9} d_{A_1} A_1^{\text{LN}}.$$

Numerically solving this using the ode15s integrator leads to $\int_0^{395} A_1^{LN}(s) \approx 7.83 \times 10^{-3}$ (g/cm³) day, so that $K_{P_D^{LN}A_1^{LN}} = 6.33 \times 10^{-2}$ (g/cm³) day.

C.7.31 Estimate for d_Q

The dissociation rate of PD-1/PD-L1 was found to be 1.44 s^{-1} in [25]. Thus, we have that

$$d_Q = 60 \times 60 \times 24 \times 1.44 \text{ s}^{-1} = 1.24 \times 10^5 \text{ d}^{-1}.$$

C.7.32 Estimate for $\alpha_{P_D P_L}$

The formation rate of PD-1/PD-L1 was found to be $1.84 \times 10^5 \text{ M}^{-1} \text{ s}^{-1}$ in [25]. We need to convert this to units of $(\text{molec}/\text{cm}^3)^{-1} \text{ d}^{-1}$. We recall that $1 \text{ M} = 1 \text{ mol}/\text{L} = 10^{-3} \text{ mol}/\text{cm}^3 = 6.02 \times 10^{20} \text{ molec}/\text{cm}^3$. Thus, we have that

$$\alpha_{P_D P_L} = 60 \times 60 \times 24 \times 1.84 \times 10^5 \times (6.02 \times 10^{20})^{-1} = 2.64 \times 10^{-11} (\text{molec}/\text{cm}^3)^{-1} \text{ d}^{-1}.$$

C.8 DAMP and TS Cell Parameters

C.8.1 Estimates for H

Considering (2.3) at steady state, we have that

$$\lambda_{HN_c} \overline{N_c} + \lambda_{HC_F} \overline{C_F} - d_H \overline{H} = 0.$$

Since HMGB1 is released more by necrotic cancer cells than CAFs, we assume that

$$\frac{\lambda_{HN_c}}{9} = \frac{\lambda_{HC_F}}{1}.$$

Solving these simultaneously leads to

$$\begin{aligned} \lambda_{HN_c} &= 1.57 \times 10^{-14} (\text{g}/\text{cell}) \text{ day}^{-1}, \\ \lambda_{HC_F} &= 1.74 \times 10^{-15} (\text{g}/\text{cell}) \text{ day}^{-1}. \end{aligned}$$

C.8.2 Estimates for A

Considering (2.4) at steady state leads to

$$\lambda_{AN_c} \overline{N_c} - d_A \overline{A} = 0 \implies \lambda_{AN_c} = 1.93 \times 10^{-8} (\text{g}/\text{cell}) \text{ day}^{-1}.$$

C.8.3 Estimates for S

Considering (2.5) at steady state leads to the equation

$$\lambda_{SN_c} \overline{N_c} - d_S \overline{S} = 0.$$

This leads to

$$\lambda_{SN_c} = 1.70 \times 10^{-14} (\text{g}/\text{cell}) \text{ day}^{-1}.$$

C.8.4 Estimates for D_0 and D

Adding (2.6) and (2.7) at steady state, leads to

$$\mathcal{A}_{D_0} - \lambda_{D_0K} \overline{D_0K} - d_{D_0} \overline{D_0} - \lambda_{DDLN} \overline{D} - d_D \overline{D} = 0.$$

We assume that HMGB1 is the most potent inducer of DC maturation, followed by extracellular ATP, with surface calreticulin being the weakest inducer. As such, at steady state, we assume that

$$\frac{\lambda_{DH}}{2 \times 10} = \frac{\lambda_{DA}}{2 \times 2} = \frac{\lambda_{DS}}{2 \times 1}.$$

In [69], it was also shown that the percentage of immature DCs that were lysed as a result of NK cells is roughly linear in the ratio of NK cells to immature DCs. When a 1:1 ratio of activated NK cells to immature DCs is present, after 24 hours, roughly 35.5% of immature DCs are lysed, whereas if a 5:1 ratio is present, 85.5% of immature DCs are lysed. At steady state, the ratio of NK cells to immature DCs is $\approx 2.39 : 1$, corresponding to an approximate 52.85% being lysed. However, if we consider only immature DC loss due to degradation, after 24 hours, only $1 - e^{-d_{D_0}} \approx 3.54\%$ are lost to it. Thus, we assume at steady state that

$$\frac{\lambda_{D_0K} \overline{D_0K}}{0.5285} = \frac{d_{D_0} \overline{D_0}}{0.0354} \implies \lambda_{D_0K} = 1.32 \times 10^{-7} \text{ (cell/cm}^3\text{)}^{-1} \text{ day}^{-1}.$$

Considering (2.7) at steady state leads to

$$\frac{\lambda_{DH} \overline{D_0}}{2} + \frac{\lambda_{DA} \overline{D_0}}{2} + \frac{\lambda_{DS} \overline{D_0}}{2} - \lambda_{DDLN} \overline{D} - d_D \overline{D} = 0.$$

Finally, it was found in [70] that only a limited number of DCs migrate up to the TDLN, with at most 4% of DCs reaching the TDLN in melanoma patients when DCs were injected intradermally. We assume at steady state that this holds too for MSI-H/dMMR CRC. Taking into account that only $e^{-d_D \tau_m}$ of mature DCs that leave the TS, survive their migration to the TDLN, we have that

$$\frac{\lambda_{DDLN}}{0.04 e^{d_D \tau_m}} = \frac{d_D}{1 - 0.04 e^{d_D \tau_m}}$$

Solving these simultaneously leads to

$$\begin{aligned} \mathcal{A}_{D_0} &= 1.20 \times 10^6 \text{ (cell/cm}^3\text{)} \text{ day}^{-1}, \\ \lambda_{DH} &= 2.04 \times 10^{-1} \text{ day}^{-1}, \\ \lambda_{DA} &= 4.07 \times 10^{-2} \text{ day}^{-1}, \\ \lambda_{DS} &= 2.04 \times 10^{-2} \text{ day}^{-1}, \\ \lambda_{D_0K} &= 1.32 \times 10^{-7} \text{ (cell/cm}^3\text{)}^{-1} \text{ day}^{-1}, \\ \lambda_{DDLN} &= 1.71 \times 10^{-2} \text{ day}^{-1}. \end{aligned}$$

C.8.5 Estimates for C_F

We consider (2.26) at steady state, which leads to

$$\left(\lambda_{C_F} + \frac{\lambda_{C_F I_\beta}}{2} + \frac{\lambda_{C_F I_{1\beta}}}{2} \right) \left(1 - \frac{\overline{C_F}}{C_{F0}} \right) - d_{C_F} = 0.$$

We assume that TGF- β is more potent than IL-1 β at promoting CAF growth in CRC, so that at steady state

$$\frac{\lambda_{C_F I_\beta}}{2 \times 4} = \frac{\lambda_{C_F I_{1\beta}}}{2 \times 1}.$$

We assume that the carrying capacity of CAFs is 20% of its steady state, so that

$$C_{F0} = 1.2 \overline{C_F} = 1.12 \times 10^7 \text{ cell/cm}^3.$$

The mean doubling time of CAFs in CRC was estimated to be 24 h in [71], so we set

$$\lambda_{C_F} = \frac{\ln 2}{24 \text{ h}} = 6.93 \times 10^{-1} \text{ d}^{-1}. \quad (\text{C.4})$$

Solving these simultaneously leads to

$$\begin{aligned} \lambda_{C_F I_\beta} &= 7.89 \times 10^{-1} \text{ day}^{-1}, \\ \lambda_{C_F I_{1\beta}} &= 1.97 \times 10^{-1} \text{ day}^{-1}. \end{aligned}$$

C.8.6 Estimates for $N_0/N_1/N_2$

Adding (2.27), (2.28), and (2.29) at steady state leads to

$$\mathcal{A}_{N_0} - d_{N_0} \overline{N_0} - d_{N_1} \overline{N_1} - d_{N_2} \overline{N_2} = 0 \implies \mathcal{A}_{N_0} = 4.38 \times 10^6 \text{ (cell/cm}^3\text{) day}^{-1}.$$

To estimate the other neutrophil production constants, we consider (2.27), (2.28), (2.29) at steady state, and use the data from [72]. We assume that the magnitude of response to a specific cytokine is proportional to its corresponding neutrophil polarisation rate, where the response is defined as the Euclidean distance between the centroid vectors of cytokine-treated neutrophils and PBS-treated neutrophils.

Using values from [72], and considering (2.27), (2.28), and (2.29) at steady state leads to the equations

$$\begin{aligned} \mathcal{A}_{N_0} - \frac{\lambda_{N_1 I_{1\beta}} \overline{N_0}}{2} - \frac{\lambda_{N_1 I_\gamma} \overline{N_0}}{2} - \frac{\lambda_{N_2 I_6} \overline{N_0}}{2} - \frac{\lambda_{N_2 I_\beta} \overline{N_0}}{2} - d_{N_0} \overline{N_0} &= 0, \\ \frac{\lambda_{N_1 I_{1\beta}} \overline{N_0}}{2} + \frac{\lambda_{N_1 I_\gamma} \overline{N_0}}{2} - d_{N_1} \overline{N_1} &= 0, \\ \frac{\lambda_{N_2 I_6} \overline{N_0}}{2} + \frac{\lambda_{N_2 I_\beta} \overline{N_0}}{2} - d_{N_2} \overline{N_2} &= 0, \\ \frac{\lambda_{N_1 I_{1\beta}}}{2 \times 19.41} &= \frac{\lambda_{N_1 I_\gamma}}{2 \times 23.05}, \\ \frac{\lambda_{N_2 I_6}}{2 \times 19.97} &= \frac{\lambda_{N_2 I_\beta}}{2 \times 16.99}. \end{aligned}$$

Solving these simultaneously leads to

$$\begin{aligned}\lambda_{N_1 I_1 \beta} &= 1.72 \text{ day}^{-1}, \\ \lambda_{N_1 I_1 \gamma} &= 2.04 \text{ day}^{-1}, \\ \lambda_{N_2 I_6} &= 4.06 \text{ day}^{-1}, \\ \lambda_{N_2 I_6 \beta} &= 3.46 \text{ day}^{-1}.\end{aligned}$$

C.8.7 Estimates for $M_0/M_1/M_2$

To estimate macrophage production parameters, we do a similar process to neutrophils. Adding (2.30), (2.31), and (2.32) at steady state, leads to

$$\mathcal{A}_{M_0} - d_{M_0} \overline{M_0} - d_{M_1} \overline{M_1} - d_{M_2} \overline{M_2} = 0 \implies \mathcal{A}_{M_0} = 8.75 \times 10^5 \text{ (cell/cm}^3\text{) day}^{-1}.$$

Using values from [72], and considering (2.30) at steady state, leads to the equations

$$\begin{aligned}\mathcal{A}_{M_0} - \frac{\lambda_{M_1 I_\alpha} \overline{M_0}}{2} - \frac{\lambda_{M_1 I_\gamma} \overline{M_0}}{2} - \frac{\lambda_{M_2 I_4} \overline{M_0}}{2} - \frac{\lambda_{M_2 I_{10}} \overline{M_0}}{2} - \frac{\lambda_{M_2 P_L} \overline{M_0}}{2} - d_{M_0} \overline{M_0} &= 0, \\ \frac{\lambda_{M_1 I_\alpha}}{2 \times 10.77} = \frac{\lambda_{M_1 I_\gamma}}{2 \times 12.54} = \frac{\lambda_{M_2 I_4}}{2 \times 7.39} = \frac{\lambda_{M_2 I_{10}}}{2 \times 6.81}.\end{aligned}$$

We assume that TGF- β repolarises M1 macrophages to the M2 phenotype more potently than IL-6, so that at steady state

$$\frac{\lambda_{M I_\beta}}{2 \times 5} = \frac{\lambda_{M I_6}}{2 \times 1}.$$

We also assume that IFN- γ repolarises M2 macrophages to the M1 phenotype slightly more potently than TNF, which repolarises more slightly than IL-12. Hence, at steady state

$$\frac{\lambda_{M I_\gamma}}{2 \times 6} = \frac{\lambda_{M I_\alpha}}{2 \times 5} = \frac{\lambda_{M I_{12}}}{2 \times 1}.$$

At steady state, we assume that

$$\frac{\lambda_{M_1 I_\alpha}/2 + \lambda_{M_1 I_\gamma}/2}{\overline{M_1}} = \frac{\lambda_{M_2 I_4}/2 + \lambda_{M_2 I_{10}}/2 + \lambda_{M_2 P_L}/2}{\overline{M_2}},$$

and that

$$\frac{\lambda_{M I_{12}} M_1}{2} + \frac{\lambda_{M I_\gamma} M_1}{2} + \frac{\lambda_{M I_\alpha} M_1}{2} = \frac{\lambda_{M I_\beta} M_2}{2} + \frac{\lambda_{M I_6} M_2}{2}$$

to ensure equilibrium is maintained. Solving these simultaneously leads to,

$$\begin{aligned}\lambda_{M_1 I_\alpha} &= 2.71 \times 10^{-1} \text{ day}^{-1}, \\ \lambda_{M_1 I_\gamma} &= 3.15 \times 10^{-1} \text{ day}^{-1}, \\ \lambda_{M_2 I_4} &= 1.86 \times 10^{-1} \text{ day}^{-1}, \\ \lambda_{M_2 I_{10}} &= 1.71 \times 10^{-1} \text{ day}^{-1}, \\ \lambda_{M_2 P_L} &= 2.36 \text{ day}^{-1}, \\ \lambda_{M I_{12}} &= 2.65 \times 10^{-2} \text{ day}^{-1},\end{aligned}$$

$$\begin{aligned}
\lambda_{MI_\gamma} &= 1.59 \times 10^{-1} \text{ day}^{-1}, \\
\lambda_{MI_\alpha} &= 1.32 \times 10^{-1} \text{ day}^{-1}, \\
\lambda_{MI_\beta} &= 5.71 \times 10^{-2} \text{ day}^{-1}, \\
\lambda_{MI_6} &= 1.14 \times 10^{-2} \text{ day}^{-1}.
\end{aligned}$$

C.8.8 Estimates for K_0/K

To estimate NK cell production parameters, we do a similar process to neutrophils and macrophages. Adding (2.33) and (2.34) at steady state, leads to

$$\mathcal{A}_{K_0} - d_{K_0}\overline{K_0} - d_K\overline{K} = 0 \implies \mathcal{A}_{K_0} = 3.82 \times 10^5 \text{ (cell/cm}^3\text{) day}^{-1}.$$

Using values from [72], and considering (2.34) at steady state, leads to the equations

$$\begin{aligned}
\frac{\lambda_{KI_2}\overline{K_0}}{2} + \frac{\lambda_{KI_{12}}\overline{K_0}}{2} + \frac{\lambda_{KD_0}\overline{K_0}}{2} + \frac{\lambda_{KD}\overline{K_0}}{2} - d_K\overline{K} &= 0, \\
\frac{\lambda_{KI_2}}{15.4} &= \frac{\lambda_{KI_{12}}}{14.83}.
\end{aligned}$$

We assume that mature DCs are more potent activators of NK cells than immature DCs so that at steady state

$$\frac{\lambda_{KD}}{2 \times 5} = \frac{\lambda_{KD_0}}{2 \times 1}.$$

We finally assume that DC-mediated NK-cell activation is twice as potent as cytokine-induced activation at steady state, so that

$$\frac{\lambda_{KD_0}/2 + \lambda_{KD}/2}{2} = \frac{\lambda_{KI_2}/2 + \lambda_{KI_{12}}/2}{1}.$$

Solving these simultaneously leads to

$$\begin{aligned}
\lambda_{KI_2} &= 6.94 \times 10^{-2} \text{ day}^{-1}, \\
\lambda_{KI_{12}} &= 6.69 \times 10^{-2} \text{ day}^{-1}, \\
\lambda_{KD_0} &= 4.54 \times 10^{-2} \text{ day}^{-1}, \\
\lambda_{KD} &= 2.27 \times 10^{-1} \text{ day}^{-1}.
\end{aligned}$$

C.9 Cytokine Production Constants

To estimate many of the cytokine production constants, we consider (2.35) - (2.43) at steady state and use the data from [72]. For each immune cell, we assume that each cytokine's corresponding gene expression is proportional to its production rate by that cell. We assume that the results for fibroblastic reticular cells in [73] translate directly to results for CAFs, recalling that CAFs are considered to be all fibroblasts found in the TME [73].

C.9.1 Estimates for I_2

Using values from [72], and considering (2.35) at steady state leads to the equations

$$\frac{\lambda_{I_2T_8}}{0.114615876287774} = \frac{\lambda_{I_2T_1}}{0.335763693785869}$$

and

$$\lambda_{I_2 T_8} \overline{T_8} + \lambda_{I_2 T_1} \overline{T_1} - d_{I_2} \overline{I_2} = 0.$$

Solving these simultaneously leads to

$$\begin{aligned}\lambda_{I_2 T_8} &= 5.79 \times 10^{-13} \text{ (g/cell)}^{-1} \text{ day}^{-1}, \\ \lambda_{I_2 T_1} &= 1.70 \times 10^{-12} \text{ (g/cell)}^{-1} \text{ day}^{-1}.\end{aligned}$$

C.9.2 Estimates for I_γ

Using values from [72], and considering (2.36) at steady state leads to the equations

$$\frac{\lambda_{I_\gamma T_8}}{2 \times 0.0539973307184416} = \frac{\lambda_{I_\gamma T_1}}{2 \times 0.0188926732394088} = \frac{\lambda_{I_\gamma K}}{2}$$

and

$$(\lambda_{I_\gamma T_8} \overline{T_8} + \lambda_{I_\gamma T_1} \overline{T_1}) \frac{1}{2} + \lambda_{I_\gamma K} \frac{\overline{K}}{2} - d_{I_\gamma} \overline{I_\gamma} = 0.$$

Solving these simultaneously leads to

$$\begin{aligned}\lambda_{I_\gamma T_8} &= 1.49 \times 10^{-14} \text{ (g/cell)}^{-1} \text{ day}^{-1}, \\ \lambda_{I_\gamma T_1} &= 5.22 \times 10^{-15} \text{ (g/cell)}^{-1} \text{ day}^{-1}, \\ \lambda_{I_\gamma K} &= 2.76 \times 10^{-13} \text{ (g/cell)}^{-1} \text{ day}^{-1}.\end{aligned}$$

C.9.3 Estimates for I_α

Using values from [72], and considering (2.37) at steady state leads to the equations

$$\frac{\lambda_{I_\alpha T_8}}{0.0654443776961264} = \frac{\lambda_{I_\alpha T_1}}{0.108187215112606} = \frac{\lambda_{I_\alpha M_1}}{0.0396575742078822} = \frac{\lambda_{I_\alpha N_1}}{0.543182158054752} = \frac{\lambda_{I_\alpha K}}{0.114108294134927}$$

and

$$\lambda_{I_\alpha T_8} \overline{T_8} + \lambda_{I_\alpha T_1} \overline{T_1} + \lambda_{I_\alpha M_1} \overline{M_1} + \lambda_{I_\alpha N_1} \overline{N_1} + \lambda_{I_\alpha K} \overline{K} - d_{I_\alpha} \overline{I_\alpha} = 0.$$

Solving these simultaneously leads to

$$\begin{aligned}\lambda_{I_\alpha T_8} &= 2.71 \times 10^{-13} \text{ (g/cell)}^{-1} \text{ day}^{-1}, \\ \lambda_{I_\alpha T_1} &= 4.48 \times 10^{-13} \text{ (g/cell)}^{-1} \text{ day}^{-1}, \\ \lambda_{I_\alpha M_1} &= 1.64 \times 10^{-13} \text{ (g/cell)}^{-1} \text{ day}^{-1}, \\ \lambda_{I_\alpha N_1} &= 2.25 \times 10^{-12} \text{ (g/cell)}^{-1} \text{ day}^{-1}, \\ \lambda_{I_\alpha K} &= 4.72 \times 10^{-13} \text{ (g/cell)}^{-1} \text{ day}^{-1}.\end{aligned}$$

C.9.4 Estimates for I_β

We assume that at steady state, CAFs produce twice as much TGF- β than cancer cells in the TME. This, in conjunction with values from [72], and considering (2.38) at steady state leads to the equations

$$\frac{\lambda_{I_\beta C_F}}{2} = \frac{\lambda_{I_\beta C}}{1}$$

and

$$\frac{\lambda_{I_\beta C_F}}{0.175283003265127} = \frac{\lambda_{I_\beta T_r}}{0.507677682409403}$$

and

$$\lambda_{I_\beta C} \bar{C} + \lambda_{I_\beta T_r} \bar{T}_r + \lambda_{I_\beta C_F} \bar{C}_F - d_{I_\beta} \bar{I}_\beta = 0.$$

Solving these simultaneously leads to

$$\begin{aligned} \lambda_{I_\beta C} &= 6.74 \times 10^{-9} \text{ (g/cell)}^{-1} \text{ day}^{-1}, \\ \lambda_{I_\beta T_r} &= 3.90 \times 10^{-8} \text{ (g/cell)}^{-1} \text{ day}^{-1}, \\ \lambda_{I_\beta C_F} &= 1.35 \times 10^{-8} \text{ (g/cell)}^{-1} \text{ day}^{-1}. \end{aligned}$$

C.9.5 Estimates for I_{12}

Using values from [72], and considering (2.39) at steady state leads to the equations

$$\frac{\lambda_{I_{12}D}}{2 \times 0.330046991455334} = \frac{\lambda_{I_{12}N_1}}{0.038490607327517} = \frac{\lambda_{I_{12}M_1}}{2 \times 0.375922019952045}$$

and

$$\frac{\lambda_{I_{12}D} \bar{D}}{2} + \lambda_{I_{12}N_1} \bar{N}_1 + \frac{\lambda_{I_{12}M_1} \bar{M}_1}{2} - d_{I_{12}} \bar{I}_{12} = 0.$$

Solving these simultaneously leads to

$$\begin{aligned} \lambda_{I_{12}D} &= 2.05 \times 10^{-15} \text{ (g/cell)}^{-1} \text{ day}^{-1}, \\ \lambda_{I_{12}N_1} &= 1.20 \times 10^{-16} \text{ (g/cell)}^{-1} \text{ day}^{-1}, \\ \lambda_{I_{12}M_1} &= 2.34 \times 10^{-15} \text{ (g/cell)}^{-1} \text{ day}^{-1}. \end{aligned}$$

C.9.6 Estimates for I_{10}

Amongst 48 different cell lines tested, it was found in [74], that cancer IL-10 production was maximised in cell lines derived from colon carcinomas. As such, we assume that at steady state, cancer production of IL-10 is equal to half of that by M2 macrophages. We assume that the enhancement factor of IL-2 for IL-10 production by Tregs is similar in CRC to that of inflammatory bowel disease, and use the estimate of $\lambda_{I_{10}I_2} = 3$ that was used in [75]. This, in conjunction with values from [72], and considering (2.40) at steady state leads to the equations

$$\frac{\lambda_{I_{10}C}}{1} = \frac{\lambda_{I_{10}M_2}}{2} \tag{C.5}$$

and

$$\frac{\lambda_{I_{10}T_2}}{0.0165868439434975} = \frac{\lambda_{I_{10}M_2}}{1} = \frac{\lambda_{I_{10}T_r} \left(1 + \frac{\lambda_{I_{10}I_2}}{2}\right)}{0.472157630570674}$$

and

$$\lambda_{I_{10}C} \bar{C} + \lambda_{I_{10}T_2} \bar{T}_2 + \lambda_{I_{10}M_2} \bar{M}_2 + \lambda_{I_{10}T_r} \left(1 + \frac{\lambda_{I_{10}I_2}}{2}\right) \bar{T}_r - d_{I_{10}} \bar{I}_{10} = 0.$$

Solving these simultaneously leads to

$$\lambda_{I_{10}C} = 1.54 \times 10^{-14} \text{ (g/cell)}^{-1} \text{ day}^{-1},$$

$$\begin{aligned}
\lambda_{I_{10}T_2} &= 5.12 \times 10^{-16} \text{ (g/cell)}^{-1}\text{day}^{-1}, \\
\lambda_{I_{10}M_2} &= 3.09 \times 10^{-14} \text{ (g/cell)}^{-1}\text{day}^{-1}, \\
\lambda_{I_{10}T_r} &= 5.83 \times 10^{-13} \text{ (g/cell)}^{-1}\text{day}^{-1}, \\
\lambda_{I_{10}I_2} &= 3.
\end{aligned}$$

C.9.7 Estimates for I_4

Considering (2.41) at steady state leads to the equations

$$\lambda_{I_4T_2}\bar{T}_2 - d_4\bar{I}_4 = 0.$$

This leads to

$$\lambda_{I_4T_2} = 3.35 \times 10^{-11} \text{ (g/cell)}^{-1}\text{day}^{-1}.$$

C.9.8 Estimates for I_6

Using values from [72], and considering (2.42) at steady state leads to the equations

$$\frac{\lambda_{I_6D}}{0.0101779065606832} = \frac{\lambda_{I_6C_F}}{0.0881605096837823}$$

and

$$\lambda_{I_6D}\bar{D} + \lambda_{I_6C_F}\bar{C}_F - d_{I_6}\bar{I}_6.$$

Solving these simultaneously leads to

$$\begin{aligned}
\lambda_{I_6D} &= 4.24 \times 10^{-11} \text{ (g/cell)}^{-1}\text{day}^{-1}, \\
\lambda_{I_6C_F} &= 3.67 \times 10^{-10} \text{ (g/cell)}^{-1}\text{day}^{-1}.
\end{aligned}$$

C.9.9 Estimates for $I_{1\beta}$

Using values from [72], and considering (2.43) at steady state leads to the equations

$$\frac{\lambda_{I_{1\beta}D}}{0.714110468057273} = \frac{\lambda_{I_{1\beta}N_1}}{1} = \frac{\lambda_{I_{1\beta}M_1}}{0.0662745236861768},$$

and

$$\lambda_{I_{1\beta}D}\bar{D} + \lambda_{I_{1\beta}N_1}\bar{N}_1 + \lambda_{I_{1\beta}M_1}\bar{M}_1 - d_{I_{1\beta}}\bar{I}_{1\beta}.$$

Solving these simultaneously leads to

$$\begin{aligned}
\lambda_{I_{1\beta}D} &= 3.68 \times 10^{-13} \text{ (g/cell)}^{-1}\text{day}^{-1}, \\
\lambda_{I_{1\beta}N_1} &= 5.15 \times 10^{-13} \text{ (g/cell)}^{-1}\text{day}^{-1}, \\
\lambda_{I_{1\beta}M_1} &= 3.41 \times 10^{-14} \text{ (g/cell)}^{-1}\text{day}^{-1}.
\end{aligned}$$

C.10 TDLN subsystem constants

C.10.1 Estimate for V_{TS}

The mean tumour volume in stage III colorectal patients was found to be 27.08 cm^3 in [76]. We thus set $V_{LN} = 2.71 \times 10^1 \text{ cm}^3$.

C.10.2 Estimate for V_{LN}

The mean diameter of lymph nodes in CRC patients where cancer has metastasised was found to be 5.6 mm in [77]. Assuming a spherical lymph node, this corresponds to $V_{LN} = \frac{4}{3} \times 2.8^3 \pi \text{ mm}^3 = 9.20 \times 10^{-2} \text{ cm}^3$.

C.10.3 Estimate for τ_m

In [78], it took 18 hours for DCs, which acquired antigen from a site of subcutaneous injection to arrive at the lymph node. We assume that this migration time is the same for DCs acquiring cancer antigens from the TS so that $\tau_m = 18 \text{ h} = 0.75 \text{ d}$.

C.10.4 Estimate for τ_a

To estimate τ_a , we note that T cells in the TDLN travel at speeds of $11 \sim 14 \mu\text{m}/\text{min}$, in comparison to DCs which migrate at speeds of $3 - 6 \mu\text{m}/\text{min}$ [79]. We thus have that $\tau_a = \frac{4.5}{12.5} \tau_m \approx 0.27 \text{ d}$.

C.10.5 Estimates for CD8+ T cells

It was found in [80] that activated CD8+ T cells required 39 hours on average to complete their first cell division, and so we set $\Delta_8^0 = 39 \text{ h} = 1.63 \text{ d}$. Furthermore, the average division time for subsequent cell cycles is 8.6 hours [80], however, can vary between 5 – 28 hours. Thus, we set $\Delta_8 = 8.6 \text{ h} = 0.36 \text{ d}$. It was shown in [81], that fully activated CD8+ T cells divide a minimum of 7 – 10 times, however can divide more if persistent antigen exposure is present. Indeed, in Lymphocytic Choriomeningitis Virus (LCV), CD8+ T cells can divide more than 15 times [82]. We perform a compromise and set $n_{\max}^8 = 10$. We thus have that $\tau_{T_A^8} = 4.87 \text{ d}$. Finally, it is widely accepted that T cell exhaustion can arise only days to weeks from the initial antigen exposure in the case of chronic antigen stimulation [83, 84] so that we take $\tau_l = 10 \text{ d}$.

C.10.6 Estimates for Th1 and Th2 cells

For simplicity, we use the same parameters for Th1 and Th2 cells, noting that they are phenotypes of CD4+ T helper cells. It was found in [85] that CD4 T cell priming takes between 1 – 2 days, and so we set $\tau_4^{\text{act}} = 1.5 \text{ d}$. Compared to CD8+ T cells, CD4+ T cells appear to divide less, with only approximately 9 cell divisions as in LCV [86]. We assume this is similar in MSI-H/dMMR CRC, and so set $n_{\max}^1 = n_{\max}^2 = 9$. It takes between 12 and 24 hours for the first CD4+ T cell division to occur, with subsequent divisions occurring at a rate of approximately 10 hours per cell division [87]. We thus set $\Delta_1^0 = \Delta_2^0 = 18.5 \text{ h} = 0.77 \text{ d}$, and $\Delta_1 = \Delta_2 = 10 \text{ h} = 0.42 \text{ d}$. We thus have that $\tau_{T_A^1} = \tau_{T_A^2} = 4.13 \text{ d}$.

C.10.7 Estimates for Tregs

We assume that the activation of Tregs takes the amount of time as that of CD4+ T helper cells so that $\tau_4^{\text{act}} = 1.5 \text{ d}$. It was found in [88], that in mice, 6 days after tumour implantation, 45% of Tregs

in the TDLN had undergone at least 1 division, and 14% had undergone more than 6 divisions. We thus set $n_{\max}^r = 6$ and assume that the cell division rates of Tregs and CD4+ T helper cells are the same so that $\Delta_r^0 = 0.77$ d and $\Delta_r = 0.42$ d. We thus have that $\tau_{T_A^r} = 2.87$ d.

C.11 T Cell Parameters and Estimates

C.11.1 Estimates for T_0^8 , T_A^8 , T_8 and T_{ex}

Considering (2.9) at steady state leads to

$$\mathcal{A}_{T_0^8} - \frac{\lambda_{T_0^8 T_A^8} e^{-d_{T_0^8} \tau_8^{\text{act}}} \overline{D^{\text{LN}} T_0^8}}{4} - d_{T_0^8} \overline{T_0^8} = 0,$$

and in particular,

$$\overline{R^8} = \frac{\lambda_{T_0^8 T_A^8} e^{-d_{T_0^8} \tau_8^{\text{act}}} \overline{D^{\text{LN}} T_0^8}}{4}.$$

Considering (2.24) at steady state leads to

$$\frac{2^{n_{\max}^8} e^{-d_{T_0^8} \tau_{T_A^8}} \overline{R^8}}{4} - \lambda_{T_A^8 T_8} \overline{T_A^8} - d_{T_8} \overline{T_A^8} = 0.$$

We first consider the case where no pembrolizumab is present. Considering (2.13) and (2.14) at steady state leads to

$$\begin{aligned} \lambda_{T_A^8 T_8} e^{-d_{T_8} \tau_a} \overline{T_A^8} + \frac{\lambda_{T_8 I_2} \overline{T_8}}{4} - \frac{\lambda_{T_8 C} \overline{T_8}}{2} - \frac{d_{T_8} \overline{T_8}}{2} &= 0, \\ \frac{\lambda_{T_8 C} \overline{T_8}}{2} - \frac{d_{T_{\text{ex}}} \overline{T_{\text{ex}}}}{2} &= 0. \end{aligned}$$

We assume that at steady state, 95% of positive T_8 growth is due to T_A^8 migration to the TS, and the other 5% is due to IL-2-induced proliferation. Thus, we have that

$$\frac{\lambda_{T_A^8 T_8} e^{-d_{T_8} \tau_a} \overline{T_A^8}}{0.95} = \frac{\lambda_{T_8 I_2} \overline{T_8^{\text{TS}}} / 4}{0.05}.$$

To determine $\lambda_{T_{\text{ex}} A_1}$, we assume that when pembrolizumab is present, at steady state 20% of exhausted CD8+ T cells are reinvigorated. That is, we assume that

$$\frac{\lambda_{T_{\text{ex}} A_1} \overline{T_{\text{ex}}} / 2}{0.2} = \frac{d_{T_{\text{ex}}} \overline{T_{\text{ex}}} / 2}{0.8}.$$

Solving these equations simultaneously leads to

$$\begin{aligned} \mathcal{A}_{T_0^8} &= 3.72 \times 10^5 \text{ (cell/cm}^3\text{) day}^{-1}, \\ \lambda_{T_0^8 T_A^8} &= 8.64 \times 10^{-11} \text{ (cell/cm}^3\text{)}^{-1}, \\ \overline{R^8} &= 2.55 \times 10^3 \text{ (cell/cm}^3\text{) day}^{-1}, \\ \lambda_{T_A^8 T_8} &= 3.42 \times 10^{-1} \text{ day}^{-1}, \\ \lambda_{T_8 I_2} &= 1.62 \times 10^{-3} \text{ day}^{-1}, \end{aligned}$$

$$\begin{aligned}\lambda_{T_8C} &= 7.16 \times 10^{-3} \text{ day}^{-1}, \\ \lambda_{T_{\text{ex}A_1}} &= 2.25 \times 10^{-3} \text{ day}^{-1}.\end{aligned}$$

C.11.2 Estimates for T_0^4 , T_A^1 , T_A^2 , T_1 , T_2

Considering (2.15) at steady state leads to

$$\mathcal{A}_{T_0^4} - \frac{\left(\lambda_{T_0^4 T_A^1} + \lambda_{T_0^4 T_A^2}\right) e^{-d_{T_0^4} \tau_{\text{act}}^4} \overline{D^{\text{LN}} T_0^4}}{4} - d_{T_0^4} \overline{T_0^4} = 0,$$

where for $i = 1, 2$,

$$\overline{R^i} = \frac{\lambda_{T_0^4 T_A^i} e^{-d_{T_0^4} \tau_{\text{act}}^4} \overline{D^{\text{LN}} T_0^4}}{4}.$$

Considering (2.12) at steady state leads to

$$\frac{2^{n_{\text{max}}^i} e^{-d_{T_0^4} \tau_{T_A^i}} \overline{R^i}}{4} - \lambda_{T_A^i T_i} \overline{T_A^i} - d_{T_i} \overline{T_A^i} = 0.$$

Finally, considering (2.19) and (2.20) at steady state leads to

$$\begin{aligned}\lambda_{T_A^1 T_1} e^{-d_{T_1} \tau_a} \overline{T_A^1} + \frac{\lambda_{T_1 I_2} \overline{T_1}}{4} - d_{T_1} \overline{T_1} &= 0, \\ \lambda_{T_A^2 T_2} e^{-d_{T_2} \tau_a} \overline{T_A^2} - d_{T_2} \overline{T_2} &= 0.\end{aligned}$$

We assume, like for CD8+ T cells, that at steady state, 95% of positive T_1 growth is due to $T_A^1(n_{\text{max}}^1, t)$ migration to the TS, and the other 5% is due to IL-2-induced proliferation. Thus, we have that

$$\frac{\lambda_{T_A^1 T_1} e^{-d_{T_1} \tau_a} \overline{T_A^1}}{0.95} = \frac{\lambda_{T_1 I_2} \overline{T_1} / 4}{0.05}.$$

Solving these equations simultaneously leads to

$$\begin{aligned}\mathcal{A}_{T_0^4} &= 2.75 \times 10^5 \text{ (cell/cm}^3\text{) day}^{-1}, \\ \lambda_{T_0^4 T_A^1} &= 2.06 \times 10^{-10} \text{ (cell/cm}^3\text{)}^{-1}, \\ \lambda_{T_0^4 T_A^2} &= 3.48 \times 10^{-10} \text{ (cell/cm}^3\text{)}^{-1}, \\ \overline{R^1} &= 2.66 \times 10^3 \text{ (cell/cm}^3\text{) day}^{-1}, \\ \overline{R^2} &= 4.48 \times 10^3 \text{ (cell/cm}^3\text{) day}^{-1}, \\ \lambda_{T_A^1 T_1} &= 4.22 \times 10^{-2} \text{ day}^{-1}, \\ \lambda_{T_A^2 T_2} &= 1.86 \times 10^{-2} \text{ day}^{-1}, \\ \lambda_{T_1 I_2} &= 1.60 \times 10^{-3} \text{ day}^{-1}.\end{aligned}$$

C.11.3 Estimates for T_0^r and T_A^r

Considering (2.21) at steady state leads to

$$\mathcal{A}_{T_0^r} - \frac{\lambda_{T_0^r T_A^r} e^{-d_{T_0^r} \tau_{\text{act}}^4} \overline{D^{\text{LN}} T_0^r}}{4} - d_{T_0^r} \overline{T_0^r} = 0,$$

where

$$\overline{R^r} = \frac{\lambda_{T_0^r T_A^r} e^{-d_{T_0^r} \tau_{\text{act}}^r} \overline{D^{\text{LN}} T_0^r}}{4}.$$

Considering (2.24) at steady state leads to

$$\frac{2^{n_{\text{max}}^r} e^{-d_{T_0^r} \tau_{T_A^r}} \overline{R^r}}{4} - \lambda_{T_A^r T_r} \overline{T_A^r} - d_{T_r} \overline{T_A^r} = 0.$$

Finally, considering (2.25) at steady state leads to

$$\lambda_{T_A^r T_r} e^{-d_{T_r} \tau_a} \overline{T_A^r} - d_{T_r} \overline{T_r} = 0.$$

Solving these equations simultaneously leads to

$$\begin{aligned} \mathcal{A}_{T_0^r} &= 2.36 \times 10^5 \text{ (cell/cm}^3\text{) day}^{-1}, \\ \lambda_{T_0^r T_A^r} &= 1.07 \times 10^{-7} \text{ (cell/cm}^3\text{)}^{-1}, \\ \overline{R^r} &= 2.34 \times 10^5 \text{ (cell/cm}^3\text{) day}^{-1}, \\ \lambda_{T_A^r T_r} &= 7.13 \times 10^{-1} \text{ day}^{-1}. \end{aligned}$$

C.12 Estimates for C and N_c

C.12.1 Estimates for C

Since CD8+ T cells are more effective at lysing cancer cells than Th1 cells, we approximate

$$\frac{\lambda_{CT_8}/4}{8} = \lambda_{CT_1}.$$

We assume that CD8+ T cells and NK cells kill cancer cells with similar potency, so we approximate

$$\lambda_{CK}/4 = \lambda_{CT_8}/4.$$

We also assume that the rate that TNF induces tumour necroptosis is larger than that for IFN- γ , so we approximate

$$\frac{\lambda_{CI_\alpha}}{2 \times 5} = \frac{\lambda_{CI_\gamma}}{2}.$$

Via fitting to experimental data, it was found in [89] that the optimal C_0 for colon cancer, where logistic growth is assumed, is $C_0 = 8.02 \times 10^8 \text{ cell/cm}^3$, which we assume to be the case for CRC, and this is consistent with the estimate in [90].

We note that not using the steady-state equation, (2.1), as part of the parameter estimation pro-

cess results in more accurate trajectories for the time period of interest. However, this may result in reduced accuracy for trajectories extending significantly beyond this timeframe.

C.12.2 Estimates for N_c

Considering (2.2) at steady state leads to the equation

$$\frac{\lambda_{CI_\alpha}\bar{C}}{2} + \frac{\lambda_{CI_\gamma}\bar{C}}{2} - d_{N_c}\bar{N}_c = 0.$$

C.12.3 Fitting λ_C , λ_{CT_8} , and λ_{CI_α}

We fit λ_C , λ_{CT_8} , and λ_{CI_α} by choosing the values such that the steady state value of C and N_c is reached at 155 days, in particular ensuring that C and N_c reach steady state at exactly 155 days. Furthermore, we expect monotonicity in the growth of the total cancer population ($C + N_c$), as the cancer progresses without treatment, and so we aim to minimise the objective function

$$\text{Objective} = \frac{|C(155) - \bar{C}|}{\bar{C}} + \frac{|N_c(155) - \bar{N}_c|}{\bar{N}_c} + \frac{\left| \max_{t \in [0, 155]} (C(t) + N_c(t)) - (\bar{C} + \bar{N}_c) \right|}{\bar{C} + \bar{N}_c}. \quad (\text{C.6})$$

We use perform a parameter sweep to minimise (C.6), and set the parameter space to be $\lambda_C \in (0 \text{ day}^{-1}, 2 \text{ day}^{-1}]$, $\lambda_{CT_8} \in (0 \text{ day}^{-1}, 1 \times 10^{-6} \text{ day}^{-1}]$, and $\lambda_{CI_\alpha} \in (0 \text{ day}^{-1}, 1 \text{ day}^{-1}]$, ensuring that all model parameters are positive. The optimal values of λ_C , λ_{CT_8} , and λ_{CI_α} were found to be

$$\begin{aligned} \lambda_C &= 6.27 \times 10^{-1} \text{ day}^{-1}, \\ \lambda_{CT_8} &= 5.22 \times 10^{-7} (\text{cell/cm}^3)^{-1} \text{ day}^{-1}, \\ \lambda_{CI_\alpha} &= 4.69 \times 10^{-2} \text{ day}^{-1}, \end{aligned}$$

which implies that

$$\begin{aligned} \lambda_{CT_1} &= 1.63 \times 10^{-8} (\text{cell/cm}^3)^{-1} \text{ day}^{-1}, \\ \lambda_{CK} &= 5.22 \times 10^{-7} (\text{cell/cm}^3)^{-1} \text{ day}^{-1}, \\ \lambda_{CI_\gamma} &= 9.38 \times 10^{-3} \text{ day}^{-1}, \\ d_{N_c} &= 5.34 \times 10^{-1} \text{ day}^{-1}. \end{aligned}$$

In particular, we observe that λ_C is rather consistent with [89] where λ_C , in the absence of immune cells, was estimated to be 0.5775 in CRC.

References

- [1] Siewe N, Friedman A. TGF- β inhibition can overcome cancer primary resistance to PD-1 blockade: A mathematical model. PLOS ONE. 2021 Jun;16(6):e0252620. Available from: <http://dx.doi.org/10.1371/journal.pone.0252620>.
- [2] Siewe N, Friedman A. Optimal timing of steroid initiation in response to CTLA-4 antibody in metastatic cancer: A mathematical model. PLOS ONE. 2022 Nov;17(11):e0277248. Available from: <http://dx.doi.org/10.1371/journal.pone.0277248>.

- [3] Siewe N, Friedman A. Cancer therapy with immune checkpoint inhibitor and CSF-1 blockade: A mathematical model. *Journal of Theoretical Biology*. 2023 Jan;556:111297. Available from: <http://dx.doi.org/10.1016/j.jtbi.2022.111297>.
- [4] Han Y, Liu D, Li L. PD-1/PD-L1 pathway: current researches in cancer. *American journal of cancer research*. 2020;10(3):727. Available from: <https://pmc.ncbi.nlm.nih.gov/articles/PMC7136921/>.
- [5] Zhang W, An F, Xia M, Zhan Q, Tian W, Jiao Y. Increased HMGB1 expression correlates with higher expression of c-IAP2 and pERK in colorectal cancer. *Medicine*. 2019 Jan;98(3):e14069. Available from: <http://dx.doi.org/10.1097/MD.0000000000014069>.
- [6] Di Virgilio F, Adinolfi E. Extracellular purines, purinergic receptors and tumor growth. *Oncogene*. 2016 Jun;36(3):293–303. Available from: <http://dx.doi.org/10.1038/onc.2016.206>.
- [7] Pellegatti P, Raffaghello L, Bianchi G, Piccardi F, Pistoia V, Di Virgilio F. Increased Level of Extracellular ATP at Tumor Sites: In Vivo Imaging with Plasma Membrane Luciferase. *PLoS ONE*. 2008 Jul;3(7):e2599. Available from: <http://dx.doi.org/10.1371/journal.pone.0002599>.
- [8] Cao Y, Chen E, Wang X, Song J, Zhang H, Chen X. An emerging master inducer and regulator for epithelial-mesenchymal transition and tumor metastasis: extracellular and intracellular ATP and its molecular functions and therapeutic potential. *Cancer Cell International*. 2023 Feb;23(1). Available from: <http://dx.doi.org/10.1186/s12935-023-02859-0>.
- [9] Ghosh P, Ghosh S, Basu K, Das S, Daefer S. An analytical model to estimate the time taken for cytoplasmic reactions for stochastic simulation of complex biological systems. In: 2006 IEEE International Conference on Granular Computing. IEEE; 2006. Available from: <http://dx.doi.org/10.1109/GRC.2006.1635762>.
- [10] Abdullah TM, Whatmore J, Bremer E, Slibinskas R, Michalak M, Eggleton P. Endoplasmic reticulum stress-induced release and binding of calreticulin from human ovarian cancer cells. *Cancer Immunology, Immunotherapy*. 2021 Nov;71(7):1655–1669. Available from: <http://dx.doi.org/10.1007/s00262-021-03072-6>.
- [11] Calu V, Ionescu A, Stanca L, Geicu OI, Iordache F, Pisoschi AM, et al. Key biomarkers within the colorectal cancer related inflammatory microenvironment. *Scientific Reports*. 2021 Apr;11(1). Available from: <http://dx.doi.org/10.1038/s41598-021-86941-5>.
- [12] Kim YW, Kim SK, Kim CS, Kim IY, Cho MY, Kim NK. Association of Serum and Intratumoral Cytokine Profiles with Tumor Stage and Neutrophil Lymphocyte Ratio in Colorectal Cancer. *Anticancer research*. 2014;34(7):3481-7. Available from: <https://ar.iiarjournals.org/content/34/7/3481.long>.
- [13] Autenshlyus AI, Arkhipov SA, Kunts TA, Marinkin IO, Mikhailova ES, Karpukhina XV, et al. Cytokine profiles of tumor supernatants in invasive ductal cancer and fibroadenoma of the breast and its relationship with VEGF-A expression in the tumors. *International Journal of Immunopathology and Pharmacology*. 2017 Jan;30(1):83–88. Available from: <http://dx.doi.org/10.1177/0394632016681306>.
- [14] Zhao H, Wu L, Yan G, Chen Y, Zhou M, Wu Y, et al. Inflammation and tumor progression: signaling pathways and targeted intervention. *Signal Transduction and Targeted Therapy*. 2021 Jul;6(1). Available from: <http://dx.doi.org/10.1038/s41392-021-00658-5>.

- [15] West WH. Continuous infusion recombinant interleukin-2 (rIL-2) in adoptive cellular therapy of renal carcinoma and other malignancies. *Cancer Treatment Reviews*. 1989 Jun;16:83–89. Available from: [http://dx.doi.org/10.1016/0305-7372\(89\)90027-3](http://dx.doi.org/10.1016/0305-7372(89)90027-3).
- [16] Czajka-Francuz P, Francuz T, Cisoń-Jurek S, Czajka A, Fajkis M, Szymczak B, et al. Serum cytokine profile as a potential prognostic tool in colorectal cancer patients – one center study. *Reports of Practical Oncology & Radiotherapy*. 2020 Nov;25(6):867–875. Available from: <http://dx.doi.org/10.1016/j.rpor.2020.08.004>.
- [17] Sharp SP, Avram D, Stain SC, Lee EC. Local and systemic Th17 immune response associated with advanced stage colon cancer. *Journal of Surgical Research*. 2017 Feb;208:180–186. Available from: <http://dx.doi.org/10.1016/j.jss.2016.09.038>.
- [18] Krzystek-Korpacka M, Diakowska D, Kapturkiewicz B, Bębenek M, Gamian A. Profiles of circulating inflammatory cytokines in colorectal cancer (CRC), high cancer risk conditions, and health are distinct. Possible implications for CRC screening and surveillance. *Cancer Letters*. 2013 Aug;337(1):107–114. Available from: <http://dx.doi.org/10.1016/j.canlet.2013.05.033>.
- [19] Wang J, Xu K, Wu J, Luo C, Li Y, Wu X, et al. The changes of Th17 cells and the related cytokines in the progression of human colorectal cancers. *BMC Cancer*. 2012 Sep;12(1). Available from: <http://dx.doi.org/10.1186/1471-2407-12-418>.
- [20] Shim KS, Kim KH, Han WS, Park EB. Elevated serum levels of transforming growth factor beta 1 in patients with colorectal carcinoma. *Cancer*. 1999 Feb;85(3):554–561. Available from: [http://dx.doi.org/10.1002/\(SICI\)1097-0142\(19990201\)85:3<554::AID-CNCR6>3.0.CO;2-X](http://dx.doi.org/10.1002/(SICI)1097-0142(19990201)85:3<554::AID-CNCR6>3.0.CO;2-X).
- [21] Bersano J, Lashuk K, Edinger A, Schueler J. A Subset of Colon Cancer Cell Lines Displays a Cytokine Profile Linked to Angiogenesis, EMT and Invasion Which Is Modulated by the Culture Conditions In Vitro. *Cells*. 2023 Oct;12(21):2539. Available from: <http://dx.doi.org/10.3390/cells12212539>.
- [22] Stanilov N, Miteva L, Deliysky T, Jovchev J, Stanilova S. Advanced Colorectal Cancer Is Associated With Enhanced IL-23 and IL-10 Serum Levels. *Laboratory Medicine*. 2010 Mar;41(3):159–163. Available from: <http://dx.doi.org/10.1309/LM7T43AQZIUPIOWZ>.
- [23] Pluim D, Ros W, Miedema IHC, Beijnen JH, Schellens JHM. Multiparameter Flow Cytometry Assay for Quantification of Immune Cell Subsets, PD-1 Expression Levels and PD-1 Receptor Occupancy by Nivolumab and Pembrolizumab. *Cytometry Part A*. 2019 Aug;95(10):1053–1065. Available from: <http://dx.doi.org/10.1002/cyto.a.23873>.
- [24] Jiang Y, Li Y, Zhu B. T-cell exhaustion in the tumor microenvironment. *Cell Death & Disease*. 2015 Jun;6(6):e1792–e1792. Available from: <http://dx.doi.org/10.1038/cddis.2015.162>.
- [25] Cheng X, Veverka V, Radhakrishnan A, Waters LC, Muskett FW, Morgan SH, et al. Structure and Interactions of the Human Programmed Cell Death 1 Receptor. *Journal of Biological Chemistry*. 2013 Apr;288(17):11771–11785. Available from: <http://dx.doi.org/10.1074/jbc.M112.448126>.
- [26] Saito A, Tojo M, Kumagai Y, Ohzawa H, Yamaguchi H, Miyato H, et al. Flow cytometry detection of cell type-specific expression of programmed death receptor ligand-1 (PD-L1) in colorectal cancer specimens. *Heliyon*. 2021 Jan;7(1):e05880. Available from: <http://dx.doi.org/10.1016/j.heliyon.2020.e05880>.

- [27] Moreira TG, Mangani D, Cox LM, Leibowitz J, Lobo ELC, Oliveira MA, et al. PD-L1+ and XCR1+ dendritic cells are region-specific regulators of gut homeostasis. *Nature Communications*. 2021 Aug;12(1). Available from: <http://dx.doi.org/10.1038/s41467-021-25115-3>.
- [28] Lai X, Friedman A. Mathematical modeling of cancer treatment with radiation and PD-L1 inhibitor. *Science China Mathematics*. 2020 Feb;63(3):465–484. Available from: <http://dx.doi.org/10.1007/s11425-019-1648-6>.
- [29] Takahashi T, Tagami T, Yamazaki S, Uede T, Shimizu J, Sakaguchi N, et al. Immunologic Self-Tolerance Maintained by Cd25+ Cd4+ Regulatory T Cells Constitutively Expressing Cytotoxic T Lymphocyte-Associated Antigen 4. *The Journal of Experimental Medicine*. 2000 Jul;192(2):303–310. Available from: <http://dx.doi.org/10.1084/jem.192.2.303>.
- [30] Waldman AD, Fritz JM, Lenardo MJ. A guide to cancer immunotherapy: from T cell basic science to clinical practice. *Nature Reviews Immunology*. 2020 May;20(11):651–668. Available from: <http://dx.doi.org/10.1038/s41577-020-0306-5>.
- [31] Rudd CE. CTLA-4 co-receptor impacts on the function of Treg and CD8+ T-cell subsets. *European Journal of Immunology*. 2009 Mar;39(3):687–690. Available from: <http://dx.doi.org/10.1002/eji.200939261>.
- [32] Grebinoski S, Zhang Q, Cillo AR, Manne S, Xiao H, Brunazzi EA, et al. Autoreactive CD8+ T cells are restrained by an exhaustion-like program that is maintained by LAG3. *Nature Immunology*. 2022 May;23(6):868–877. Available from: <http://dx.doi.org/10.1038/s41590-022-01210-5>.
- [33] Wang XB, Zheng CY, Giscombe R, Lefvert AK. Regulation of Surface and Intracellular Expression of CTLA-4 on Human Peripheral T Cells. *Scandinavian Journal of Immunology*. 2001 Nov;54(5):453–458. Available from: <http://dx.doi.org/10.1046/j.1365-3083.2001.00985.x>.
- [34] Lala M, Li TR, de Alwis DP, Sinha V, Mayawala K, Yamamoto N, et al. A six-weekly dosing schedule for pembrolizumab in patients with cancer based on evaluation using modelling and simulation. *European Journal of Cancer*. 2020 May;131:68–75. Available from: <http://dx.doi.org/10.1016/j.ejca.2020.02.016>.
- [35] Zandarashvili L, Sahu D, Lee K, Lee YS, Singh P, Rajarathnam K, et al. Real-time Kinetics of High-mobility Group Box 1 (HMGB1) Oxidation in Extracellular Fluids Studied by in Situ Protein NMR Spectroscopy. *Journal of Biological Chemistry*. 2013 Apr;288(17):11621–11627. Available from: <http://dx.doi.org/10.1074/jbc.M113.449942>.
- [36] Nandigama R, Padmasekar M, Wartenberg M, Sauer H. Feed Forward Cycle of Hypotonic Stress-induced ATP Release, Purinergic Receptor Activation, and Growth Stimulation of Prostate Cancer Cells. *Journal of Biological Chemistry*. 2006 Mar;281(9):5686–5693. Available from: <http://dx.doi.org/10.1074/jbc.M510452200>.
- [37] Zhang Y, Thangam R, You SH, Sultonova RD, Venu A, Min JJ, et al. Engineering Calreticulin-Targeting Monobodies to Detect Immunogenic Cell Death in Cancer Chemotherapy. *Cancers*. 2021 Jun;13(11):2801. Available from: <http://dx.doi.org/10.3390/cancers13112801>.
- [38] Goicoechea SM, Murphy-Ullrich JE. In: *Cell Surface Calreticulin: Role in Signaling Thrombospondin Anti-Adhesive Activity*. Springer US; 2003. p. 193–204. Available from: http://dx.doi.org/10.1007/978-1-4419-9258-1_18.

- [39] Ruedl C, Koebel P, Bachmann M, Hess M, Karjalainen K. Anatomical Origin of Dendritic Cells Determines Their Life Span in Peripheral Lymph Nodes. *The Journal of Immunology*. 2000 Nov;165(9):4910–4916. Available from: <http://dx.doi.org/10.4049/jimmunol.165.9.4910>.
- [40] Kamath AT, Henri S, Battye F, Tough DF, Shortman K. Developmental kinetics and lifespan of dendritic cells in mouse lymphoid organs. *Blood*. 2002 Sep;100(5):1734–1741. Available from: http://dx.doi.org/10.1182/blood.V100.5.1734.h81702001734_1734_1741.
- [41] Takada K, Jameson SC. Self-class I MHC molecules support survival of naive CD8 T cells, but depress their functional sensitivity through regulation of CD8 expression levels. *Journal of Experimental Medicine*. 2009 Sep;206(10):2253–2269. Available from: <http://dx.doi.org/10.1084/jem.20082553>.
- [42] Hellerstein M, Hanley MB, Cesar D, Siler S, Papageorgopoulos C, Wieder E, et al. Directly measured kinetics of circulating T lymphocytes in normal and HIV-1-infected humans. *Nature Medicine*. 1999 Jan;5(1):83–89. Available from: <http://dx.doi.org/10.1038/4772>.
- [43] Kumbhari A, Egelston CA, Lee PP, Kim PS. Mature Dendritic Cells May Promote High-Avidity Tuning of Vaccine T Cell Responses. *Frontiers in Immunology*. 2020 Oct;11. Available from: <http://dx.doi.org/10.3389/fimmu.2020.584680>.
- [44] Vukmanovic-Stejic M, Zhang Y, Cook JE, Fletcher JM, McQuaid A, Masters JE, et al. Human CD4+ CD25hi Foxp3+ regulatory T cells are derived by rapid turnover of memory populations in vivo. *Journal of Clinical Investigation*. 2006 Sep;116(9):2423–2433. Available from: <http://dx.doi.org/10.1172/JCI28941>.
- [45] Louzoun Y, Xue C, Lesinski GB, Friedman A. A mathematical model for pancreatic cancer growth and treatments. *Journal of Theoretical Biology*. 2014 Jun;351:74–82. Available from: <http://dx.doi.org/10.1016/j.jtbi.2014.02.028>.
- [46] Coffelt SB, Wellenstein MD, de Visser KE. Neutrophils in cancer: neutral no more. *Nature Reviews Cancer*. 2016 Jun;16(7):431–446. Available from: <http://dx.doi.org/10.1038/nrc.2016.52>.
- [47] Ocana A, Nieto-Jiménez C, Pandiella A, Templeton AJ. Neutrophils in cancer: prognostic role and therapeutic strategies. *Molecular Cancer*. 2017 Aug;16(1). Available from: <http://dx.doi.org/10.1186/s12943-017-0707-7>.
- [48] Patel AA, Zhang Y, Fullerton JN, Boelen L, Rongvaux A, Maini AA, et al. The fate and lifespan of human monocyte subsets in steady state and systemic inflammation. *Journal of Experimental Medicine*. 2017 Jun;214(7):1913–1923. Available from: <http://dx.doi.org/10.1084/jem.20170355>.
- [49] Wu SY, Fu T, Jiang YZ, Shao ZM. Natural killer cells in cancer biology and therapy. *Molecular Cancer*. 2020 Aug;19(1). Available from: <http://dx.doi.org/10.1186/s12943-020-01238-x>.
- [50] Vivier E, Tomasello E, Baratin M, Walzer T, Ugolini S. Functions of natural killer cells. *Nature Immunology*. 2008 Apr;9(5):503–510. Available from: <http://dx.doi.org/10.1038/ni1582>.
- [51] Lowry LE, Zehring WA. Potentiation of Natural Killer Cells for Cancer Immunotherapy: A Review of Literature. *Frontiers in Immunology*. 2017 Sep;8. Available from: <http://dx.doi.org/10.3389/fimmu.2017.01061>.

- [52] Lotze MT, Matory YL, Ettinghausen SE, Rayner AA, Sharrow SO, Seipp CA, et al. In vivo administration of purified human interleukin 2. II. Half life, immunologic effects, and expansion of peripheral lymphoid cells in vivo with recombinant IL 2. *The Journal of Immunology*. 1985 Oct;135(4):2865–2875. Available from: <http://dx.doi.org/10.4049/jimmunol.135.4.2865>.
- [53] Lotze MT, Matory YL, Ettinghausen SE, Rayner AA, Sharrow SO, Seipp CA, et al. In vivo administration of purified human interleukin 2. II. Half life, immunologic effects, and expansion of peripheral lymphoid cells in vivo with recombinant IL 2. *The Journal of Immunology*. 1985 Oct;135(4):2865–2875. Available from: <http://dx.doi.org/10.4049/jimmunol.135.4.2865>.
- [54] Balachandran S, Adams GP. Interferon- γ -Induced Necrosis: An Antitumor Biotherapeutic Perspective. *Journal of Interferon & Cytokine Research*. 2013 Apr;33(4):171–180. Available from: <http://dx.doi.org/10.1089/jir.2012.0087>.
- [55] Ma Y, Zhao S, Shen S, Fang S, Ye Z, Shi Z, et al. A novel recombinant slow-release TNF α -derived peptide effectively inhibits tumor growth and angiogenesis. *Scientific Reports*. 2015 Sep;5(1). Available from: <http://dx.doi.org/10.1038/srep13595>.
- [56] Oliver J, Bland L, Oettinger C, Arduino M, McAllister S, Agüero S, et al. Cytokine kinetics in an in vitro whole blood model following an endotoxin challenge. *Lymphokine and cytokine research*. 1993 April;12(2):115–120. Available from: <https://pubmed.ncbi.nlm.nih.gov/8324076/>.
- [57] Tirado-Rodríguez B, Ortega E, Segura-Medina P, Huerta-Yepez S. TGF- β : An Important Mediator of Allergic Disease and a Molecule with Dual Activity in Cancer Development. *Journal of Immunology Research*. 2014;2014:1–15. Available from: <http://dx.doi.org/10.1155/2014/318481>.
- [58] Jung K, Ha JH, Kim JE, Kim JA, Kim YJ, Kim CH, et al. Heterodimeric Fc-fused IL12 shows potent antitumor activity by generating memory CD8+ T cells. *OncoImmunology*. 2018 Mar;7(7):e1438800. Available from: <http://dx.doi.org/10.1080/2162402X.2018.1438800>.
- [59] Huhn RD, Radwanski E, Gallo J, Affrime MB, Sabo R, Gonyo G, et al. Pharmacodynamics of subcutaneous recombinant human interleukin-10 in healthy volunteers. *Clinical Pharmacology & Therapeutics*. 1997 Aug;62(2):171–180. Available from: [http://dx.doi.org/10.1016/S0009-9236\(97\)90065-5](http://dx.doi.org/10.1016/S0009-9236(97)90065-5).
- [60] Prendiville J, Thatcher N, Lind M, McIntosh R, Ghosh A, Stern P, et al. Recombinant human interleukin-4 (rhu IL-4) administered by the intravenous and subcutaneous routes in patients with advanced cancer—A phase I toxicity study and pharmacokinetic analysis. *European Journal of Cancer*. 1993 Jan;29(12):1700–1707. Available from: [http://dx.doi.org/10.1016/0959-8049\(93\)90108-r](http://dx.doi.org/10.1016/0959-8049(93)90108-r).
- [61] Waage A, Brandtzaeg P, Halstensen A, Kierulf P, Espevik T. The complex pattern of cytokines in serum from patients with meningococcal septic shock. Association between interleukin 6, interleukin 1, and fatal outcome. *The Journal of experimental medicine*. 1989 Jan;169(1):333–338. Available from: <http://dx.doi.org/10.1084/jem.169.1.333>.
- [62] Wirtz DC, Heller KD, Miltner O, Zilkens KW, Wolff JM. Interleukin-6: a potential inflammatory marker after total joint replacement. *International Orthopaedics*. 2000 Oct;24(4):194–196. Available from: <http://dx.doi.org/10.1007/s002640000136>.

- [63] Lachmann HJ, Lowe P, Felix SD, Rordorf C, Leslie K, Madhoo S, et al. In vivo regulation of interleukin 1 β in patients with cryopyrin-associated periodic syndromes. *Journal of Experimental Medicine*. 2009 Apr;206(5):1029–1036. Available from: <http://dx.doi.org/10.1084/jem.20082481>.
- [64] Yan T, Yu L, Shangguan D, Li W, Liu N, Chen Y, et al. Advances in pharmacokinetics and pharmacodynamics of PD-1/PD-L1 inhibitors. *International Immunopharmacology*. 2023 Feb;115:109638. Available from: <http://dx.doi.org/10.1016/j.intimp.2022.109638>.
- [65] Longoria TC, Tewari KS. Evaluation of the pharmacokinetics and metabolism of pembrolizumab in the treatment of melanoma. *Expert Opinion on Drug Metabolism & Toxicology*. 2016 Aug;12(10):1247–1253. Available from: <http://dx.doi.org/10.1080/17425255.2016.1216976>.
- [66] Dang TO, Ogunniyi A, Barbee MS, Drilon A. Pembrolizumab for the treatment of PD-L1 positive advanced or metastatic non-small cell lung cancer. *Expert Review of Anticancer Therapy*. 2015 Dec;16(1):13–20. Available from: <http://dx.doi.org/10.1586/14737140.2016.1123626>.
- [67] Schoenfeld AJ, Hellmann MD. Acquired Resistance to Immune Checkpoint Inhibitors. *Cancer Cell*. 2020 Apr;37(4):443–455. Available from: <http://dx.doi.org/10.1016/j.ccell.2020.03.017>.
- [68] Le DT, Durham JN, Smith KN, Wang H, Bartlett BR, Aulakh LK, et al. Mismatch repair deficiency predicts response of solid tumors to PD-1 blockade. *Science*. 2017 Jul;357(6349):409–413. Available from: <http://dx.doi.org/10.1126/science.aan6733>.
- [69] Piccioli D, Sbrana S, Melandri E, Valiante NM. Contact-dependent Stimulation and Inhibition of Dendritic Cells by Natural Killer Cells. *The Journal of Experimental Medicine*. 2002 Feb;195(3):335–341. Available from: <http://dx.doi.org/10.1084/jem.20010934>.
- [70] Verdijk P, Aarntzen EHJG, Lesterhuis WJ, Boullart ACI, Kok E, van Rossum MM, et al. Limited Amounts of Dendritic Cells Migrate into the T-Cell Area of Lymph Nodes but Have High Immune Activating Potential in Melanoma Patients. *Clinical Cancer Research*. 2009 Apr;15(7):2531–2540. Available from: <http://dx.doi.org/10.1158/1078-0432.CCR-08-2729>.
- [71] Potdar PD, Chaudhary S. Molecular characterization of cancer-associated fibroblasts isolated from human colorectal cancer as a major stromal cell component promoting metastasis. *Journal of Unexplored Medical Data*. 2017 Feb;2(1). Available from: <http://dx.doi.org/10.20517/2572-8180.2016.10>.
- [72] Cui A, Huang T, Li S, Ma A, Pérez JL, Sander C, et al. Dictionary of immune responses to cytokines at single-cell resolution. *Nature*. 2023 Dec;625(7994):377–384. Available from: <http://dx.doi.org/10.1038/s41586-023-06816-9>.
- [73] Zhang Y, Lv N, Li M, Liu M, Wu C. Cancer-associated fibroblasts: tumor defenders in radiation therapy. *Cell Death & Disease*. 2023 Aug;14(8). Available from: <http://dx.doi.org/10.1038/s41419-023-06060-z>.
- [74] Gastl GA, Abrams JS, Nanus DM, Oosterkamp R, Silver J, Liu F, et al. Interleukin-10 production by human carcinoma cell lines and its relationship to interleukin-6 expression. *International Journal of Cancer*. 1993 Aug;55(1):96–101. Available from: <http://dx.doi.org/10.1002/ijc.2910550118>.

- [75] Lo WC, Arsenescu V, Arsenescu RI, Friedman A. Inflammatory Bowel Disease: How Effective Is TNF- α Suppression? PLOS ONE. 2016 Nov;11(11):e0165782. Available from: <http://dx.doi.org/10.1371/journal.pone.0165782>.
- [76] Park JY, Kim SH, Lee SM, Lee JS, Han JK. CT volumetric measurement of colorectal cancer helps predict tumor staging and prognosis. PLOS ONE. 2017 Jun;12(6):e0178522. Available from: <http://dx.doi.org/10.1371/journal.pone.0178522>.
- [77] Rössler O, Betge J, Harbaum L, Mrak K, Tschmelitsch J, Langner C. Tumor size, tumor location, and antitumor inflammatory response are associated with lymph node size in colorectal cancer patients. Modern Pathology. 2017 Jun;30(6):897–904. Available from: <http://dx.doi.org/10.1038/modpathol.2016.227>.
- [78] Catron DM, Itano AA, Pape KA, Mueller DL, Jenkins MK. Visualizing the First 50 Hr of the Primary Immune Response to a Soluble Antigen. Immunity. 2004 Sep;21(3):341–347. Available from: <http://dx.doi.org/10.1016/j.immuni.2004.08.007>.
- [79] Anaya JM, Shoenfeld Y, Rojas-Villarraga A, Levy RA, Cervera R. Autoimmunity: from bench to bedside. El Rosario University Press; 2013.
- [80] Plambeck M, Kazeroonian A, Loeffler D, Kretschmer L, Salinno C, Schroeder T, et al. Heritable changes in division speed accompany the diversification of single T cell fate. Proceedings of the National Academy of Sciences. 2022 Feb;119(9). Available from: <http://dx.doi.org/10.1073/pnas.2116260119>.
- [81] Kaech SM, Ahmed R. Memory CD8⁺ T cell differentiation: initial antigen encounter triggers a developmental program in naïve cells. Nature Immunology. 2001 May;2(5):415–422. Available from: <http://dx.doi.org/10.1038/87720>.
- [82] Masopust D, Murali-Krishna K, Ahmed R. Quantitating the Magnitude of the Lymphocytic Choriomeningitis Virus-Specific CD8 T-Cell Response: It Is Even Bigger than We Thought. Journal of Virology. 2007 Feb;81(4):2002–2011. Available from: <http://dx.doi.org/10.1128/jvi.01459-06>.
- [83] Blank CU, Haining WN, Held W, Hogan PG, Kallies A, Lugli E, et al. Defining ‘T cell exhaustion’. Nature Reviews Immunology. 2019 Sep;19(11):665–674. Available from: <http://dx.doi.org/10.1038/s41577-019-0221-9>.
- [84] McLane LM, Abdel-Hakeem MS, Wherry EJ. CD8 T Cell Exhaustion During Chronic Viral Infection and Cancer. Annual Review of Immunology. 2019 Apr;37(1):457–495. Available from: <http://dx.doi.org/10.1146/annurev-immunol-041015-055318>.
- [85] Jolley-Gibbs DM, Lepak NM, Yen M, Swain SL. Two Distinct Stages in the Transition from Naïve CD4 T Cells to Effectors, Early Antigen-Dependent and Late Cytokine-Driven Expansion and Differentiation. The Journal of Immunology. 2000 Nov;165(9):5017–5026. Available from: <http://dx.doi.org/10.4049/jimmunol.165.9.5017>.
- [86] Homann D, Teyton L, Oldstone MBA. Differential regulation of antiviral T-cell immunity results in stable CD8⁺ but declining CD4⁺ T-cell memory. Nature Medicine. 2001 Aug;7(8):913–919. Available from: <http://dx.doi.org/10.1038/90950>.

- [87] Kaech SM, Wherry EJ, Ahmed R. Effector and memory T-cell differentiation: implications for vaccine development. *Nature Reviews Immunology*. 2002 Apr;2(4):251–262. Available from: <http://dx.doi.org/10.1038/nri778>.
- [88] Darrasse-Jèze G, Bergot AS, Durgeau A, Billiard F, Salomon BL, Cohen JL, et al. Tumor emergence is sensed by self-specific CD44hi memory Tregs that create a dominant tolerogenic environment for tumors in mice. *Journal of Clinical Investigation*. 2009 Aug. Available from: <http://dx.doi.org/10.1172/JCI36628>.
- [89] Sarapata EA, de Pillis LG. A Comparison and Catalog of Intrinsic Tumor Growth Models. *Bulletin of Mathematical Biology*. 2014 Aug;76(8):2010–2024. Available from: <http://dx.doi.org/10.1007/s11538-014-9986-y>.
- [90] dePillis LG, Savage H, Radunskaya AE. Mathematical Model of Colorectal Cancer with Monoclonal Antibody Treatments. arXiv; 2013. Available from: <https://arxiv.org/abs/1312.3023>.